

**SEISMIC DAMAGE ASSESSMENT  
OF MOMENT RESISTING  
STEEL FRAMES**

by

**Karim Helmi**

**A Thesis  
Submitted to the College of Graduate Studies and Research  
through Civil & Environmental Engineering  
in Partial Fulfillment of the Requirements for  
the Degree of Master of Applied Science at the  
University of Windsor**

**Windsor, Ontario, Canada**

**1999**

**© 1999 Karim Helmi**



**National Library  
of Canada**

**Acquisitions and  
Bibliographic Services**

395 Wellington Street  
Ottawa ON K1A 0N4  
Canada

**Bibliothèque nationale  
du Canada**

**Acquisitions et  
services bibliographiques**

395, rue Wellington  
Ottawa ON K1A 0N4  
Canada

*Your file Votre référence*

*Our file Notre référence*

**The author has granted a non-exclusive licence allowing the National Library of Canada to reproduce, loan, distribute or sell copies of this thesis in microform, paper or electronic formats.**

**The author retains ownership of the copyright in this thesis. Neither the thesis nor substantial extracts from it may be printed or otherwise reproduced without the author's permission.**

**L'auteur a accordé une licence non exclusive permettant à la Bibliothèque nationale du Canada de reproduire, prêter, distribuer ou vendre des copies de cette thèse sous la forme de microfiche/film, de reproduction sur papier ou sur format électronique.**

**L'auteur conserve la propriété du droit d'auteur qui protège cette thèse. Ni la thèse ni des extraits substantiels de celle-ci ne doivent être imprimés ou autrement reproduits sans son autorisation.**

**0-612-52568-6**

**Canada**

## **ABSTRACT**

In designing earthquake resistant structures, the codes of practice assume a monotonic push-over collapse scenario. Equivalent static forces are applied and design is based only on these forces, not taking into account the cyclic effect of the earthquake loads which, in the case of a severe earthquake, almost certainly will cause a number of load reversals in the inelastic range and some level of structural damage is to be expected. The purpose of this thesis is to assess the level of damage experienced by a structure that is designed and detailed according to the Canadian design codes and standards.

The investigation included the elastic and inelastic analyses of the structure by the computer program DRAIN-2DX. Ground acceleration records from real earthquakes were used as input. The damage was calculated using an empirical strength deterioration formula suggested in the literature by other researchers.

The damage patterns were found to vary from one earthquake record to another. This variation seemed to be the effect of different modes on the structural response. The role of modal participation on the damage patterns has been explained by investigating the response spectra and the Fourier amplitude spectra of roof displacement and base shear histories.

The damage distribution changes from uniform to a localised pattern, as the participation of higher modes tends to supersede that of first mode. Parametric analyses have also revealed that a qualitative prediction of where the damage would localise can be made based on the envelope of the maximum elastic interstorey drift ratios.

**DEDICATION**

**TO MY PARENTS  
AND MY BROTHER**

## **ACKNOWLEDGEMENTS**

The author wishes to express his deep gratitude to his advisor, Dr. Sudip Bhattacharjee, for his support, guidance, effort and time throughout the course of this research. His most helpful supervision is greatly appreciated.

The author wishes to thank Dr. Faouzi Ghib for giving time and help with the DRAIN-2DX program.

Financial assistance received from the Natural Sciences and Engineering Research Council of Canada and the University of Windsor is thankfully acknowledged.

# TABLE OF CONTENTS

<b>ABSTRACT</b>	<b>iii</b>
<b>DEDICATION</b>	<b>iv</b>
<b>ACKNOWLEDGEMENTS</b>	<b>v</b>
<b>LIST OF FIGURES</b>	<b>viii</b>
<b>LIST OF TABLES</b>	<b>xii</b>
<b>LIST OF SYMBOLS</b>	<b>xiii</b>
<b>1. INTRODUCTION</b>	<b>1</b>
1.1. General	1
1.2. Design concepts and procedures of earthquake resistant structures	2
1.2.1. Design concepts	2
1.2.2. Design procedures	3
1.3. Types of damage variables and indices	4
1.4. Research objectives	6
<b>2. LITERATURE REVIEW</b>	<b>8</b>
2.1. General	8
2.2. Damage in steel structures	8
2.3. Cyclic damage in steel structures	10
2.4. Comments on the cyclic damage models	14
2.4.1. The Daali-Korol strength deterioration model	14
2.4.2. The Daali-Korol damage models	14
2.4.3. The Ballio-Castiglioni approach	15
<b>3. METHODOLOGY DESCRIPTION</b>	<b>17</b>
3.1. General	17
3.2. Description of the building	17
3.2.1. General description of the building	17
3.2.2. Structural system, loading and design of the building	18
3.3. The finite element method	20
3.4. The DRAIN-2DX program	22
3.5. Modelling	23
3.5.1. Basic modelling assumptions	23
3.5.2. Element modelling	24
3.5.2.1. General	24
3.5.2.2. Yield surface	24

3.5.2.3. Strain Hardening	25
3.5.3. Masses and Loads	26
3.5.4. Damping	26
3.5.5. Natural Frequencies and periods	26
3.6. Analysis	27
3.7. Earthquake records	27
3.8. Analysis results and damage calculation	28
3.8.1. General	28
3.8.2. Damage calculations	29
<b>4. RESULTS AND DISCUSSION</b>	<b>31</b>
4.1. Introduction	31
4.2. Description of behaviour	31
4.2.1. Record # 1 (Loma Prieta record #1)	32
4.2.2. Record # 2 (Loma Prieta record #2)	34
4.2.3. Record # 3 (The Northridge record)	35
4.2.4. Record # 4 (The Long Beach record)	36
4.2.5. Record # 5 (The Morgan Hill record)	37
4.3. General comments and observations	39
4.4. Effect of higher modes on the damage patterns	40
4.5. The relation between interstorey drift ratio and damage	42
4.6. The relation between the maximum inelastic base shear and the total damage	43
<b>5. SUMMARY AND CONCLUSIONS</b>	<b>45</b>
5.1. Summary	44
5.2. Conclusions	45
5.3. Recommendations for future research	47
<b>REFERENCES</b>	<b>49</b>
<b>APPENDIX A</b>	<b>54</b>
<b>APPENDIX B</b>	<b>104</b>
<b>APPENDIX C</b>	<b>107</b>
<b>APPENDIX D</b>	<b>116</b>
<b>VITA AUCTORIS</b>	<b>119</b>

## LIST OF FIGURES

2.1	Profile of an I section showing notations of the different dimensions	11
3.1	Plan of the building	18
3.2	Elevation of a typical moment resisting frame	19
3.3	Element type 02	24
3.4	Yield surface of element type 02	25
3.5	Strain hardening model	25
A.1	Unscaled ground acceleration record # 1 (Loma Prieta record # 1)	55
A.2	Unscaled ground acceleration record # 2 (Loma Prieta record # 2)	56
A.3	Unscaled ground acceleration record # 3 (Northridge record)	57
A.4	Unscaled ground acceleration record # 4 (Long Beach record)	58
A.5	Unscaled ground acceleration record # 5 (Morgan Hill record)	59
A.6	Response spectrum for unscaled ground acceleration record # 1 (Loma Prieta record # 1)	60
A.7	Response spectrum for unscaled ground acceleration record # 2 (Loma Prieta record # 2)	61
A.8	Response spectrum for unscaled ground acceleration record # 3 (Northridge)	62
A.9	Response spectrum for unscaled ground acceleration record # 4 (Long Beach record)	63
A.10	Response spectrum for unscaled ground acceleration record # 5 (Morgan Hill record)	64
A.11	Strength deterioration in percent for record # 1 (Loma Prieta record # 1) 2.5% strain hardening ratio	65
A.12	Strength deterioration in percent for record # 1 (Loma Prieta record # 1) 5% strain hardening ratio	66
A.13	Strength deterioration in percent for record # 1 (Loma Prieta record # 1)	



10% strain hardening ratio	67
A.14 Normalized roof displacement record # 1 (Loma Prieta record #1)	68
A.15 Normalized inelastic roof displacement record # 1 (Loma Prieta record #1)	69
A.16 Maximum interstorey drift ratio for record #1 (Loma Prieta record # 1)	70
A.17 Strength deterioration in percent for record # 1 (Loma Prieta record # 2) 5% strain hardening ratio	71
A.18 Normalized roof displacement record # 2 (Loma Prieta record #2)	72
A.19 Maximum interstorey drift ratio for record #2 (Loma Prieta record # 2)	73
A.20 Strength deterioration in percent for record # 3 (Northridge record) 5% strain hardening ratio	74
A.21 Normalized roof displacement record # 3 (Northridge record)	75
A.22 Maximum interstorey drift ratio for record #3 (Northridge record)	76
A.23 Strength deterioration in percent for record # 1 (Long Beach record) 5% strain hardening ratio	77
A.24 Normalized roof displacement record # 1 (Long Beach record)	78
A.25 Maximum interstorey drift ratio for record #1 (Long Beach record)	79
A.26 Strength deterioration in percent for record # 5 (Morgan Hill record) 2.5% strain hardening ratio	80
A.27 Strength deterioration in percent for record # 5 (Morgan Hill record) 5% strain hardening ratio	81
A.28 Strength deterioration in percent for record # 5 (Morgan Hill record) 10% strain hardening ratio	82
A.29 Normalized roof displacement record # 5 (Morgan Hill record)	83
A.30 Normalized inelastic roof displacement record # 5 (Morgan Hill record)	84
A.31 Maximum interstorey drift ratio for record # 5 (Morgan Hill record)	85
A.32 Fourier spectrum for base shear history record #1	

	(Loma Prieta record # 1)	86
A.33	Fourier spectrum for base shear history record #2 (Loma Prieta record # 2)	87
A.34	Fourier spectrum for base shear history record #3 (Northridge record)	88
A.35	Fourier spectrum for base shear history record #4 (Long Beach record)	89
A.36	Fourier spectrum for base shear history record #5 (Morgan Hill record)	90
A.37	Fourier spectrum for roof displacement history record #1 (Loma Prieta record # 1)	91
A.38	Fourier spectrum for roof displacement history record #2 (Loma Prieta record # 2)	92
A.39	Fourier spectrum for roof displacement history record #3 (Northridge record)	93
A.40	Fourier spectrum for roof displacement history record #4 (Long Beach record)	94
A.41	Fourier spectrum for roof displacement history record #5 (Morgan Hill record)	95
A.42	Percentage strength deterioration versus maximum interstorey drift ratio record #1 (Loma Prieta record # 1)	96
A.43	Percentage strength deterioration versus maximum interstorey drift ratio record #2 (Loma Prieta record # 2)	97
A.44	Percentage strength deterioration versus maximum interstorey drift ratio record #3 (Northridge record)	98
A.45	Percentage strength deterioration versus maximum interstorey drift ratio record #4 (Long Beach record)	99
A.46	Percentage strength deterioration versus maximum interstorey drift ratio record #5 (Morgan Hill record)	100
A.47	Elastic maximum interstorey drift ratio versus damage	101

<b>A.48</b>	<b>Base shear versus total averaged damage</b>	<b>102</b>
<b>A.49</b>	<b>Base shear versus total weighted damage</b>	<b>103</b>

## **LIST OF TABLES**

3.1	First five natural frequencies and damping of the structure	26
3.2	Summary of ground acceleration data	28
3.3	Values of “a” for beams	30
4.1	Summary of analysis results	31

## LIST OF SYMBOLS

<b>A</b>	fatigue variable
<b>A<sub>i</sub></b>	the hysteretic energy dissipated in the <i>i</i> th cycle
<b>A<sub>yi</sub></b>	the energy that the element would dissipate if it had an elasto-plastic behavior
<b>a</b>	section variable
<b>a</b>	fatigue exponent
<b>b</b>	half of the flange's width
<b>b</b>	damage exponent
<b>C</b>	damping matrix
<b>d</b>	percentage of strength deterioration or damage
<b>E</b>	Elastic modulus
<b>F</b>	foundation factor
<b>F<sub>y</sub></b>	force causing first yield
<b>h</b>	clear height of the web
<b>I</b>	seismic importance factor of the structure
<b>i</b>	unit vector
<b>L</b>	cantilever length
<b>l</b>	unbraced length
<b>M</b>	structural mass matrix
<b>P</b>	applied load vector at the nodes
<b>R</b>	force modification factor that reflects the capability of the structure to dissipate energy through inelastic behaviour
<b>r<sub>y</sub></b>	moment of inertia about the weak axis
<b>S</b>	seismic response factor, for unit value of zonal velocity ratio

$S_x$	section modulus
$t$	flange thickness
$U$	factor representing level of protection based on experience
$U$	displacement vector at the nodes
$\dot{U}$	Velocity vector at nodes
$\ddot{U}$	acceleration vector at nodes
$\ddot{u}_g(t)$	ground acceleration time history
$V$	minimum lateral seismic force at the base of the structure
$V_e$	equivalent lateral force at the base of the structure representing elastic response
$v$	zonal velocity ratio
$v_y$	tip deflection at yield,
$W$	dead load plus 25% of the design snow load plus 60% of the storage load for areas used for storage plus the full contents of any tanks
$w$	web thickness
$\alpha$	mass proportional damping factor
$\alpha_e$	equivalent slenderness ratio
$\alpha_f$	modified flange slenderness
$\alpha_l$	modified lateral slenderness
$\alpha_w$	modified web slenderness
$\beta$	stiffness proportional damping factor
$\beta$	calibration factor
$\Delta v$	tip deflection range
$\Delta \epsilon$	strain range

- $\delta_p$  plastic deformation  $\delta$
- $\mu_i$  is the ductility measured from zero load intercept and experienced in the  $i$ th reversal
- $\mu_m$  is the maximum ductility under monotonic loading
- $\mu_{max}$  is the maximum amount of ductility experienced during the loading history
- $\theta_p$  plastic hinge rotation
- $\sigma^*$  equivalent stress
- $\sigma_y$  yield stress

# **CHAPTER 1**

## **INTRODUCTION**

### **1.1 General**

In designing an earthquake resistant structure, it is expected that, for minor earthquakes, the structure will not suffer any damage, and, in the case of moderate earthquakes, only non-structural damage will occur (i.e. the structural behaviour will remain in the elastic range). However, for the case of severe earthquakes, it is not practical or economical to expect that no damage will occur to the structure. Most design codes allow some level of damage, without jeopardising the overall structural integrity. A structure subjected to a severe earthquake will almost certainly be subjected to a number of load reversals in the inelastic range: thus causing damage that may take several forms. For example, yielding of reinforcing steel, crushing of concrete cover in reinforced concrete structures, buckling of bracing members or beam flanges causing a deterioration of the member strength, and connection failure in steel structures are the common types of earthquake induced structural damage. A method for assessing damage in a structure is, therefore, required in order to predict the probable damage that a structure will suffer during an earthquake and to determine the acceptable level of damage. Moreover, damage assessment could be used to determine the performance of existing structures and their safety. The damage assessment tools can also be applied for post-earthquake condition assessment of structures.



## **1.2 Design concepts and procedures of earthquake resistant structures**

### **1.2.1 Design concepts**

In designing earthquake resistant buildings, it is usually assumed, for practical and economical reasons, that the lateral forces resulting from the earthquake are not resisted by the whole structure, but rather by certain elements in the structure through different mechanisms. The following is a summary of some of these resisting mechanisms:

- Concrete or masonry walls (reinforced or plain) can resist the lateral forces through shearing forces and bending moments about their strong axis.
- Concentric steel bracing can resist the lateral forces through axial forces in the braces. In the case of a severe earthquake, part of the seismic input energy is dissipated through the yielding of bracing members. Bracings can also be eccentric that resist the lateral forces through the combined actions of normal force in the braces and the bending in connecting beams.
- Moment resisting frames can be reinforced concrete or steel, and can resist the lateral forces through bending moment and shearing forces in the frame members. Previously, the only accepted concept was the strong column weak beam, in which only beams were allowed to undergo inelastic deformation. The dissipation of energy occurred through the formation of plastic hinges at the beam ends. Lately, other concepts and energy dissipation mechanisms, such as the strong beam weak column and the weak panel zone in steel beam-column connections, were accepted under certain conditions <sup>[33]</sup>.

In addition to the above schemes, a combination of these schemes can be used, such as the

combination of concrete shear walls with moment resisting frames.

### 1.2.2 Design procedures

Design codes generally assume a monotonic push-over collapse scenario for the earthquake effect, although the earthquake loading is dynamic in nature. A possible maximum snap shot of the dynamic time history is used for the design process. This is interpreted onto the structure by an equivalent static force, the magnitude of which depends on the weight of the structure, its natural period, its material, the mechanism of resisting the lateral forces, the type of soil in the site and the probable ground acceleration in the location of the structure. The National Building code of Canada NBCC 1995<sup>[31]</sup>, for example, calculates an equivalent elastic base shear based on the formula:

$$V_e = v \cdot S \cdot I \cdot F \cdot W \quad (1.1)$$

where,

v = zonal velocity ratio

S = seismic response factor, for unit value of zonal velocity ratio

I = seismic importance factor of the structure

F = foundation factor

W = dead load plus 25% of the design snow load plus 60% of the storage load for areas used for storage plus the full contents of any tanks

The design base shear is then calculated by  $V = (V_e / R)U$  (1.2),

where  $U=0.6$  and "R" is a force modification factor that reflects the capability of the structure to dissipate energy through inelastic behaviour<sup>[31]</sup>. For example,  $R=4$ , for the case of moment resisting steel frames, reflects the large capability of this structure to dissipate

energy through the formation of plastic hinges.

The reduced base shear is then distributed throughout the height of the structure by means of an inverted triangle scheme, which is an approximation for the first mode shape of the structure. The resulting forces are used to design the structure in combination with other forces like dead loads and live loads.

The previous summary shows that the design procedures do appreciate the fact that the real life seismic force demand will possibly exceed the elastic capacity of a structure. However, no specific indication is given about how the structure, designed for a reduced elastic base shear capacity, will perform during a severe earthquake.

It is therefore necessary to develop some kind of damage index to evaluate the performance of a structure under a severe earthquake, and study whether the performance will be acceptable or not. It would also help determine whether the seismic force reduction factors provide a safe structural design.

### **1.3 Types of damage variables and indices**

A damage variable is a quantity that is used for estimating the damage. This variable could be a force, displacement, strength deterioration etc., while a damage index is a value that is equal to zero when there is no damage and is equal to unity when total collapse or failure occurs to the structure. A damage index may include one or more damage variables in its calculation.

There are many types of indices in the literature with different classification schemes; such as:

- **local and global indices**

A local index is related to a single element, which may be a beam, a column or a connection. A local index may involve a single damage parameter, such as maximum deformation or dissipated energy, or two or more parameters. The most widely used damage index that involves several damage parameters is that of Park & Ang<sup>[34]</sup> for reinforced concrete which combines ductility and dissipated energy. A global index on the other hand is related to the whole structure or a substructure and is defined in terms of a global parameter, for example a global ductility factor (based on storey displacements), or softening indices relating the initial fundamental period of the structure to the final one. Global indices can also be defined as the weighted averages of individual member indices.

- **Classification based on the type of analysis**

Most damage indices require some sort of analysis, which could be static or dynamic, elastic or inelastic. A damage index may require no analysis at all and would be based on field measurements like the interstorey drift, and then calculated based on statistical studies or experimentally calibrated models.

- **Structural and economic indices**

A structural index would include structural quantities while an economic index would be based on economic quantities, for example the cost of repair as compared to the cost of replacement, i.e. demolition and rebuilding. An economic damage index is useful when making insurance decisions as it provides a convenient way of defining the appropriate premium. Several studies have been made to correlate structural and economical indices<sup>[19,22,23,40]</sup>.

- **Classification based on the approach used in defining the damage index**

The damage index could be based on one of the following approaches:

- The demand versus capacity approach is based on estimation of some demand on a structure, sub-structure or member, and estimation of the corresponding capacity. Possible choices for the demand and capacity include strength, displacement and energy dissipation. The damage variable in each case maybe based on a single maximum value, a maximum range or some cumulative value. A maximum single value appears to be most appropriate when the damage variable is based on strength or energy dissipation, and a cumulative value when it is based on deformations, which reflect inelastic exertions.
- In the second approach, the calculated degradation of a certain structural variable, like stiffness or energy dissipation, is compared with a predetermined critical value, and is usually expressed as a percentage of the initial value corresponding to the undamaged state.

- **Structural and non-structural elements**

Although the focus of research is often on structural elements, the economic consequence of damage to non-structural elements often exceeds that of structural damage. Therefore, a damage index for non-structural elements is needed. Several researchers have proposed damage indices to non-structural elements, by correlating masonry infills damage to interstorey drift and developing loss curves for non-structural elements based on maximum storey drift and acceleration <sup>[19,22,23]</sup>.

## **1.4 Research objectives**

The objectives of this research are

- To evaluate the performance of moment resisting steel frames, designed according to the NBCC 1995<sup>[31]</sup> under earthquake loading, with respect to the damage to the members.
- To study the possible damage patterns in a structure and the effects of vibration modes and the properties of the ground motions on them.
- To explore the possibility of using the results of a dynamic elastic time history analysis for estimating damage.

## **CHAPTER 2**

### **LITERATURE REVIEW**

#### **2.1 General**

A survey of the literature showed that systematic attempts, to estimate quantitatively the degree of seismic damage that a structure suffers, have been made since about 1980. Of course, the use of well known ductility factors as damage variables was suggested in the late 1950s. However, the incorporation of damage variables into actual damage indices, and, more importantly, the attempt to calibrate these indices against available experimental data, have only been carried out during the past 20 years.

The survey showed as well that research in the field of damage assessment for reinforced concrete structures was more than that for steel structures and that several damage indices were developed for reinforced concrete structures. A good compilation of the research done on reinforced concrete structures could be found in the paper by Kappos<sup>[21]</sup>, where, from the analysis of commonly used indices, the author concluded that the best results were given by the Park et al. index<sup>[36]</sup>.

#### **2.2 Damage in steel structures**

Although several researchers have studied the seismic behaviour of steel members and connections, many of which included cyclic testing, it was mainly focussed on the general behaviour, and the performance was considered adequate if the member or connection could achieve a certain ductility ratio before failure; the cycle to cycle damage was rarely considered. In spite of the widespread damage to the connections of moment resisting steel frames during the Northridge earthquake 1994, the issue of cyclic damage has not been addressed. Achieving a certain ductility ratio is the main concern

for research that is carried out either for the investigation of the repair methods or for finding other alternatives for the commonly used connection detail. This can be attributed in part to the fact that the low toughness of the welding metal, used in the joint detail prior to the Northridge earthquake (known as the pre-Northridge detail), was not able to resist stresses near the yield stress of the base metal, and thus fractured in a brittle manner.

Engelhardt & Sabol (1998)<sup>[16]</sup> studied reinforcing the pre-Northridge detail with cover plates. Chen et al. (1996)<sup>[10]</sup>, Engelhardt et al. (1996)<sup>[18]</sup> and Iwankiw and Carter 1996<sup>[20]</sup> studied the possibility of modifying the connections by creating a weak section away from the joint at which the plastic hinge would form in order to relieve the stress concentration at the joint. This was accomplished by trimming the flanges of the beam, and was named the dogbone connection. Chi et al. (1997)<sup>[12]</sup> examined methods to quantify fracture toughness demand in seismically designed beam-to-column connections through 2-D and 3-D finite element fracture analyses. Engelhardt & Sabol (1997)<sup>[17]</sup> summarised the research done in this area until 1997 in a comprehensive review.

Researchers trying to simulate damage in existing structures do not usually consider the cyclic effect. Song and Ellingwood<sup>[41]</sup> assumed that a brittle fracture would occur in a connection at a certain stress level followed by a degradation in the connection stiffness. They used a degraded  $M-\phi$  model for the connection, assuming sudden fracture in the bottom weld, and studied the behaviour of the structure after fracture and its effect on further damage to other connections. Chi et al.<sup>[11]</sup>, on the other hand, assumed a continuously degraded model to account for weld fracture and correlated the possibility



of damage to certain values of the ductility ratios related to their model of distributed plasticity.

### **2.3 Cyclic damage in steel structures**

Bertero & Popov (1965)<sup>[3]</sup> studied the effect of large alternating stresses on I-beams. They observed that local buckling always occurred in the beam flanges (although not in the first cycle), even though the  $b/t$  ratio was within the limit allowed by the codes for plastic sections. It was observed as well that local buckling caused a large reduction in the number of cycles to failure as compared to the case of simple axial loading of the same metal. For example, in a strain controlled test with a control strain of 2.5%, the beam failed after 16 cycles, while in a uniaxial test the expected number of cycles to failure would be greater than 400.

Krawinkler & Zohrei (1983)<sup>[26]</sup> studied two possible types of failure, one due to local buckling of flanges and the other due to weld fracture of the connection. Two sets of experiments were carried out on cantilever I-beams for each type of failure. For the case of failure by local buckling, degradation in the strength and stiffness of the beams in the first few cycles continued at a constant rate until a certain value was reached after which the hysteresis loops stabilized. This was followed by another rapid degradation and the eventual failure in a few cycles. They also represented these three stages of damage growth by 3 lines on a semi log plot. They concluded as well that the degradation per cycle in the first two stages could be represented by the Coffin-Manson law<sup>[42]</sup>

$$\Delta d = A(\Delta \delta_p)^u \quad (2.1),$$

and that the parameter “a” was more stable than “A” which should be considered as a variable. For the case of failure by weld fracture, they observed that little or no deterioration occurred during the propagation of the crack until the crack length reached a certain critical value (a crack length of 0.5 of the flange thickness was considered a critical value), after which very rapid deterioration occurred and failure was almost sudden. They developed a formula for the calculation of damage and discovered that it depended in a large part on the initial crack size which showed very large scatter

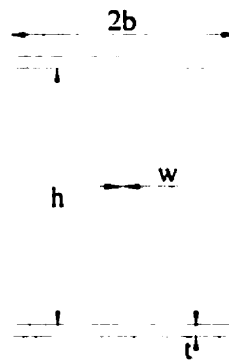


Figure 2.1 Profile of an I section showing notations of the different dimensions

Castiglioni & Di Palma (1989)<sup>[9]</sup> conducted several tests on different beams with different flange slenderness ( $b/t$ ) and web slenderness ( $h/w$ ) ratios. They confirmed the previous findings of Krawinkler & Zohrei<sup>[26]</sup> regarding the local buckling failure mode and concluded as well that the rate of deterioration did not depend solely on the flange’s width to thickness ratio  $b/t$ ; and that the web’s height to thickness ratio,  $h/w$ , had an effect on the rate of deterioration as well.

Calado & Azevedo (1989)<sup>[5]</sup>, after conducting several tests on cantilever beams and bracings, concluded that damage was sensitive to the  $b/t$  ratio as well as the steel grade.

They also concluded that a linear damage rule (Miner's rule<sup>[29]</sup>) could be used. A failure criterion was proposed as being,

$$\eta_i = A_i / A_{yi} < \gamma, \quad (2.2)$$

where  $A_i$  represented the hysteretic energy dissipated in the  $i$ th cycle and  $A_{yi}$  the energy that the element would dissipate if it had an elasto-plastic behavior. A value of  $\gamma=0.5$  was suggested for failure.

Ballio & Castiglioni (1994)<sup>[11]</sup> investigated the possibility of developing a damage model based on tip deflection of cantilever beams and concluded that the use of Miner's<sup>[29]</sup> rule was adequate for the cumulative damage of steel members.

Daali & Korol (1995)<sup>[14]</sup>, based on the work of Krawinkler and Zohrie<sup>[26]</sup>, suggested a model for the calculation of strength deterioration per reversal due to local buckling; a formula,

$$d = a \Sigma (\theta_{pi})^b \quad (2.3)$$

was suggested. Based on experimental results<sup>[8,14,26]</sup> and the suggestions of Krawinkler, the exponent "b" was considered constant and given a value of 1.65, while "a" was considered a variable and was found to be dependant on an equivalent slenderness factor  $\alpha_e$  that combines the  $b/t$ ,  $h/w$  and  $l/r_y$  ratios in one value, through the following formula:

$$a = -1.98 + 14.3 \alpha_e \quad (2.4)$$

where,  $\alpha_e = \frac{\alpha_f \alpha_w \alpha_t}{30072} \quad (2.5)$

and,

$$\alpha_f = \frac{b}{t} \sqrt{\frac{\sigma_y}{300}} \quad (2.6), \quad \alpha_w = \frac{h}{w} \sqrt{\frac{\sigma_y}{300}} \quad (2.7), \quad \alpha_t = \frac{l}{r_y} \sqrt{\frac{\sigma_y}{300}} \quad (2.8); \quad "l"$$

being the unsupported span length and  $r_y$  the radius of gyration about the weak axis.

Daali & Korol (1996)<sup>[15]</sup> suggested two damage models; one based on the Park & Ang model<sup>[34]</sup>,

$$D = \frac{\mu_{max}}{\mu_m} + \beta_2 \frac{\sum(\mu_i - 1)}{\mu_m} \quad (2.9)$$

and another suggested by them,

$$D = \frac{\mu_{max}}{\mu_m} + \beta_1 \sum \left( \frac{\mu_i - 1}{\mu_m - 1} \right)^{1.15} \quad (2.10)$$

where,  $\mu_i$  is the ductility measured from zero load intercept and experienced in the  $i$ th reversal,  $\mu_m$  is the maximum ductility under monotonic loading,  $\mu_{max}$  is the maximum amount of ductility experienced during the loading history, and  $\beta_1, \beta_2$  are calibration factors. These models combined the maximum damage during the loading history and the cyclic deterioration; and were based on the assumption that a drop of 15 to 20% in strength constituted failure. A formula for the calculation of  $\mu_m$ , using tests done by them and others<sup>[24,27,28]</sup> was suggested based on the equivalent slenderness factor  $\alpha_e$ . The value of  $\beta$  was calibrated for different  $b/t$  ratio based on test results by them and others<sup>[9,24,25]</sup>.

Ballio & castiglioni (1995)<sup>[2]</sup> presented a unified approach for damage assessment of steel structures that combined low and high cycle fatigue. This approach used the Wöhler<sup>[43]</sup> (S-N) curves (their research was mainly focussed on the curves proposed by the

Eurocode 3<sup>[13]</sup>) for the calculation of both low and high cycle fatigue. The low cycle fatigue was incorporated into this method through an equivalent stress,

$$(\Delta\sigma^* = \Delta\epsilon E) \quad (2.11)$$

and they concluded that by using this method the Wöhler<sup>[43]</sup> (S-N) curves proposed by the Eurocode 3<sup>[13]</sup> could be used for the prediction of low cycle fatigue failure.

Calado & Castiglioni (1996)<sup>[4]</sup> continued to investigate the same unified approach suggested by Ballio & Castiglioni<sup>[2]</sup>, by testing several connection details. They reached the same conclusion that the Wöhler<sup>[43]</sup> (S-N) lines proposed by the Eurocode 3<sup>[13]</sup> can be used for the prediction of connection failure by low cycle fatigue.

## **2.4 Comments on the cyclic damage models**

### **2.4.1 The Daali-Korol strength deterioration model<sup>[14]</sup>**

This model, although was based on few experimental results, has a very good base. The model takes all the slenderness ratios into account in the calculation of the degradation, although it is the opinion of the author that the lateral slenderness should not be included in the model. The reason for this is that it is a member property and not a section property, and does not have a significant effect on the cyclic damage as concluded by Calado & Azevedo<sup>[5]</sup>. The model is based on the plastic rotation as a response parameter which is an available output in many analysis programs and does not restrict the use of the model to the experimental conditions. A shortcoming of the model is that it cannot be used to determine the damage in very compact sections, because for a value of  $\alpha_c$  less than 0.138, the value of “a” would be negative which is physically impossible and means that this formula has limited application scope.

## 2.4.2 The Daali-Korol damage models<sup>[15]</sup>

The two damage calculation models, one based on the Park & Ang<sup>[34]</sup> model and the other suggested by them, assume failure when the section capacity is reduced by 15-20%. Both models combine the damage due to maximum response and the cyclic damage, a concept that is more appropriate for reinforced concrete members in which maximum response induces irreversible damage due to yielding of steel and crushing of concrete. On the other hand, a steel member, subjected to a relatively high response cycle, will be able to withstand lower response cycles without much loss in strength, and, the main effect would be due to the cyclic damage which would be included in the cyclic damage calculations. In the case of steel connections, however, the maximum response could cause an irreversible damage and the use of such combination would be appropriate.

## 2.4.3 The Ballio-Castiglioni<sup>[21]</sup> approach

This approach presents a unique and easy formula; however, it is based on tests conducted on cantilever beams in which the tip deflection was the controlled and measured parameter; this limits the use of this model. This approach calculates the equivalent stress by the formula.

$$E\Delta\varepsilon = (\Delta v / v_y) (F_y L / 4S_x) \quad (2.12)$$

where, E = Elastic modulus,  $\Delta\varepsilon$  = strain range,  $\Delta v$  = tip deflection range,  $v_y$  = tip deflection at yield,  $F_y$  = force causing first yield, L = cantilever length and  $S_x$  = section modulus

It is known that the displacement and strain ductility ratios do not remain proportional in the inelastic curve, and, thus, it would not be possible to replace the displacement ductility ratio in the formula with another ductility ratio which would be more

appropriate for use in a more complex structure without modifications or calibrations to the model. In the case of a beam in a multi storey frame, it would be very complicated to estimate the displacement ductility ratio, and the curvature ductility ratio is normally used.

In an attempt to incorporate these models in an example study<sup>[7]</sup>, the damage in columns of low-rise steel frames was estimated by considering the deflections of the columns in the first floor as a reference for the displacement ductility ratio.

## **CHAPTER 3**

### **METHODOLOGY DESCRIPTION**

#### **3.1 General**

In designing an earthquake resistant building, the standard method in the industry and that provided by the current codes of practice, is to perform a static analysis using pseudo-static seismic loads, and then the structure is designed according to the limit state design concept. A dynamic analysis for the performance evaluation of the structure, whether elastic or inelastic, is only performed for very special structures.

In order to accomplish the objectives of the research, elastic and inelastic analyses of a building, designed and detailed according to the current codes of practice, are conducted using the special purpose computer program DRAIN-2DX<sup>[38]</sup>. Five scaled ground acceleration histories from real earthquakes are applied as input.

#### **3.2 Description of the building**

##### **3.2.1 General description of the building**

The building, subject of this study, is a multi-storey steel office building assumed to be located in Vancouver, BC, Canada. The building is square in plan. The length of each side is 40 m. The columns are arranged in a regular grid spaced at 8 m in both directions. The building is 10 storeys high. The height of the first storey is 5 m and the height of all other storeys is 4 m; thus giving a total height of 41 m. Figure 3.1 shows the plan of the building.



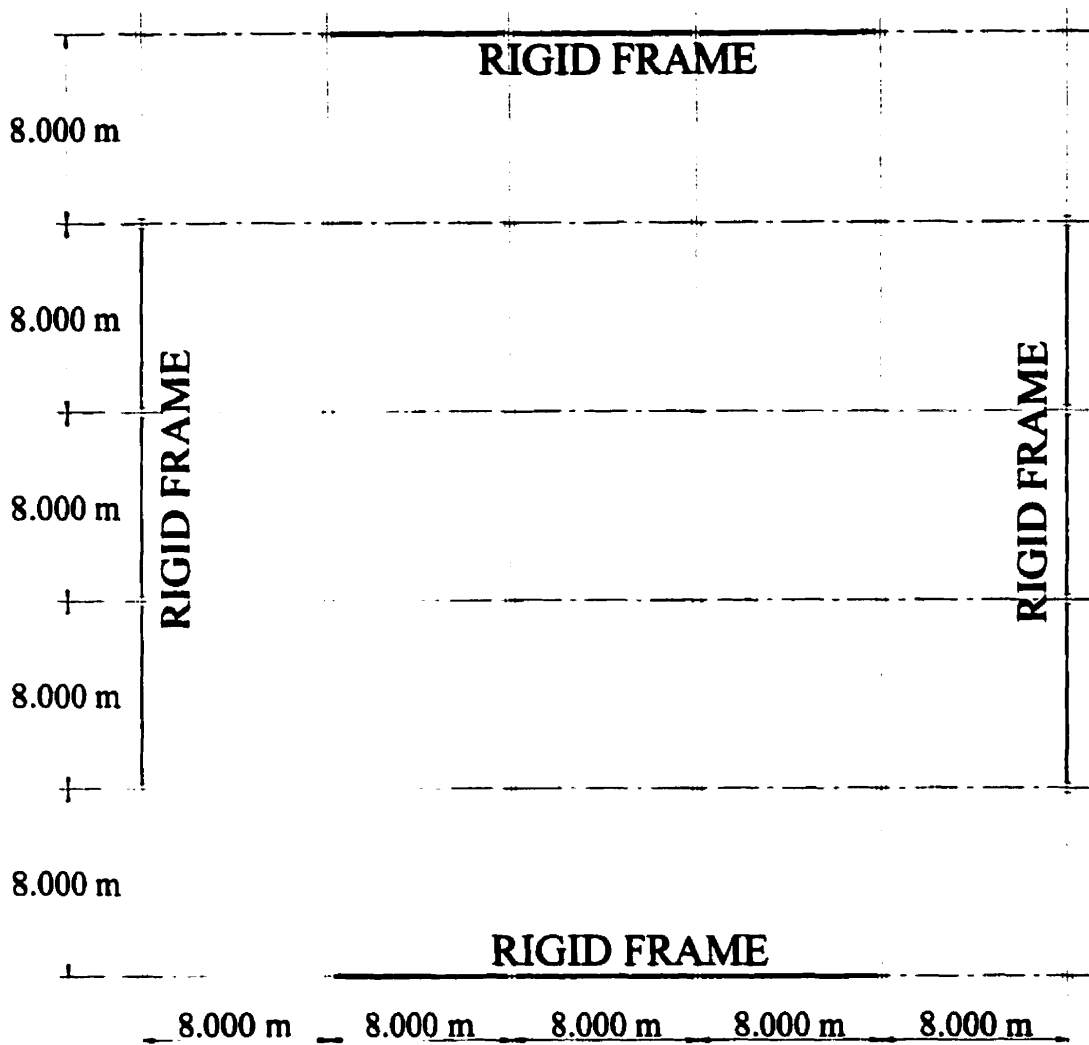


Figure 3.1 Plan of the building

### 3.2.2 Structural system, loading and design of the building

The lateral forces in the building were assumed to be resisted by 4 multi-storey rigid moment resisting steel frames, one on each side of the perimeter of the building. Frames were assumed to be fixed at the ground level. Only the inner 3 bays of each side form the moment resisting frame. The rest of the beams and columns resist only the gravity loads.

Figure 3.2 shows an elevation of a typical moment resisting frame.

The loading on the frame was determined according to the NBCC 1995<sup>[31]</sup>. The climatic information for the Vancouver area, supplied in appendix C of the Code, was used to determine the design snow, the equivalent static wind and equivalent static earthquake loads. The design dead gravity load was estimated using the handbook of steel construction<sup>[6]</sup> and the design live load was determined according to Table 4.1.6.3 of the NBCC<sup>[31]</sup>. The total elastic lateral force on the frame, due to seismic load effect, was found to be 15.92 MN.

The building was designed using the limit states design method as given by the CAN/CSA-S16.1-94<sup>[32]</sup>, thus applying the provisions and detailing requirements of moment resisting rigid frames in zones with high seismic activity. A yield stress of 300 MPa was assumed for the steel in the design.

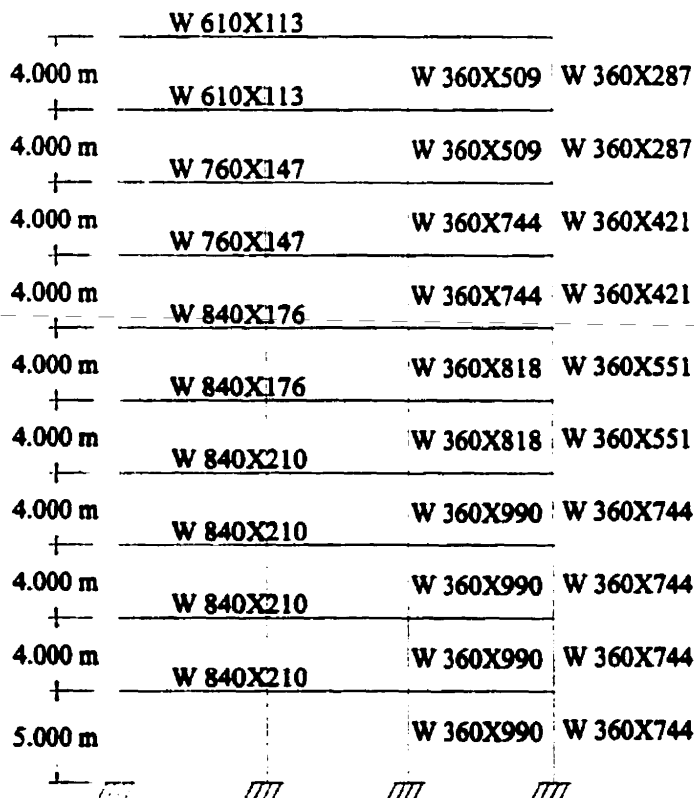


Figure 3.2 Elevation of a typical moment resisting frame

It should be mentioned that the governing factor in the design of the frame has been found to be the maximum interstorey drift limit for the seismic forces, as set by clause 4.1.9.3 of the NBCC<sup>[31]</sup>.

### **3.3 The finite element method**

The first step in a finite element analysis is to discretize the structure into a set of structural elements. Each finite element is interconnected with the adjacent elements through nodal points. Acting at each nodal point are nodal forces and displacements. For each element, a standard set of simultaneous equations can be developed to relate these physical quantities. Assembling these elements to form the whole structure is equivalent, physically, to superimposing these element equations mathematically. The result is a large set of simultaneous equations which are suited for solution by computer. Applying the loading and boundary conditions for the structural problem, the assembled set of equations can be solved and the unknown parameters found. Substitution of these values back to each element formulation provides the displacement and stress distribution within each element.

In a static analysis, the matrix equation relating the nodal displacement and the loads may be expressed as:

$$\mathbf{K U} = \mathbf{P} \quad (3.1)$$

where,

**K**= structural stiffness matrix

**U**= displacement vector at the nodes

**P**= applied load vector at the nodes

In a dynamic analysis, the time domain becomes a part of the problem; the inertial and damping forces become effective. The matrix equation relating the nodal displacement, velocity, acceleration and the loads may be expressed as:

$$\mathbf{M}\ddot{\mathbf{U}} + \mathbf{C}\dot{\mathbf{U}} + \mathbf{K}\mathbf{U} = \mathbf{P}(t) \quad (3.2)$$

where,

$\mathbf{M}$ = structural mass matrix

$\ddot{\mathbf{U}}$  = acceleration vector at nodes

$\mathbf{C}$ = damping matrix

$\dot{\mathbf{U}}$  =Velocity vector at nodes

$\mathbf{P}(t)$ = applied load vector at the nodes as a function of time

In the case of earthquake induced ground acceleration history, the equation is expressed as:

$$\mathbf{M}\ddot{\mathbf{U}} + \mathbf{C}\dot{\mathbf{U}} + \mathbf{K}\mathbf{U} = -\mathbf{M}\mathbf{i}\ddot{u}_g(t) \quad (3.3)$$

Where,

$\mathbf{i}$ = unit vector

$\ddot{u}_g(t)$ = ground acceleration time history

In the dynamic analysis, it would be difficult to find an analytical solution applicable for the complete time history for the set of equations in the case of non-linearity, whether it is due to geometry or material, or in the case of a complex load function. The time history is, therefore, divided into small time increments and the set of equations is solved for each time increment and the resulting displacements, velocities and accelerations are used as initial conditions for the next step.

In the case of inelastic analysis, whether the problem is static or dynamic, the computer program calculates the forces and displacements in the structure using the current stiffness matrix. Stiffness matrices of the elements, that exceeded the elastic limit, are modified according to the current tangent stiffness of the material's stiffness curve and the global stiffness matrix is recalculated. This procedure is repeated through an iterative process until the equilibrium is established.

### **3.4 The DRAIN-2DX program**

DRAIN-2DX<sup>[38]</sup> is an improved version of, DRAIN-2D (Dynamic Response Analysis of INelastic 2-Dimensional structures), a special purpose computer program for static and dynamic analysis of plane structures. It performs nonlinear static and dynamic analyses. For dynamic analysis, it considers ground accelerations (all supports moving in phase), ground displacements (supports may move out of phase), imposed dynamic loads (e.g., wind), and specified initial velocities (e.g., impulse loading). Static and dynamic loads can be applied in any sequence<sup>[38]</sup>.

The program is written in FORTRAN-77, and consists of a "base" program which manages the data and controls the analysis, plus a set of subroutines for each element type which control the element details. Information is transferred between the base program and the elements through an interface that is the same for all element types.

The input files are in a formatted form containing several blocks of the input data. Model data, such as the geometry and constraints, element information, data controlling the analysis parameter, such as the maximum time step for time integration and data controlling the analysis segments and loads are specified in different blocks<sup>[39]</sup>. The element library contains Type01, inelastic truss bar; Type02, simple inelastic beam-

column with a lumped plasticity model; Type04, simple inelastic connection, which allows for translational as well as rotational force transfer; Type06, elastic panel element, which allow vertical, horizontal extensional and flexural stiffness to be input; Type09, inelastic link element, that can act in compression/tension with initial gap or axial force; and Type15, "fiber" beam-column element for steel and reinforced concrete members. The elements include capabilities for event and internal energy calculations. Inelastic static analysis can be carried out, with the ability to trace sequences of hinge formation and to continue into the post-failure range.

The step-by-step integration scheme for dynamic analysis can be done using a fixed time step or a variable time step which would be varied during the analysis, on the basis of input error tolerances. Energy balance computations are performed, identifying the static work, the energy absorbed by viscous damping, the kinetic energy, and the input energy. Mode shapes and periods can be calculated at any state.

### **3.5 Modelling**

#### **3.5.1 Basic modelling assumptions**

The basic assumption in the modelling of the beam is that each component of the ground motion is resisted independently by the two frames parallel to the direction of motion, and that both frames resist this force equally. Based on this assumption, an analysis of a single two-dimensional frame was carried out assuming that it will carry half the inertia force of the structure.

The frame was discretized with the same type of element for both columns and beams. The connections were assumed rigid and the effect of the panel zones was neglected and was not included in the model.

## 3.5.2 Element modelling

### 3.5.2.1 General

The element type 02 was used for all the beams and columns. Element type 02, as shown in Figure 3.3, is a simple inelastic element for modelling beams and beam-columns of steel and reinforced concrete type. The element consists of an elastic beam, two rigid plastic hinges and an optional rigid end zone<sup>[37]</sup>. The P- $\delta$  effect was included in the analysis of the elements.

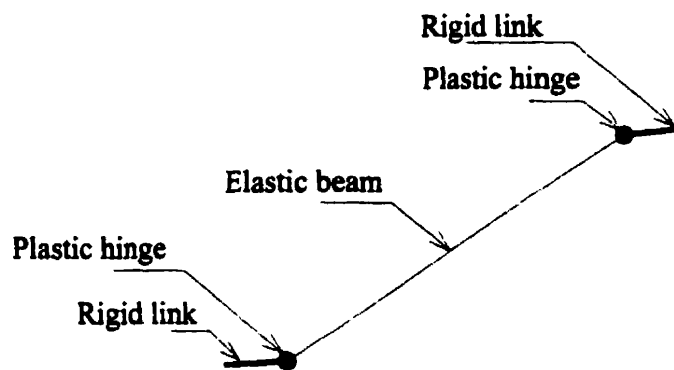


Figure 3.3: Element type 02

### 3.5.2.2 Yield surface

Yielding is assumed to take place only in the plastic hinges. The hinge yield moments can be specified different at the two element ends, and for the positive and negative bending<sup>[37]</sup>; however, it was considered the same for all. The effect of axial force on bending strength is taken into account by specifying a P-M yield surface which was assumed to be a single line connecting yield moment and yield axial force, as shown in Figure 3.4 for the case of inelastic analysis.

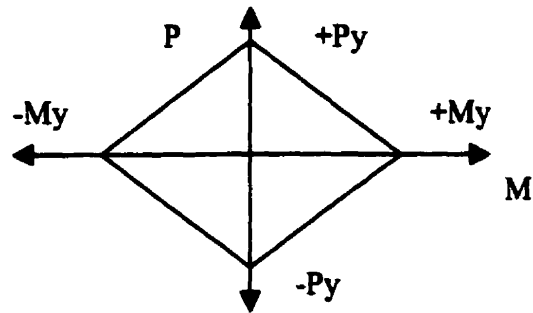


Figure 3.4 Yield surface of element type 02

### 3.5.2.3 Strain hardening

Strain hardening in bending is modelled in DRAIN-2DX assuming that the element consists of elastic and inelastic components in parallel as shown in Figure 3.5. Plastic hinges that yield at constant moment form the inelastic component. The moments in the elastic component continue to increase. The combined effect of the two result in the strain-hardening response at the post yield state<sup>[37]</sup>.

Three inelastic dynamic analyses were performed using different values of the strain hardening ratios (2.5%, 5% and 10%) for two different ground acceleration records, one creating a response dominated by the first mode and the other having significant effects from higher mode participation. Since the effect of strain hardening ratio was found not to be very high for both ground acceleration records, a typical value of 5%<sup>[30,41]</sup> strain hardening was used for all other analyses.

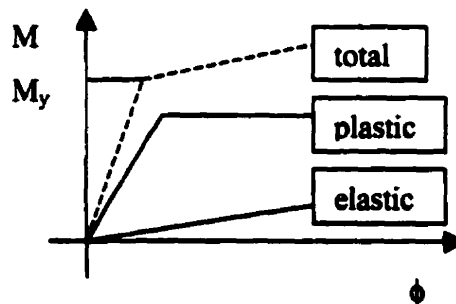


Figure 3.5 Strain hardening model



### 3.5.3 Masses and loads

For the calculation of the masses and loads, the full design dead load was applied plus 25% of the design live load. The frame was assumed to carry half of the mass of the building lumped at the nodes. For the calculation of the initial static loading only the strip adjacent to the frame was considered and the other portions were assumed to be carried by the gravity columns.

### 3.5.4 Damping

Viscous damping matrix is defined in DRAIN-2DX as proportional to the stiffness and nodal mass matrices (Rayleigh's damping) through the formula  $C = \alpha M + \beta K$ . In effect, mass dependant damping introduces transitional and rotational dampers at each node, with damping coefficients  $\alpha M$ . The damping matrix  $\beta K$  remains constant, and is set to that calculated from the initial stiffness value  $K_0$ <sup>[39]</sup>.

The values of  $\alpha$  and  $\beta$  were chosen to induce a damping equal to 2% of the critical damping at the first two modes.

### 3.5.5 Natural frequencies and periods

An analysis was carried out to determine the natural frequencies, periods and the corresponding damping ratios of the structure. Table 3.1 summarises the results of this analysis.

Table 3.1 The first five natural frequencies and damping ratios of the structure

Mode	Natural period in seconds	Natural frequency in Hz	Percentage of critical damping
1	2.793	0.358	2
2	1.0479	0.9543	2
3	0.60696	1.6476	2.845
4	0.40829	2.449	3.967
5	0.29539	3.385	5.338

### **3.6 Analysis**

The analysis is carried out in two steps, first a static analysis is performed for the gravity loads, followed by a time step dynamic analysis using the results from the previous step as initial conditions. The dynamic analysis was carried out using a fixed time step scheme. A time step of 0.005 seconds was used for the elastic analysis and a time step of 0.0025 seconds was used for the inelastic analysis. The analyses were carried out for a duration of 50 seconds.

The P- $\Delta$  effect was considered in the static and dynamic analyses. Appendix C contains sample input files for elastic and inelastic analyses.

### **3.7 Earthquake records**

Five ground acceleration histories from real earthquake events were used in this study: two records from the 1989 Loma prieta earthquake, one from the 1994 Northridge earthquake, one from the 1933 Long Beach earthquake and one from the 1984 Morgan Hill earthquake.

An elastic analysis was performed for each of the earthquakes and the maximum base shear was calculated. The record was then scaled so that the maximum base shear would be equal to the elastic lateral seismic force,  $V_e$ , calculated according to the NBCC<sup>[31]</sup> as mentioned in section 3.2.2.

Table 3.2 summarises the basic data about the records; Figures A.1 to A.5 show the unscaled acceleration time histories of the records.

A response spectra for each record was generated using a FORTRAN program given in Appendix B. Figures A.6 to A.10 show the response spectra of the unscaled records.

It is noticed from the response spectra that records 1, 2 and 4 have sharp peaks near the 1<sup>st</sup> natural frequency of the structure followed by a drop near the 2<sup>nd</sup> and 3<sup>rd</sup> frequencies.

For records 1 and 4, the values are very small near the 2<sup>nd</sup> and 3<sup>rd</sup> frequencies, while record 2 shows a considerable value near these frequencies.

Records 3 and 5, on the other hand, have more uniform shape near the first 3 modes, with record 3 more uniform than record 5.

**Table 3.2 Summary of ground acceleration data**

No.	Record	Earth-quake Mag.	Distance from epicentre in km	Scaling factor	Sampling rate Rec./sec.	Duration Sec.
1	1989 Loma Prieta Palo Alto VA – Bldg. 1 basement	7.1	47	1.607	200	40.955
2	1989 Loma Prieta Palo Alto VA – Bldg. 1 roof	7.1	47	1.316	200	39.58
3	1994 Northridge 4334 Katherine RD.	6.7	13.3	1.873	50	38.56
4	1933 Long Beach, Vernon CMD Bldg.	6.5	1.2	1.843	100	39.08
5	Morgan Hill, 1984, Gilroy	6.2	15	1.194	50	59.98

### **3.8 Analysis results and damage calculations**

#### **3.8.1 General**

The analysis results are obtained at each step and are written to a scratch file. At the end of the analysis history, results for all steps are read from the scratch file and reorganised item-by-item.

The DRAIN-2DX program has the option to calculate generalised displacements; this option was used to calculate the interstorey drift of all the storeys.

The roof displacement, the base shear and the interstorey drift for all the storeys were the output request for elastic and inelastic analyses. For the inelastic analysis, the element's forces and plastic hinge rotations were extracted as well.

The roof displacement is presented as a normalised value,  $u_{\text{roof}}/H$ , where “ $u_{\text{roof}}$ ” is the roof displacement and “ $H$ ” is the total height of the building.

### 3.8.2 Damage calculations

The following strength deterioration formula from a paper by Daali & Korol<sup>[14]</sup> was used in this study:

$$d = a \sum (\theta_{pi})^{1.65} \quad (3.4)$$

where,

$d$  = the strength deterioration ratio

$a$  = section variable

$\theta_{pi}$  = the plastic hinge rotation range

The values of “ $a$ ” for the beams were calculated based on the formula explained in Section 2.3 and assuming an unbraced length of 2.0 m in the calculation of the lateral slenderness. The values of “ $a$ ” are presented in Table 3.3. In the case of columns, the formula gave negative values, which means that the formula is not suitable for compact column sections. However a uniform value of ( $a=1$ ) was given to all columns in order to give a qualitative indication of the possible damage in the columns.

**Table 3.3 Values of “a” for beams**

<b>Beam</b>	<b>a</b>
<b>W 840 X 210</b>	<b>2.7876</b>
<b>W 840 X 176</b>	<b>5.14</b>
<b>W 760 X 147</b>	<b>5.609</b>
<b>W 610 X 113</b>	<b>4.694</b>

The plastic hinge rotation history was then extracted from the output file for all beams and columns at both ends. The full cycles were separated using a FORTRAN subroutine that uses range pair counting method and damage was calculated using the Daali-Korol formula. Appendix D contains a listing of the subroutine used for separating the complete cycles.

Two methods were used to calculate the overall damage to the building: one by simply taking the average of the damage at all beam ends, the other by taking a weighted average of the damage at the beams ends. The weighting factor was assumed to depend on the magnitude of the damage as suggested by Park et al.<sup>[35]</sup> using the following formula,

$$D_{overall} = \frac{\sum_{i=1}^n d_i^2}{\sum_{i=1}^n d_i} \quad (3.5)$$

## CHAPTER 4

### RESULTS AND DISCUSSION

#### 4.1 Introduction

Elastic and inelastic analyses of the building under study were performed using five ground acceleration records from real earthquakes; their characteristics have been given in Table 3.2. Three inelastic analyses were carried out for each of records 1 and 5, using three different strain hardening ratios of 2.5%, 5% and 10%. The rest of the analyses were carried out for a typical strain hardening ratio of 5%. Interstorey drift ratios, base shears and normalized roof displacements were extracted from elastic and inelastic analyses. Damage calculations were carried out for inelastic analyses according to the strength deterioration formula as explained in Sections 3.8.2 and 2.3.

#### 4.2 Description of behavior

Table A.2 gives a summary of the results obtained from the inelastic analyses.

Table A.2 Summary of the analysis results

Record	Earthquake *	Strain Hardening ratio	Total averaged strength deterioration	Total weighted strength deterioration	Maximum inelastic base shear (MN)
1	Loma Prieta #1	2.5%	1.97%	2.59%	5.86
1	Loma Prieta #1	5%	1.99%	2.59%	5.88
1	Loma Prieta #1	10%	1.89%	2.47%	5.58
2	Loma Prieta #2	5%	2.50%	3.05%	6.25
3	North ridge	5%	0.74%	1.67%	5.52
4	Long beach	5%	1.20%	1.80%	5.18
5	Morgan Hill	2.5%	3.19%	6.51%	5.05
5	Morgan Hill	5%	2.81%	5.89%	5.10
5	Morgan Hill	10%	2.56%	5.66%	5.27

\* Scaled to provide a maximum elastic base shear demand of 15.92 MN.

A detailed description of the behavior and observations of the building under different earthquake records is presented in the following sections.

#### **4.2.1 Record # 1 (Loma Prieta record # 1)**

An elastic analysis and three inelastic analyses using three different strain hardening ratios (2.5%, 5% and 10%) were performed for this record. The behavior of the frame in the inelastic analyses was according to the strong-column weak-beam mechanism. Plastic hinges formed at the ends of almost all beams. No yielding occurred in the columns except at the base of the frame. The general behavior and damage patterns were the same for all strain hardening ratios.

Figures A.11, A.12 and A.13 show the values of the strength deterioration in percent as compared to the original capacity for strain hardening ratios of 2.5%, 5% and 10% respectively. The average strength deterioration in the beams, for the three strain hardening cases, has been calculated to be 1.97%, 1.99% and 1.89%. The corresponding weighted damage were 2.59%, 2.59% and 2.47%. The total damage was not affected much by the strain hardening ratio; the change from 2.5% strain hardening to 5% strain hardening increased the averaged total damage by 1.1%, while the weighted average damage is almost the same. The change from 5% strain hardening to 10% strain hardening decreased both the average damage and the weighted total damage by about 5%.

The damage is fairly uniform over the frame height, and is almost symmetrical about the vertical axis in the first eight storeys, with the maximum damage at the edges of the frame. The damage patterns for the three strain hardening ratios were similar, regular with a small increase in the beams of the first four storeys followed by a sharp increase in

the 5<sup>th</sup> storey, then a small decrease in the 6<sup>th</sup> storey. This is followed by a large decrease in the 7<sup>th</sup> and 9<sup>th</sup> storeys and a moderate decrease in the 8<sup>th</sup> and 10<sup>th</sup> storeys, while the damage became almost zero in the 10<sup>th</sup> storey. The values of the damage in columns (calculated with an arbitrary value of  $a=1$  in the Daali-Korol formula) are very small and damage can be considered as negligible.

The roof displacement histories, as shown in Figures A.14 and A.15, are irregular and show an increasing trend for the first 10 seconds followed by a smooth harmonic oscillation in the first natural frequency of the structure. The amplitude and the mean value, which the curve is oscillating about, are fluctuating with a tendency for decrease in the amplitude; this is more apparent in the elastic response. As shown in Figure A.14, the elastic response is larger than the inelastic response. There is an apparent phase shift between the elastic and inelastic analyses. Three inelastic analyses, shown in Figure A.15, are completely in phase. However, the value at which the oscillation takes place about becomes different for the three values after 14 seconds; but the ranges of fluctuation seem to be the same.

The envelopes of the maximum interstorey drift ratio, as shown in Figure A.16 are fairly uniform over the height. The elastic interstorey drifts are higher than the inelastic ones, at some points twice as much. The envelope is having only a sharp increase from the 1<sup>st</sup> to the 2<sup>nd</sup> storey and a sharp decrease from the 9<sup>th</sup> to the 10<sup>th</sup> storey. The elastic and inelastic storey drifts do not seem to have any correlation; the elastic storey drift may decrease from one storey to the next while the inelastic increases and vice versa.

The increase in the strain hardening ratio causes, although not always, a decrease in the maximum interstorey drift ratio. An increase in the strain hardening ratio from 2.5% to



5% caused an average change in the maximum interstorey drift of 1.86% and a maximum value of change of 4.93%; while an increase in the strain hardening ratio from 5% to 10% caused an average change in the maximum interstorey drift of 3.32% with a maximum change of 6.99%.

The change in the strain hardening ratio did not have much effect on the maximum inelastic base shear. An increase in the strain hardening ratio from 2.5% to 5% caused an increase in the maximum base shear by 0.33%; while an increase in the strain hardening ratio from 5% to 10% caused a decrease in the maximum base shear by 1.99%.

#### **4.2.2 Record # 2 (Loma Prieta record # 2)**

The structural behavior for this earthquake record is similar to that of the previous record. The inelastic frame response showed strong-column weak-beam mechanism, yielding only at the beam ends and in the columns at the base. Figure A.17 shows the values of strength deterioration in percent at the beam ends. The damage pattern is the same as in the previous record for the first seven storeys. The damage is almost uniform in the first eight storeys; each storey having the maximum values at the extreme edges and almost symmetrical about the vertical axis. The damage increases from the 1<sup>st</sup> to 2<sup>nd</sup> storey, followed by an almost uniform damage in the 2<sup>nd</sup>, 3<sup>rd</sup> and 4<sup>th</sup> storeys. A large increase in the 5<sup>th</sup> storey is apparent, followed by a decrease in the 6<sup>th</sup> storey and a larger decrease in the 7<sup>th</sup> storey. The damage index shows an increase in the 8<sup>th</sup> storey and a sharper increase in the 9<sup>th</sup> storey, in which the damage in the storey was no longer symmetrical about the vertical axis. Finally, a sharp decrease in the damage is evident at the 10<sup>th</sup> storey.

The roof displacements, as shown in Figure A.18, are similar to those of the previous record; random vibration in the first 10 seconds, followed by a relatively regular response with a frequency of oscillation approximately equal to the first natural frequency of the structure. Once again, the elastic response is larger than the inelastic one. In this record, however, the effect of higher modes is apparent and the oscillation is not smooth in the period between 10 and 20 seconds; this effect is more apparent in the inelastic roof displacement.

The interstorey drift envelope, as shown in Figure A.19, is similar to that of the previous record; an increase in the 2<sup>nd</sup> storey followed by a uniform distribution until the 8<sup>th</sup> storey. The envelope afterwards shows a sharp increase in the 9<sup>th</sup> storey for the elastic and inelastic envelopes, followed by a decrease in the 10<sup>th</sup> storey.

Like in the record # 1, the interstorey drift ratio for the elastic analysis is larger than the inelastic one.

#### **4.2.3 Record # 3 (The Northridge record)**

The frame behavior for this record was different from the previous two. The frame behaved in the inelastic analysis according to the weak-beam strong-column mechanism, yielding occurring at the beam ends and the columns at the base. Additionally, yielding also occurred at the lower ends of the two middle columns in the 9<sup>th</sup> storey. However, the damage values for all of the columns remained very small.

Figure A.20 shows the values of strength deterioration in percent at the beam ends. The damage in all storeys is uniform and symmetrical about the vertical axis. The damage in the 1<sup>st</sup> storey is much smaller as compared to the previous records. The damage value

decreases till the 6<sup>th</sup> storey, then increases in the 7<sup>th</sup> and 8<sup>th</sup> storeys. In the 9<sup>th</sup> storey, a very sharp increase occurs followed by a large decrease in the 10<sup>th</sup> storey.

The roof displacement, as shown in Figure A.21, shows a random pattern for the first 10 seconds for the elastic and inelastic analyses, followed by a relatively regular oscillation.

The inelastic roof displacement, after about 4 seconds, shows that a permanent displacement takes place and continues throughout the rest of the history, and the oscillation takes place about it.

The maximum interstorey drift ratio envelopes for the elastic and inelastic analyses, as shown in Figure A.22, show an increase in the 2<sup>nd</sup> storey followed by a decrease in the 3<sup>rd</sup> storey; then remaining constant until the 6<sup>th</sup> storey. Two sharp increases occur in the elastic envelope in the 7<sup>th</sup> and 9<sup>th</sup> storeys followed by a decrease in the 8<sup>th</sup> and 10<sup>th</sup> storeys.

#### **4.2.4 Record # 4 (The Long Beach record)**

The behavior of the frame under this record was similar to the first two records. For the inelastic analysis, the behavior was according to the weak-beam strong-column mechanism, yielding occurring at the beam ends and at the base columns only.

The damage pattern, as shown Figure A.23, is similar to that of record # 1. The damage is fairly uniform over the height, and is almost symmetrical about the vertical axis in the first six storeys, with the maximum damage at the extreme ends of the frame. The damage pattern is regular with a small increase in the beams of the first four storeys followed by a larger increase in the 5<sup>th</sup> storey, then a small decrease in the 6<sup>th</sup> storey. This is followed by a large decrease in the 7<sup>th</sup> and 8<sup>th</sup> storeys; the damage in the last three storeys becomes almost zero.

The roof displacements for the elastic and inelastic analyses, as shown in Figure A.24, show an irregular pattern in the first 5 seconds followed by a clear smooth harmonic decaying oscillation at the first natural frequency of the structure. The elastic response is larger than the inelastic response; both are totally in phase. The inelastic response, after the first cycle, shows a large drop and oscillates about a shifted base line.

The interstorey drift ratio envelopes for both the elastic and inelastic analyses, as shown in Figure A.25, show an increase in the 2<sup>nd</sup> storey. The elastic envelope remains relatively constant up to the 9<sup>th</sup> storey, then a large decrease occurs at the 10<sup>th</sup> storey, while the inelastic envelope shows a continuous and almost regular decrease along the height of the frame.

#### **4.2.5 Record # 5 (The Morgan Hill record)**

Three inelastic analyses using three values of strain hardening ratios, 2.5%, 5% and 10%, and an elastic analysis were performed for this record. The inelastic behavior was according to the strong-column weak-beam mechanism. Plastic hinges formed at all the beam ends and yielding occurred at the base columns only. For the case of 2.5% and 5% strain hardening, yielding occurred at three columns and the fourth exterior column remained elastic, while in the case of 10% strain hardening, yielding occurred at the two exterior columns while the two interior columns remained elastic.

The damage patterns, as shown in Figures A.26, A.27 and A.28, for strain hardening ratios of 2.5%, 5% and 10 %, respectively, are similar to that of record # 3. The damage is not symmetrical about the vertical axis in most of the storeys. The damage remains very small in the first four storeys, increasing in the 2<sup>nd</sup> storey and decreasing in the

others. The damage increases sharply in the intermediate storeys, followed by sharp decreases in the last two storeys.

For record # 5, the change in the strain hardening ratio had a relatively larger effect on the total damage than in the case of record #1. The increase in the strain hardening ratio caused a decrease in the total damage. The increase in the strain hardening ratio from 2.5% to 5% caused a decrease in the average total damage of 13% and a decrease in the weighted total damage of 9%. While the increase in the strain hardening ratio from 5% to 10% caused a decrease in the average total damage of 10.4% and a decrease in the weighted total damage of 3.9%.

The roof displacement responses, as shown in Figures A.29 and A.30, show random vibrations through the time span of 50 seconds. The elastic response is higher than the inelastic one, and the inelastic response forms a permanent displacement. The strain hardening ratio changed only the value of the permanent displacement that the response oscillates about; but the range of fluctuation remained almost the same.

The maximum interstorey drift ratio envelopes, as shown in Figure A.31, increase in the 2<sup>nd</sup> storey; then, for the case of elastic response, decreases in the 3<sup>rd</sup> and 4<sup>th</sup> storeys and increases up to the 9<sup>th</sup> storey with two large increases at the 7<sup>th</sup> and 9<sup>th</sup> storeys followed by a decrease in the 10<sup>th</sup> storey. The inelastic envelopes remain almost constant from the 2<sup>nd</sup> to the 5<sup>th</sup> storeys; then increases in the 6<sup>th</sup>, 7<sup>th</sup> and 8<sup>th</sup> storeys, having the largest increase at the 7<sup>th</sup> storey. This is followed by a decrease in the 9<sup>th</sup> storey and remains almost constant in the 9<sup>th</sup> and 10<sup>th</sup> storeys.

The change in the strain hardening ratio from 2.5% to 5% decreased the average interstorey drift ratio by 8.1% with a maximum difference of 15.6%; while the change in

the strain hardening ratio from 5% to 10% decreased the average interstorey drift ratio by 7.3% with a maximum difference of 11.3%.

The change in the strain hardening ratio did not have much effect on the maximum inelastic base shear. An increase in the strain hardening ratio from 2.5% to 5% caused an increase in the maximum base shear by 1.1%; while an increase in the strain hardening ratio from 5% to 10% caused an increase in the maximum base shear by 3.2%.

#### **4.3 General comments and observations**

The behavior of the frame for all five records was in general satisfactory, although in some cases a permanent deformation occurred in the structure. However, this is to be expected, because the ground records were from relatively strong earthquakes. The frame behaved according to the strong-column weak-beam concept, forming plastic hinges at the beam ends. Yielding only occurred at the base columns with the exception of record # 3 where yielding occurred at the bottom ends of the two middle columns in the 9<sup>th</sup> storey. The reduction in beam strength was generally low, reaching a maximum value of about 5%. The exception was in the case of record # 5; the 8<sup>th</sup> storey beams reached a strength deterioration in the order of 10%. The damage calculations for columns were only qualitative; because of the approximate parameter used for the column sections. Nevertheless, the maximum strength degradation of 0.01%, observed for the columns, is indicative of low damage potentials of the columns, compared to that of beams. It can be, therefore, concluded that the damage in the columns is negligible.

The damage pattern was not uniform for all the records, and, therefore it could be concluded that the damage depends on the contribution of the higher modes in the response. This is explained in detail in a later section.

It could be noticed as well that the sharp increases in damage generally occurred in storeys where a reduction in the column sections occurred, as in the 5<sup>th</sup> storey for records 1, 2, 4 and 5; the 7<sup>th</sup> storey for records 3 and 5 and the 9<sup>th</sup> storey for records 2, 3 and 5.

The elastic displacement response was larger than the inelastic response in most cases. The elastic and inelastic roof displacements had almost the same shapes and were in phase or had a small phase shift, the earlier giving higher response.

The elastic interstorey drift ratio envelopes gave larger values than the inelastic interstorey drift ratio envelopes in almost all cases. There is no apparent correlation between them: the elastic envelope may increase, while the inelastic envelope may decrease and vice versa. However, in the cases of very sharp increases and decreases, both elastic and inelastic envelopes showed the same trend.

Changing the strain hardening ratio does not have a significant effect on the general behavior or the damage pattern, and has very little effect on the maximum base shear. The overall effect on the interstorey drift envelope and damage was more for the case of record # 5, in which the effect of higher frequencies was apparent in the response compared to the case of record # 1, where the response is dominated by the first vibration mode.

#### **4.4 Effect of higher modes on the damage pattern**

As shown from the results, the damage pattern is not same for all the records, and some damage patterns show specialized characteristics. The damage, in the cases of records 1 and 4, is mainly concentrated in the lower two thirds of the frame with very little damage in the upper third of the frame. The damage in the case of record 3 was concentrated in the upper two storeys and in the case of record 5 in the upper half of the frame with the

largest damage in the 7<sup>th</sup>, 8<sup>th</sup> and 9<sup>th</sup> storeys. The damage in case of record 2 is the same as in records 1 and 4; but has an additional concentration of damage in the upper two storeys.

By examining the response spectra of the records (Figures A.6 to A.10), it is noticed that, for records 1 and 4, the main effect on the response would be due to the first mode and the higher modes will have an insignificant effect. For records 3 and 5, on the other hand the effects of 2<sup>nd</sup> and 3<sup>rd</sup> modes would be equal and in some cases more than the 1<sup>st</sup> mode. For record 2, the main effect is of the first mode; however, the 2<sup>nd</sup> and 3<sup>rd</sup> modes have a significant effect although not as high as the 1<sup>st</sup> mode.

In order to verify the effect of the higher modes, Fourier transforms of the base shear and roof displacement histories were done for all elastic and inelastic analyses. Figures A.32 to A.36 show the Fourier amplitude spectra of the elastic and inelastic base shear responses of all five records. Figures A.37 to A.41 show the Fourier amplitude spectra of the elastic and inelastic roof displacement histories. The spectral analysis of the elastic base shear response, however, gives the clearest picture of the contribution of the higher modes which is discussed in detail.

Records 1 and 4 have large peaks at the fundamental frequency and much smaller peaks at the 2<sup>nd</sup> and 3<sup>rd</sup> frequencies. The peak at the 2<sup>nd</sup> frequency has a value that is 25% of the 1<sup>st</sup> frequency mode for record 1 and 6% for record 4. This indicates that the 1<sup>st</sup> mode is the dominant in the response; and the effect of the higher modes is insignificant, specially in the case of record 4.

The Fourier amplitude spectrum for record 2 has the largest peak at the 1<sup>st</sup> frequency, a 2<sup>nd</sup> frequency peak equal to 35% of the 1<sup>st</sup> frequency value and another peak having a



value of 18% at the third frequency. This indicates that the 1<sup>st</sup> mode is the most effective, but the effect of the higher modes is significant.

The Fourier amplitude spectrum for record 3 has the largest peak at the 2<sup>nd</sup> frequency, while the 3<sup>rd</sup> and 4<sup>th</sup> frequency peaks are comparable to that of the 1<sup>st</sup> frequency peak. This indicates that the higher frequencies dominate the response history.

The Fourier amplitude spectrum for record 5 has the largest peak at the 1<sup>st</sup> frequency and a peak having 65% of its value at the 2<sup>nd</sup> frequency and another peak having a value of 20% at the third frequency. This indicates that the effect of the higher frequency is very high although not as high as in the case of record 3.

It can be concluded that, in the case where the response is mainly in the 1<sup>st</sup> mode, the damage will concentrate in the lower two thirds of the structure and that the damage in the higher storeys will increase with the increase of the effect of the higher modes. In the case, where the effect of higher modes is large compared to the first mode, the damage will be concentrated in the upper storeys. It could be concluded as well that the damage pattern is sensitive to the effect of the higher modes.

#### **4.5 The relation between interstorey drift ratio and damage**

Although it is accepted that there is a correlation between the maximum interstorey drift ratio and the damage, the results did not show a strong correlation for both the elastic and inelastic interstorey drift ratios. In some cases the interstorey drift may increase while the damage may decrease and vice versa. Figures A.42 to A.46 show the plot of the average damage in the storeys versus the interstorey drift ratio. The plots show that, in general, there is high strength deterioration for high interstorey drift; however the scatter is large and the inelastic interstorey drift ratio shows less scatter than the elastic one. In some

records, a linear function can be fitted. However it is difficult to derive a unique relationship involving the results from different earthquake records.

Therefore, a direct relation between the maximum interstorey drift and the damage in the storey can not be concluded.

From the plot of the damage, for all points and for all records, versus the maximum elastic interstorey drift ratio, as shown in Figure A.47, it can be concluded that if the interstorey ratio is less than the 2% limit, set by the NBCC<sup>[31]</sup>, insignificant damage will occur in that storey.

From the observation of the damage pattern in Figures A.17, A.20 and A.27 and the interstorey drift ratio envelopes in Figures A.19, A.22 and A.31, it is noticed that for record # 2 two significant jumps at the 8<sup>th</sup> and 9<sup>th</sup> storeys for both the elastic interstorey drift and the damage. The same trend can be noticed for record # 3 in the 7<sup>th</sup> and 9<sup>th</sup> storeys, although the damage in the 7<sup>th</sup> storey is still low but is three times as in the 6<sup>th</sup> storey. For record # 5 a constant significant increase in the elastic interstorey drift ratio and the damage starting from the 6<sup>th</sup> floor is noticed. Therefore it can be concluded that significant increases in the interstorey drift envelopes in the upper storeys are indicative of a region of damage localization in these floors. Thus the elastic seismic analysis results can be used to obtain a general indication of the possible damage localization zones.

#### **4.6 The relation between the maximum inelastic base shear and total damage**

Figures A.48 and A.49 show the relations between maximum inelastic base shear and the total averaged damage and the total weighted damage respectively. It is observed from the figures that, for records 1, 2 and 4 in which the 1<sup>st</sup> mode is the most effective, the points show an increasing trend and a linear function can be fitted with very little scatter.

On the other hand, for records 3 and 5 where the effect of higher modes is more significant, the points show a decreasing trend that has a steeper slope and linear function can be fitted but with more scatter. In this case however, the damage is due to the vibration of the higher modes in which the correlation between the displacements and the base shear is not strong. Moreover there are insufficient data points to reach a solid conclusion.

## **CHAPTER 5**

### **SUMMARY AND CONCLUSIONS**

#### **5.1 Summary**

Elastic and inelastic dynamic analyses of a building, designed and detailed according to the Canadian Standard S16.1, were carried out using five ground acceleration histories from real earthquakes. The DRAIN-2DX computer program was used to study the general performance and level of damage the structure will suffer. A typical strain hardening ratio of 5% was used for most of the inelastic analyses. Additional parametric analyses were also conducted with the strain hardening ratios of 2.5% and 10%.

Roof displacement, interstorey drift ratio, base shear and plastic rotations were the parameters examined in this study. Damage was calculated by using an empirical equation proposed in the literature.

The response spectra and the Fourier amplitude spectra for the elastic and inelastic base shear and roof displacement were calculated to investigate the effects of higher modes on the predicted damage.

#### **5.2 Conclusions**

The following conclusions can be drawn from the results:

- The behavior of the frame for all the records was, in general, satisfactory. The frame behaved according to the strong-column weak-beam mechanism, forming plastic hinges at the beam ends. Columns experienced yielding only at the fixed bases with the exception of record # 3 where yielding occurred at the bottom ends of the two

interior columns in the 9<sup>th</sup> floor. The level of damage was low in the beams in most of the cases and negligible in the columns in all cases.

- The damage pattern is related to the contribution of the different modes of the structure. In the cases where the first mode dominates the structural response, the damage will be localised in the lower two thirds of the structure, and, in the cases where the higher modes have a significant effect, the damage will be localised at the upper floors.
- The envelope of the elastic interstorey drift ratios can be used as an indication of damage localisation in the upper storeys.
- The strain hardening ratio does not affect the general performance or the damage pattern, and has little effect on the results. It had more effect on the results, in the case where the contribution of the higher modes to the overall response is high, than in the case where the first mode is the one prevailing in the response.
- Floors at which reductions in the column sections occur suffer more damage, and almost invariably a sudden increase in the damage occurred in such floors.
- The elastic response spectra and the Fourier amplitude spectra of the elastic and inelastic base shear and roof displacement give a good indication about the effect of higher modes and what damage pattern is to be expected. The best indication,

however, can be found out from the Fourier amplitude spectrum of the elastic base shear history.

- A quantitative relation between the maximum elastic and inelastic interstorey drift ratios and the damage is not evident. Although an increased drift ratio implies an increased damage, this relation can not be represented by a unique function.
- For a value of the maximum elastic interstorey drift ratio less than 2%, no or negligible damage will occur at the particular storey.
- In the case, where the first mode dominates the structural response, a strong linear increasing relation between the maximum inelastic base shear and the total damage can be concluded. However if the higher modes have a significant effect, this relation seems to be reversed.

### **5.3 Recommendations for future research**

It is recommended that future research efforts be directed towards the following:

- The study of the damage using other failure modes, for example connection failure.
- The study of the relation between the reduction in column sections at certain floors and the sudden increase in the damage in such floors.

- **Development of a quantitative relationship between the higher mode contributions as given by the response spectrum or the Fourier amplitude spectrum of the elastic base shear, and the damage pattern.**

## REFERENCES

1. Ballio, G., and Castiglioni, C.A., 1994, "*Seismic behavior of steel sections*", Journal of Constructional Steel Research, Vol. 29, pp. 21-54.
2. Ballio, G., and Castiglioni, C.A., 1995, "*A unified approach for the design of steel structures under low and/or high cycle fatigue*", Journal of Constructional Steel Research, Vol. 34, pp. 75-101.
3. Bertero, V.V., and Popov, E.P., 1965, "*Effect of large alternating strains of steel beams*", Journal of the Structural Division, Proceedings ASCE, Vol. 91, No. 1, pp. 4217-4232.
4. Calado, L. and Castiglioni, C.A., 1996, "*Steel beam-to-column connections under low-cycle fatigue, experimental and numerical research*", Proceedings 11<sup>th</sup> World Conference on Earthquake Engineering, Acapulco, Mexico.
5. Calado, L., and Azevedo, J., 1989, "*A model for predicting the failure of structural steel elements*", Journal of Constructional Steel Research, Vol. 14, pp. 41-64.
6. Canadian Institute of Steel Construction, 1997, "*Handbook of Steel Construction*", 7<sup>th</sup> Edition, Willowdale, Ontario.
7. Castiglioni, C.A. and Calado, L., 1996, "*Comparison of two cumulative damage approaches for the assessment of behaviour factors for low-rise steel buildings*", Journal of Constructional Steel Research, Vol. 40, pp. 39-61.
8. Castiglioni, C.A. and Goss, G., 1989, "*Sulla applicabilita della regola di Miner nella fatica a basso numero di cicli*", Politecnico di Milano, 8/89.
9. Castiglioni, C.A., and Di Palma, N., 1989, "*Experimental behavior of steel members under cyclic bending*", Costruzioni Metalliche, Vol. 2/3, pp. 97-114.



10. Chen, S.J., Yeh, C.H. and Chu, J.M., 1996, "*Ductile steel beam-to-column connections for seismic design*", Journal of Structural Engineering, Vol. 122, No. 11 pp. 1292-1299.
11. Chi, W., El-Tawil, S., Deierlein, G.G. and Abel J.F., 1997, "*Inelastic analysis of a 17-story steel framed building damaged during Northridge*", Engineering Structures, Vol. 20, No. 4-6, pp. 481-495.
12. Chi, W.M., Deierlein, G.G. and Ingraffea, A.R., 1997, "*Finite element fracture mechanics investigation of welded beam-column connections*", Report No. SAC/BD-97/05, SAC joint venture.
13. Comité Européen de Normalisation, 1992, "*Eurocode 3: Design of Steel Structures, Part 1-1: general rules and rules for buildings ENV 1993-1-1*", February.
14. Daali, M.L., and Korol, R.M., 1995, "*Low cycle fatigue damage assessment in steel beams*", structural Engineering and Mechanics, Vol. 3, No. 4, pp. 341-358.
15. Daali, M.L., and Korol, R.M., 1996, "*Adequate ductility in steel beams under earthquake-type loading*", Engineering Structures, Vol. 18, No. 2, pp. 179-189.
16. Engelhardt, M.D. and Sabol, T.A., 1997, "*Reinforcing of steel moment connections with cover plates: benefits and limitations*", Engineering Structures, Vol. 20, No. 4-6, pp. 510-520.
17. Engelhardt, M.D. and Sabol, T.A., 1997, "*Seismic resistant steel moment connections: developments since the 1994 Northridge earthquake*", Progress in Structural Engineering and Materials, Vol. 1, No. 1, pp. 68-77.
18. Engelhardt, M.D., Winneberger, T., Zekany, A.J. and Potyraj, T.J., 1996, "*The dogbone connection: part II*", Modern Steel Construction, August, pp. 46-55.

19. Gunturi. S.K.V. and Shah, H.C., 1992, "*Building specific damage estimation*", Proceedings 10<sup>th</sup> World Conference on Earthquake Engineering, Madrid, Spain, pp. 6001-6006.
20. Iwankiw, N.R. and Carter, C.J., 1996, "*The dogbone: a new idea to chew on*", Modern Steel Construction, April.
21. Kappos, A.J., 1997, "*Seismic damage indices for RC buildings: evaluation of concepts and procedures*", Progress in Structural Engineering and Materials, Vol. 1, No. 1, pp. 78-87.
22. Kappos, A.J., Stylianidis, K.C. and Michailidis C.N., 1996, "*A methodology for developing loss scenarios, with an application to the city of Thessaloniki*", Proceedings 11<sup>th</sup> World Conference on Earthquake Engineering, Acapulco, Mexico, paper No. 2057.
23. Kappos, A.J., Stylianidis, K.C. and Penelis G.G., 1991, "*Analytical prediction to the response of structures to future earthquakes*", European Earthquake Engineering, Vol. 5, No. 1, pp. 10-21.
24. Korol, R.M. and Daali, M.L., 1994, "*Rotation capacity and energy absorption enhancement in beams under cyclic loading*", Engineering Mechanics Symposium of CSCE., Winnipeg.
25. Korol, R.M., Ghobarah, A. and Osman, A., 1990, "*Extended end-plate connections under cyclic loading: behavior and design*", Journal of Structural Engineering, Vol. 16, pp. 253-280.

26. Krawinkler, H., and Zohrei, M., 1983, "*Cumulative damage in steel structures subjected to earthquake ground motion*", Computers and Structures, Vol. 16, No. 1-4, pp. 531-541.
27. Kulhmann, U., 1989, "*Definition of flange slenderness limits on the basis of rotation capacity values*", Journal of Structural Engineering, Vol. 14, pp. 21-40.
28. Lukey, A.F. and Adams, P.F., 1969, "*Rotation Capacity of beams under moment gradient*" Journal of the Structural Division, Proceedings ASCE, Vol. 95, No. 6, pp. 1173-1188.
29. Miner, M.A., 1945, "*Cumulative damage in fatigue*", Journal of Applied Mechanics, September, pp. 159-164.
30. Naeim, F., DiJulio, R., Benuska, K., Reinhorn, A. M., and Li, C., 1995, "*Evaluation of the Seismic Performance of an 11 Story Steel Moment Frame Building During the 1994 Northridge Earthquake*", Report to SAC Joint Venture, SAC Task 3.1, Building No. 6, John A. Martin & Associates, Inc.
31. National research council of Canada, 1995, "*National Building Code of Canada*", Ottawa.
32. National Standards of Canada, 1994, *CAN/CSA-S16.1-94 "Limit States Design of Steel Structures"*, Ontario, Canada.
33. Osman, A., Ghobarah, A., and Korol, R.M., 1995, "*Implications of design philosophies for seismic response of steel moment frames*", Earthquake Engineering and Structural Dynamics, Vol. 24, pp. 127-143.
34. Park, Y. J. and Ang A. , 1985, "*Mechanistic seismic damage model for reinforced concrete*", Journal of Structural engineering, Vol. 111, No. 4, pp. 722-739

35. Park, Y.J., Ang, A. and Wen, Y.K., 1985, "*Seismic damage analysis of reinforced concrete structures*", Journal of Structural engineering, Vol. 111, No. 4.
36. Park, Y.J., Ang, A. and Wen, Y.K., 1987, "*Damage-limiting aseismic design of buildings*", Earthquake spectra, Vol. 3, No. 1, pp. 1-25.
37. Powell, G.H., 1993, "*DRAIN-2DX, element description and user guide for element type01, type02, type03, type06, type09, and type15*", Version 1.1, Department of Civil Engineering, University of California Berkeley, CA.
38. Prakash, V. and Powell, G.H., 1993, "*DRAIN-2DX, DRAIN-3DX and DRAIN-BUILDING: Base program design documentation*", Department of Civil Engineering, University of California Berkeley, CA.
39. Prakash, V., Powell, G.H. and Campbell, S., 1993, "*DRAIN-2DX, Base program description and user guide*", Version 1.1, Department of Civil Engineering, University of California Berkeley, CA.
40. Singhal, A. and Kiremidjian, A.S., 1995, "*Method for developing motion damage relationships for reinforced concrete frames*", Technical report NCEER 95-0008, State University of New York at Buffalo.
41. Song, J. and Ellingwood, R., 1999, "*Seismic reliability of special moment steel frames with welded connections: I*", Journal of Structural Engineering, Vol. 125, No. 4, pp. 357-371.
42. Tavernelli, J.F., and Coffin, L.F., 1961, "*Experimental support for generalized equation predicting low-cycle fatigue*", ASME, paper 61.
43. Wöhler, A., 1860, Zeitschrift für Bauwesensn, Vol. 10.

## **Appendix A**

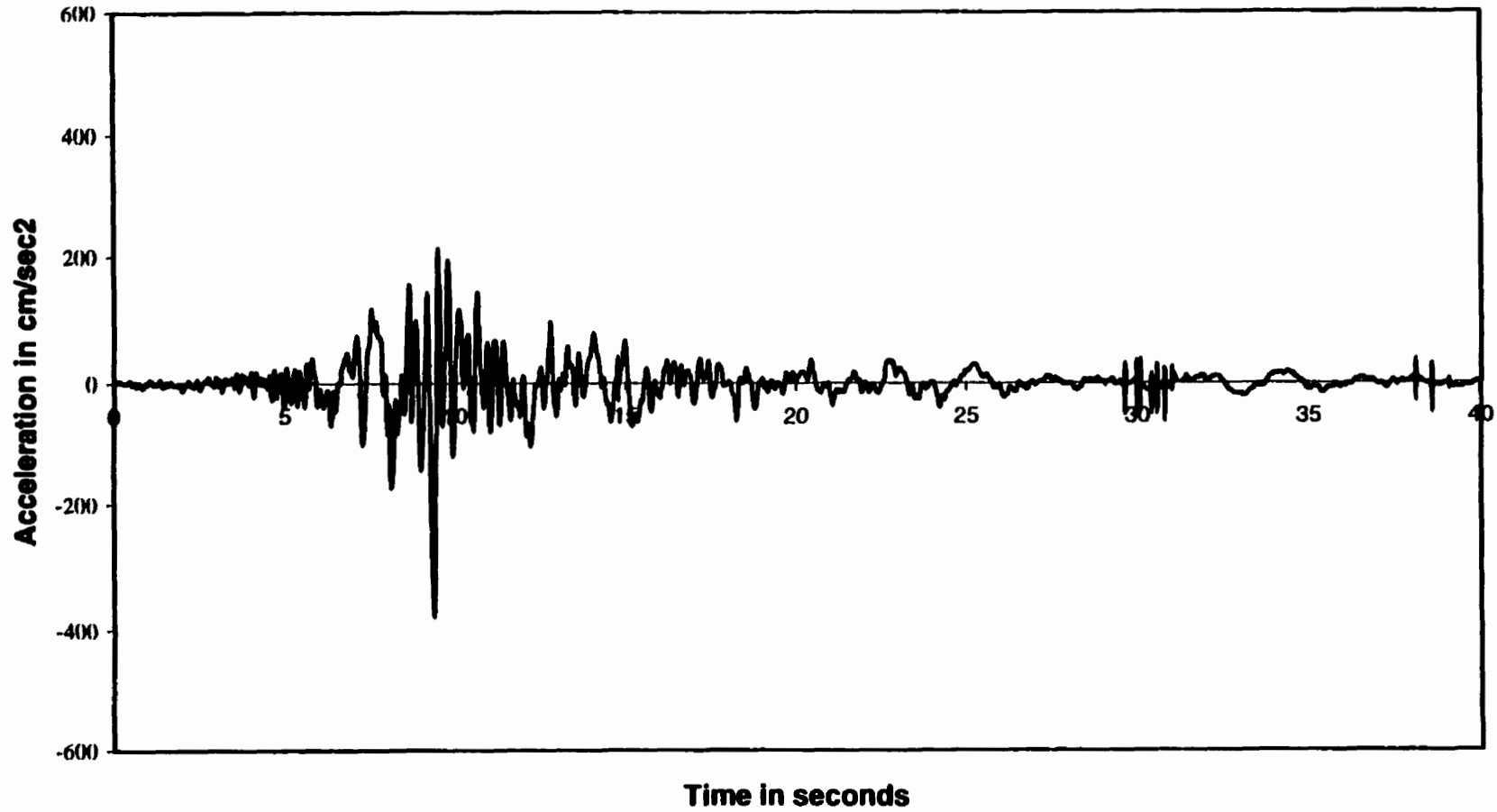
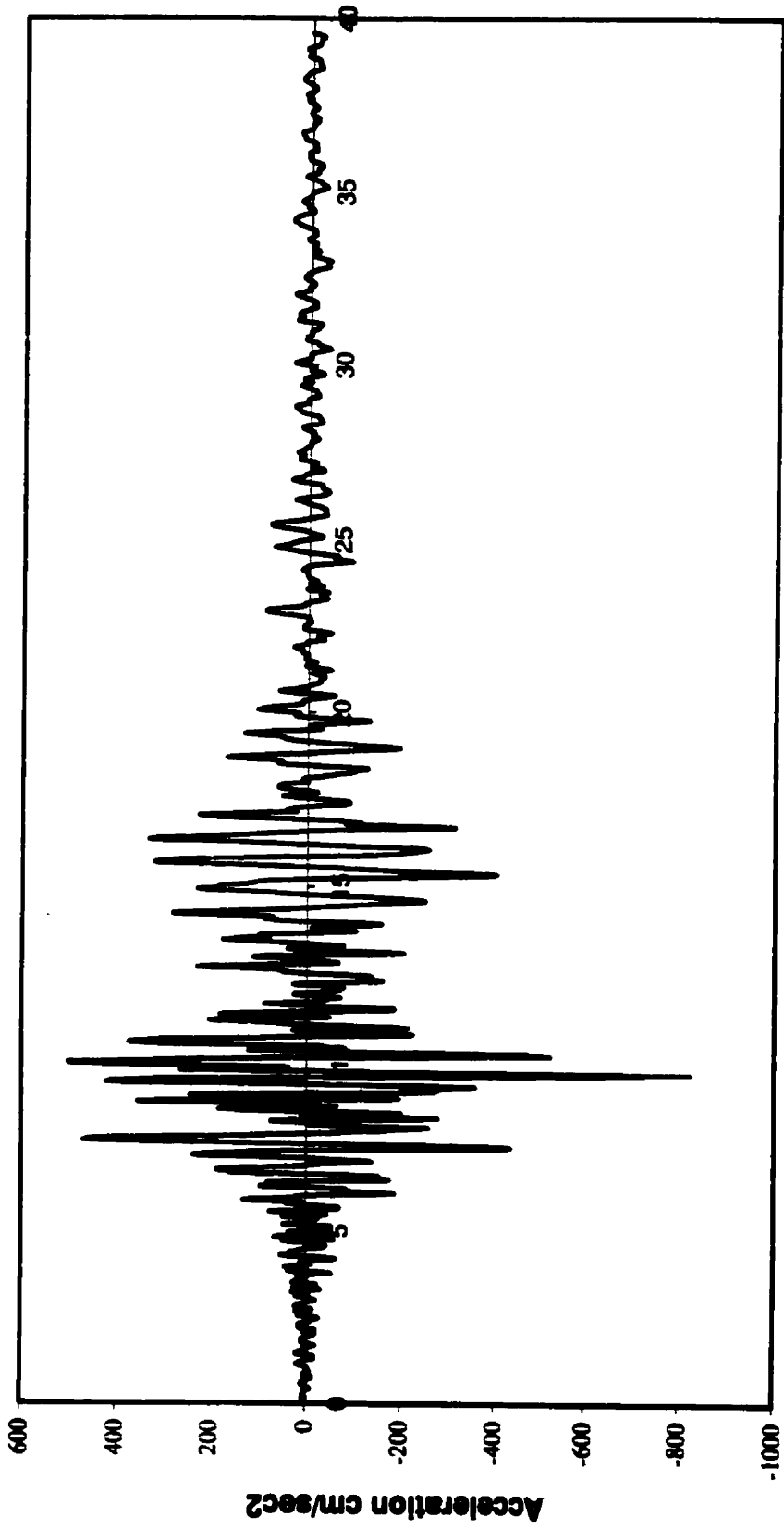
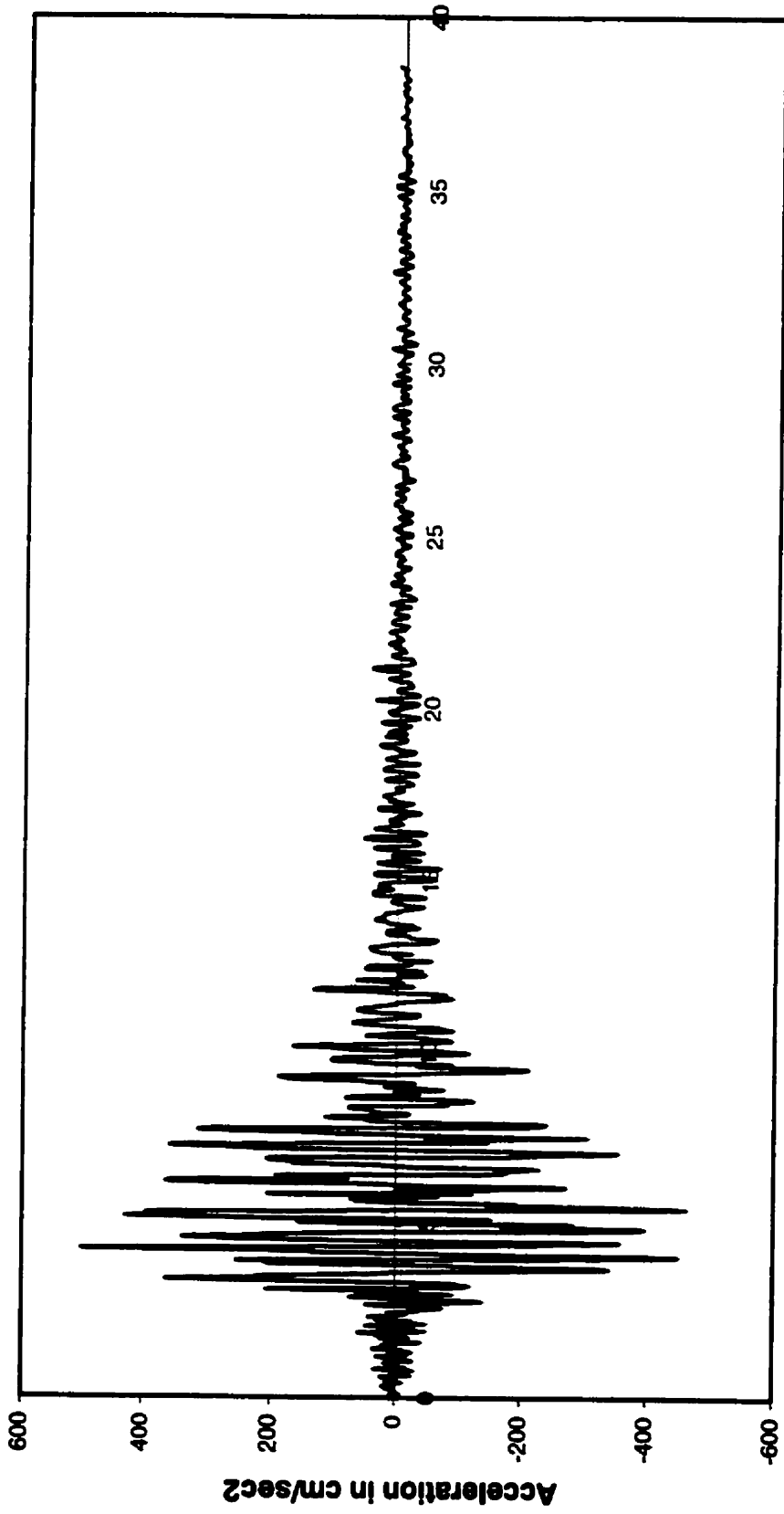


**Figure A.1**  
**Unsealed ground acceleration record # 1 (Loma Prieta record # 1)**



Time in seconds

Figure A.2  
Unscathed ground acceleration record # 2 (Loma Prieta record # 2)

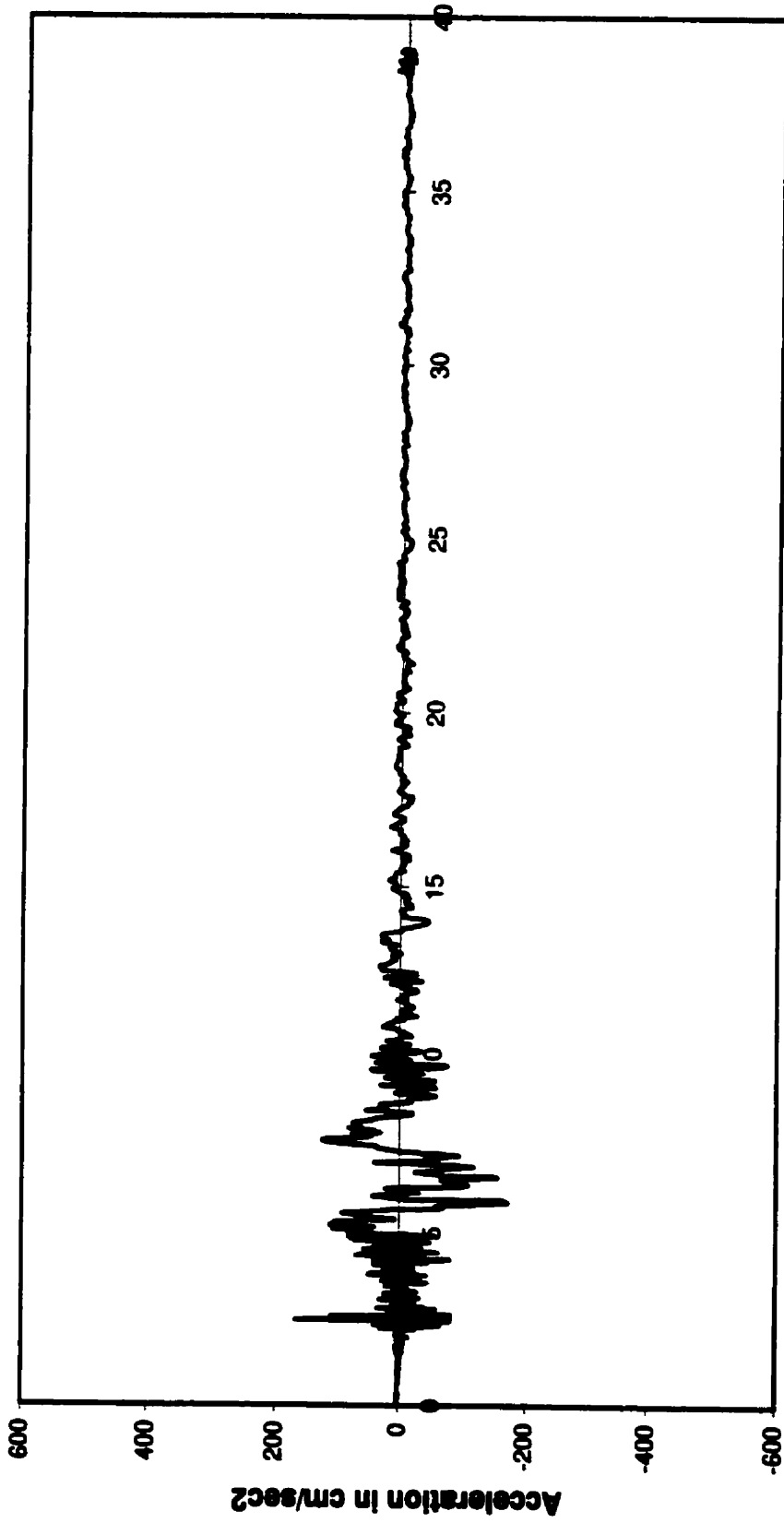


**Time in seconds**

**Figure A.3**

**Unsealed ground acceleration record # 3 (Northridge record)**

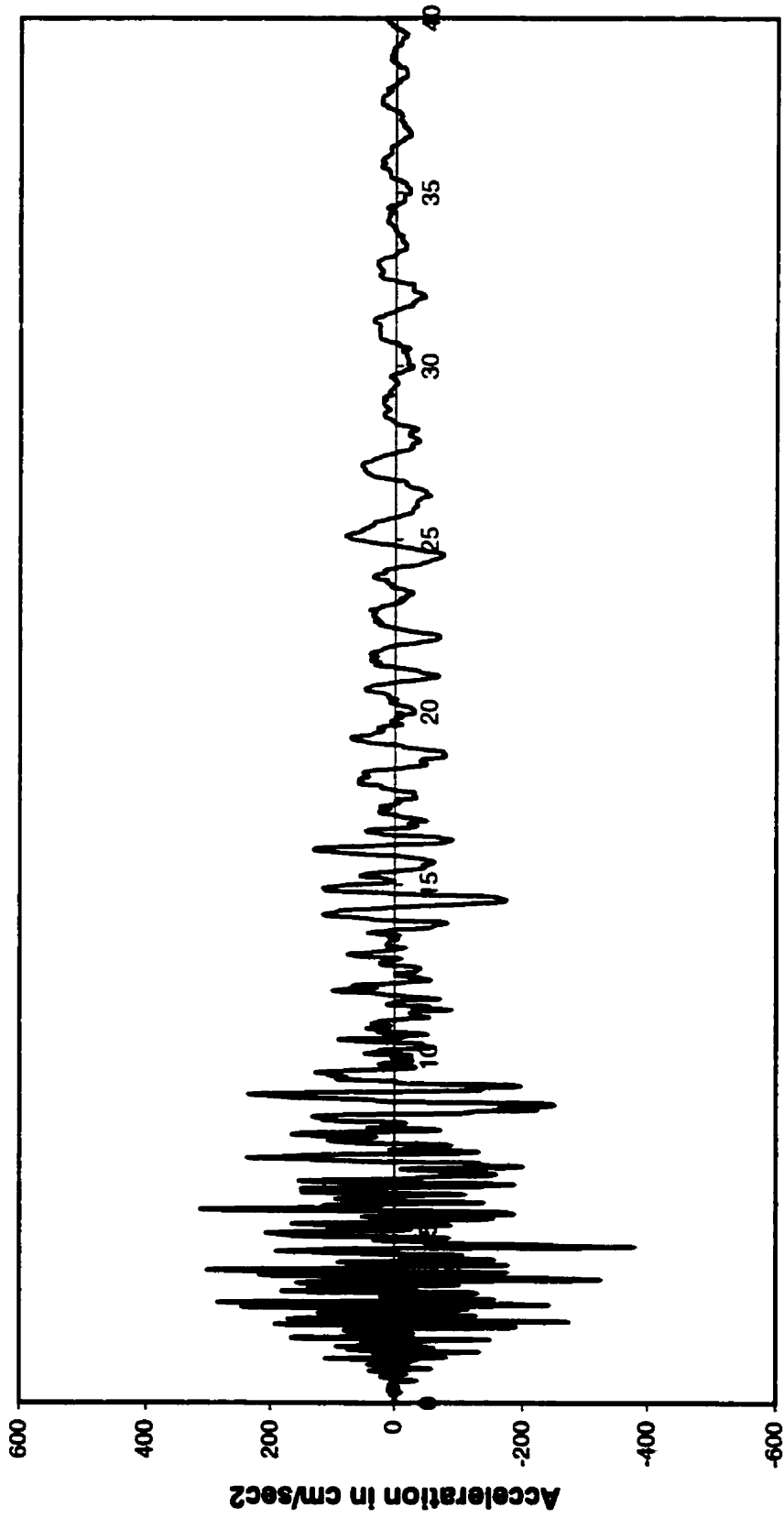




**Time in seconds**

**Figure A.4**

**Unsealed ground acceleration record # 4 (Long Beach record)**



Time in seconds

Figure A.5  
Unsealed ground acceleration record # 5 (Morgan Hill record)

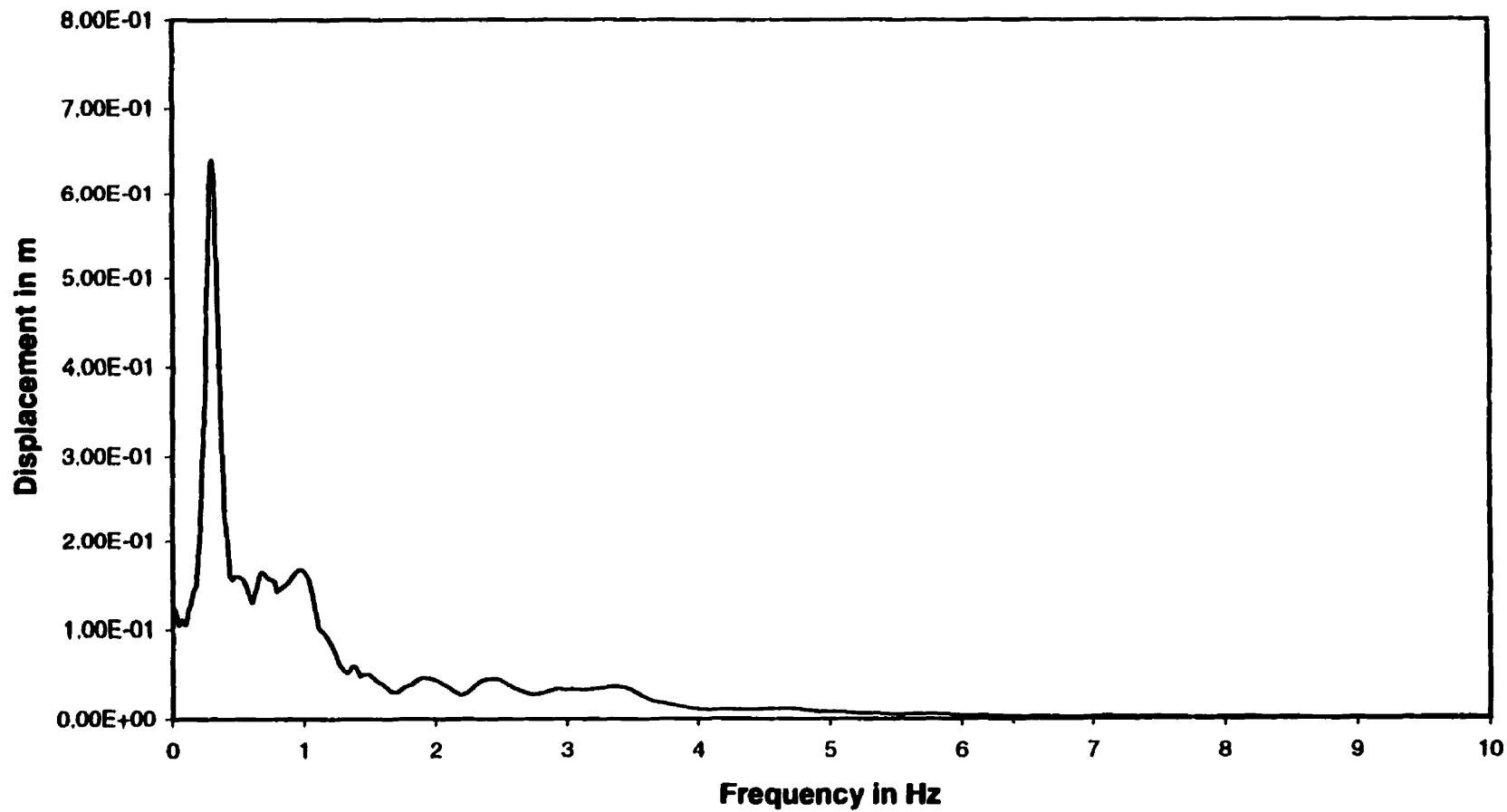


**Figure A.6**  
**Response spectrum for unscaled ground acceleration record # 1**  
**(Loma Prieta record # 1)**

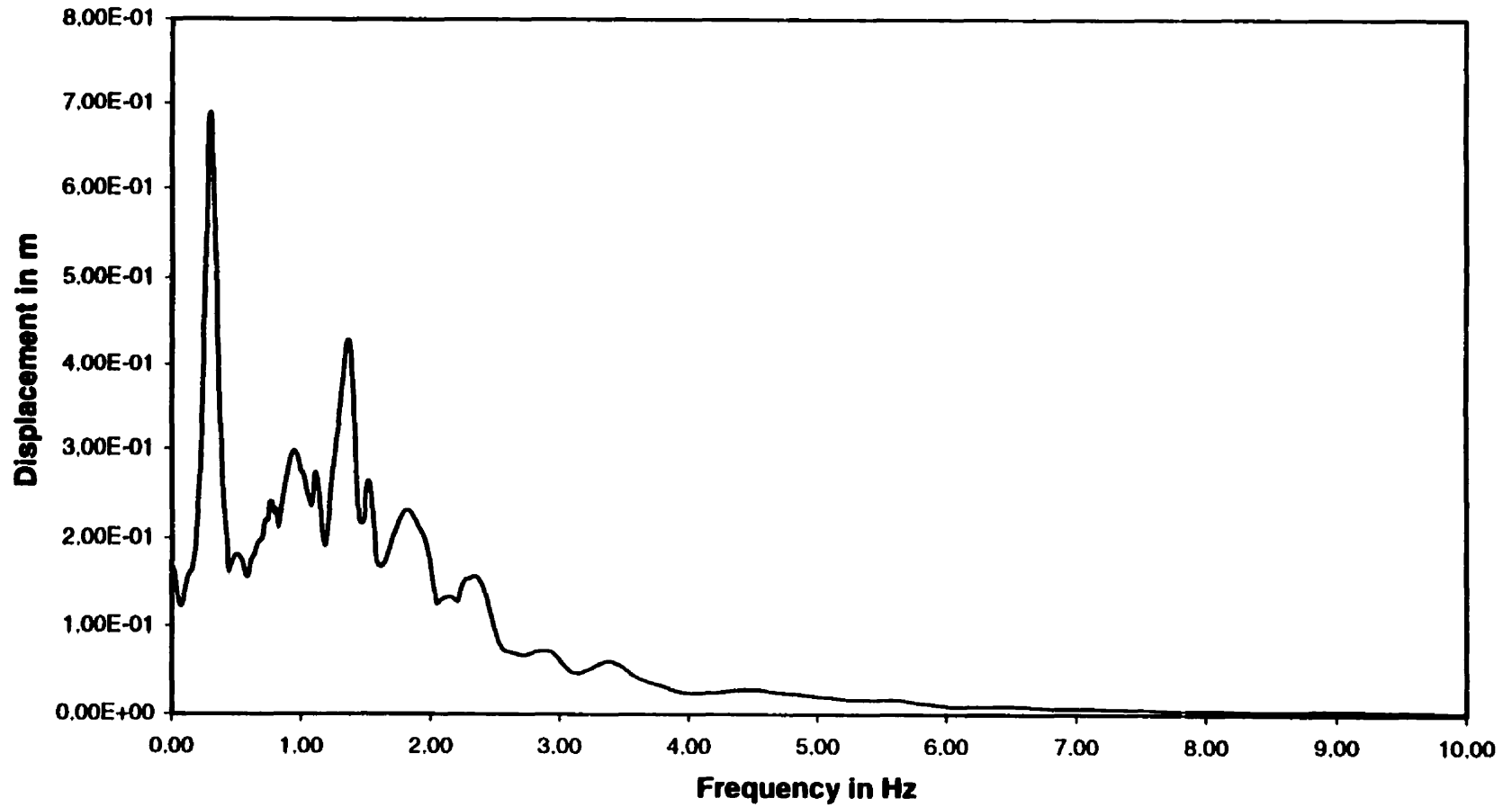


**Figure A.7**  
**Response spectrum for unscaled ground acceleration record # 2**  
**(Loma Prieta record # 2)**

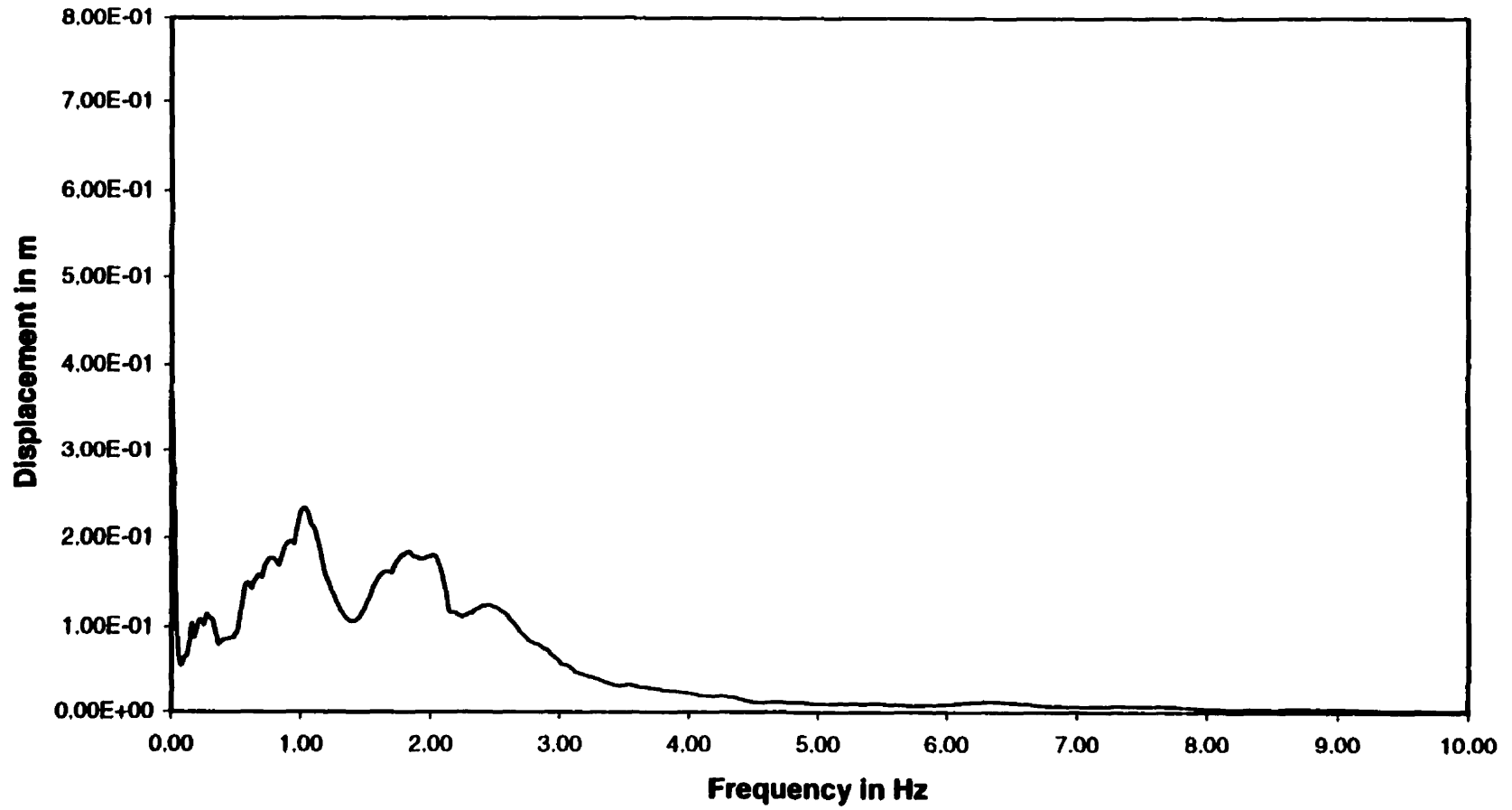


**Figure A.8**  
**Response spectrum for unscaled ground acceleration record # 3**  
**(Northridge record)**

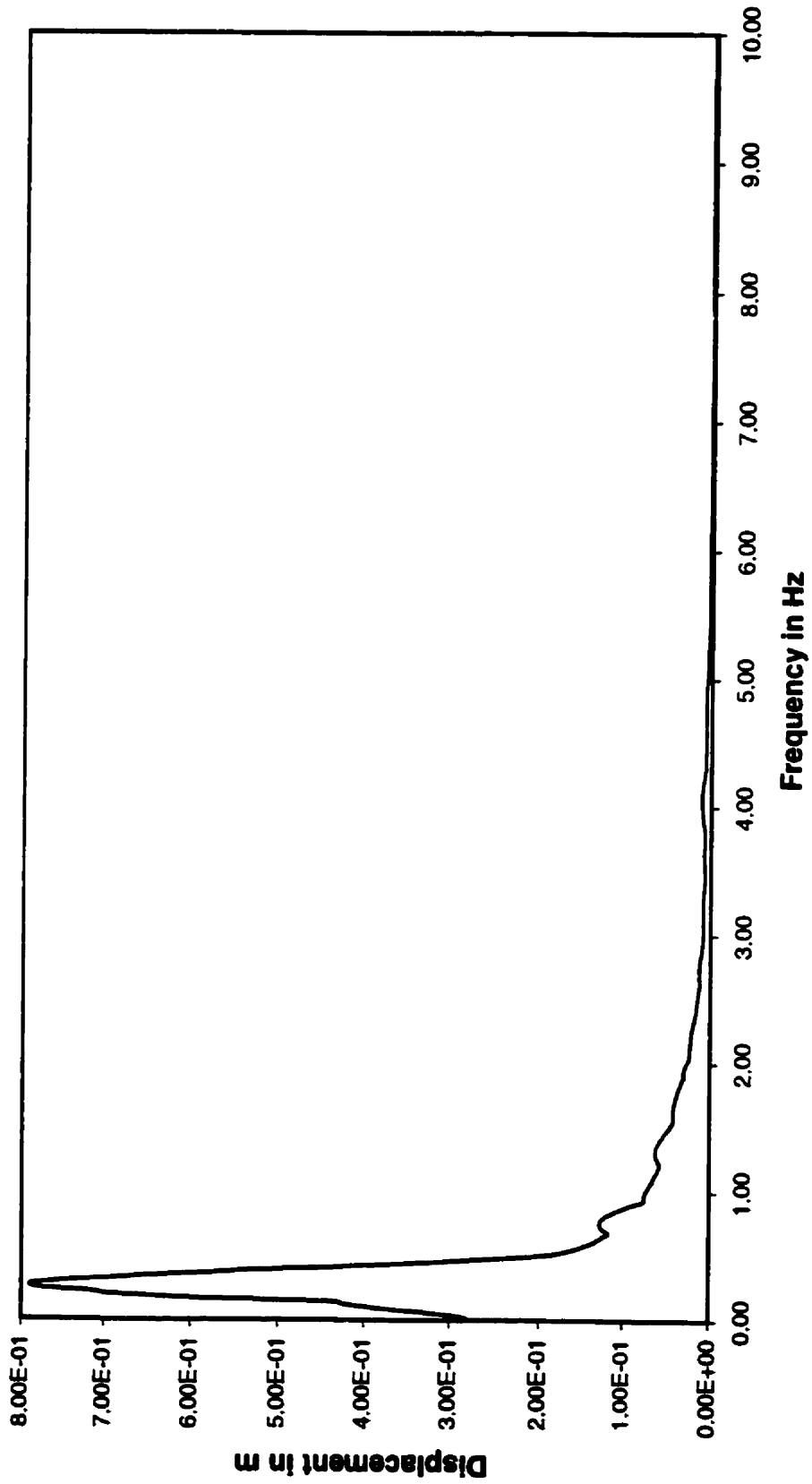


**Figure A.9**  
**Response spectrum for unscaled ground acceleration record # 4**  
**(Long Beach record)**

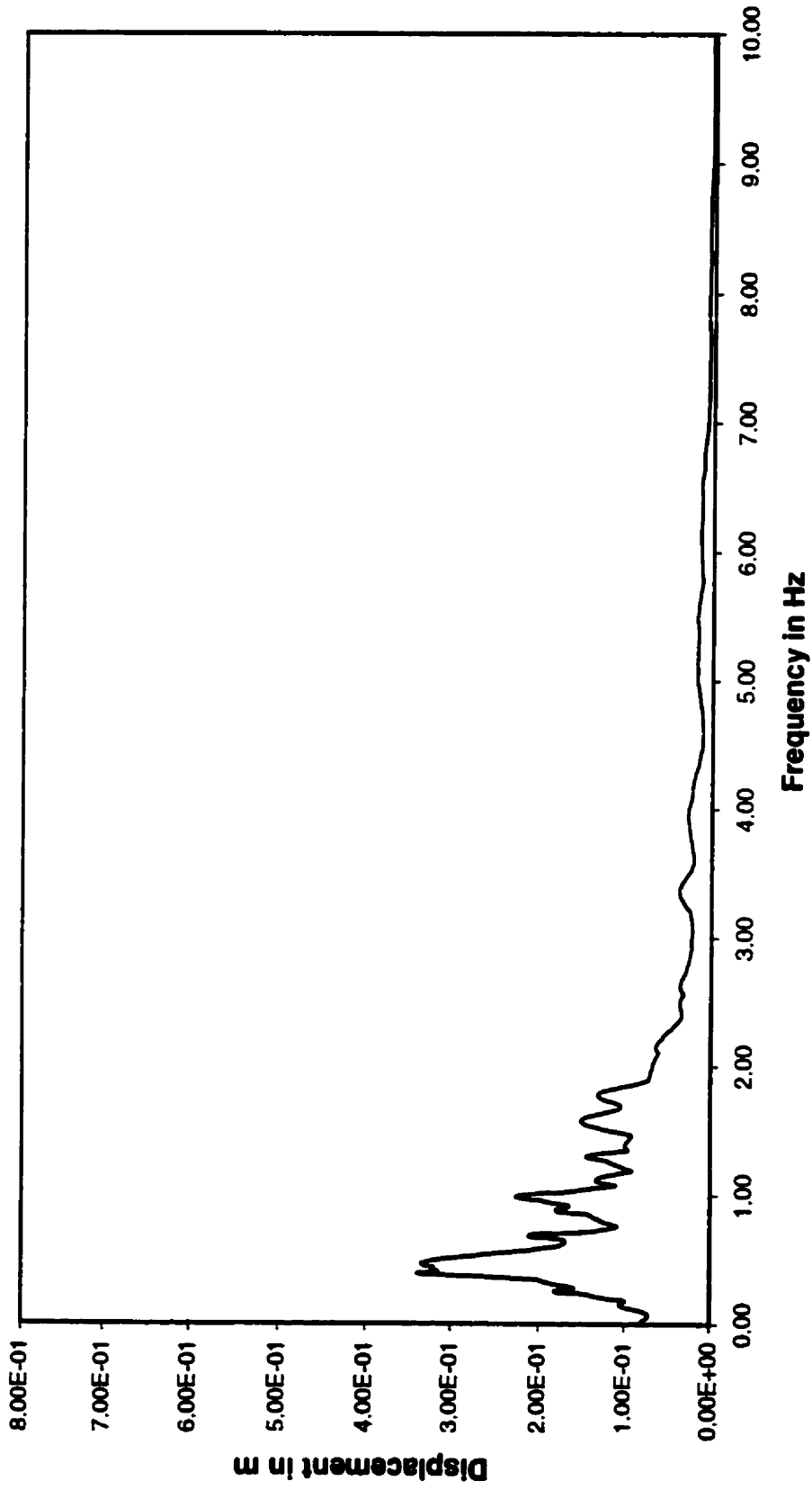


**Figure A.10**  
**Response spectrum for unscaled ground acceleration record # 5**  
**(Morgan Hill record)**

0.00	0.14	0.00	0.12	0.00	0.11
0.44	1.00	0.50	1.09	0.45	1.01
1.15	1.17	1.64	1.63	1.16	1.13
1.80	1.94	2.33	2.33	1.90	1.84
2.69	2.32	2.97	2.75	2.51	2.50
4.33	4.03	4.50	4.50	4.04	4.34
2.41	2.14	2.33	2.33	2.14	2.41
2.18	1.90	2.25	2.26	1.91	2.19
2.69	2.38	2.54	2.54	2.38	2.69
1.93	1.50	1.57	1.56	1.48	1.87



**Figure A.11**  
**Strength deterioration in percent for record # 1 (Loma Prieta record # 1)**  
**2.5% strain hardening ratio**



0.00	0.13	0.00	0.11	0.00	0.10
0.49	1.02	0.56	1.12	0.50	1.03
1.23	1.26	1.53	1.53	1.24	1.23
1.44	1.58	1.91	1.91	1.53	1.49
3.25	2.85	3.52	3.29	3.05	3.05
4.03	3.71	4.17	4.17	3.72	4.03
2.53	2.24	2.45	2.45	2.24	2.54
2.23	1.94	2.33	2.33	1.94	2.23
2.80	2.47	2.64	2.64	2.48	2.79
2.01	1.55	1.62	1.62	1.54	1.96



**Figure A.12**  
**Strength deterioration in percent for record # 1 (Loma Prieta record # 1)**  
**5% strain hardening ratio**

0.00	0.12	0.00	0.11	0.00	0.09
0.62	1.10	0.71	1.23	0.63	1.11
1.86	1.32	2.20	2.20	1.28	1.30
2.09	2.24	2.68	2.69	2.21	2.15
1.63	1.48	2.89	2.61	1.52	1.60
4.17	3.92	4.33	4.33	3.91	4.17
1.99	1.70	1.92	1.92	1.70	1.99
2.07	1.74	1.94	1.94	1.74	2.07
2.68	2.33	2.50	2.50	2.33	2.67
1.83	1.38	1.45	1.45	1.37	1.84



**Figure A.13**  
**Strength deterioration in percent for record # 1 (Loma Prieta record # 1)**  
**10% strain hardening ratio**

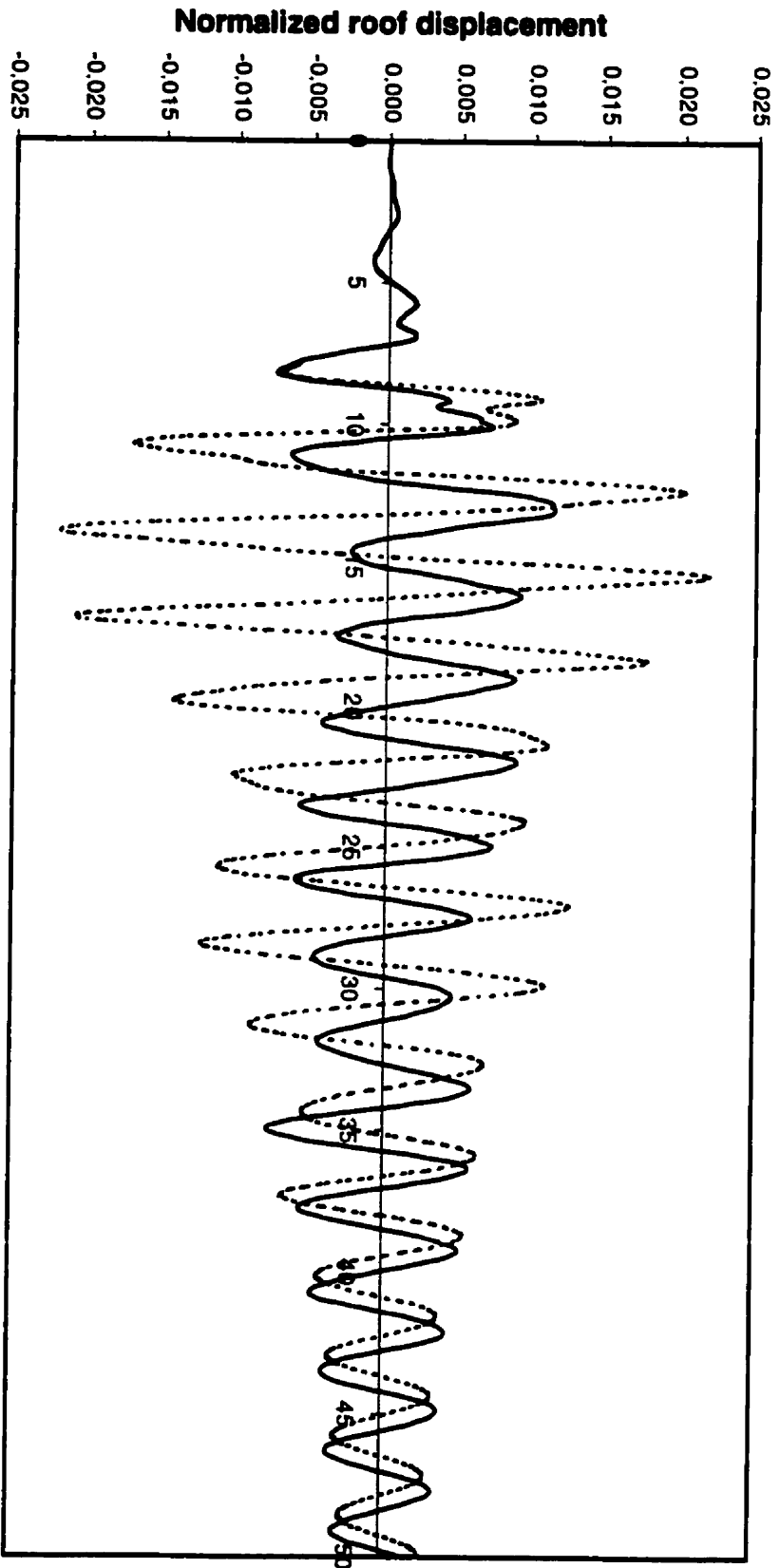
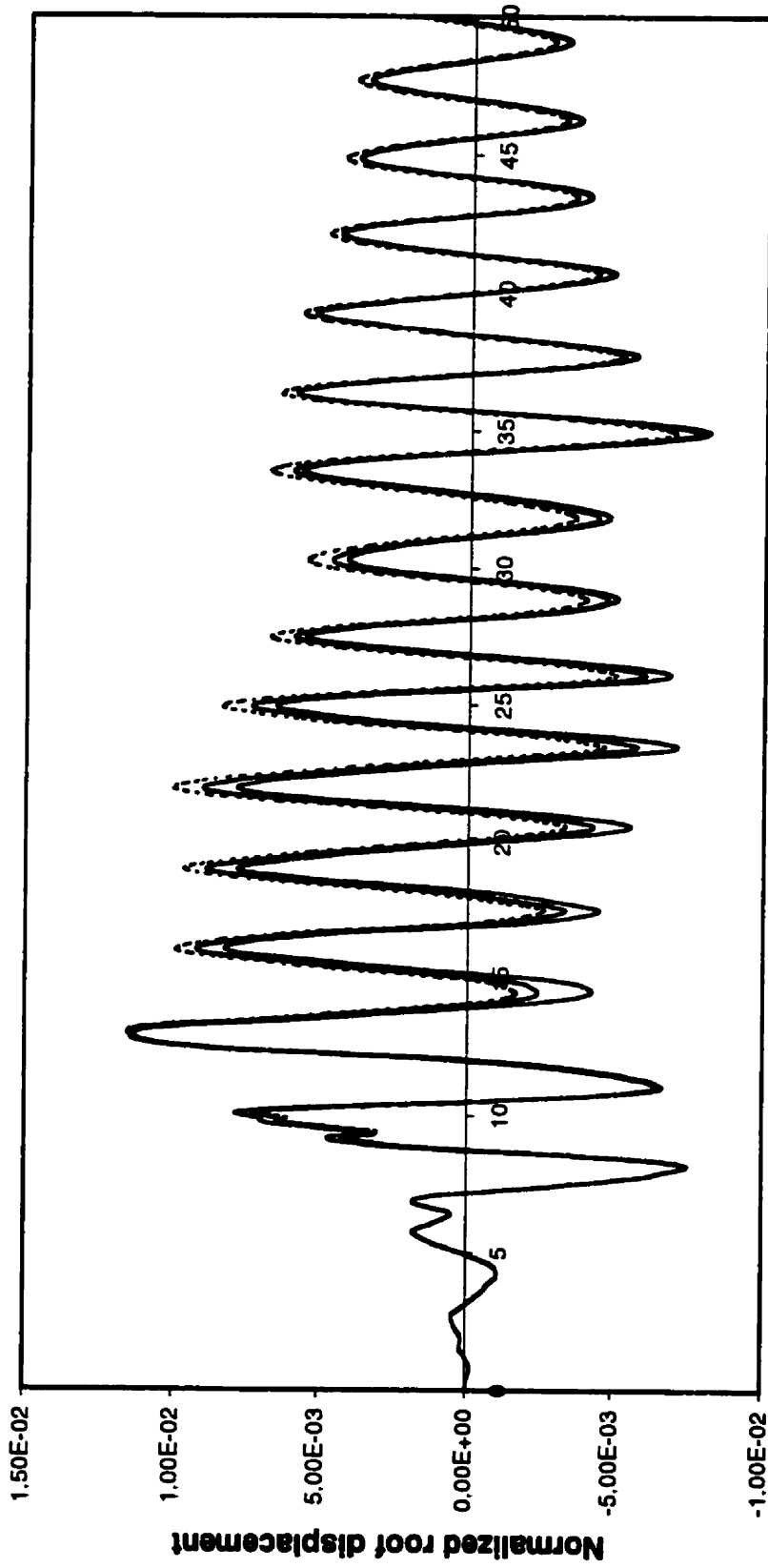


**Figure A.14**  
**Normalized roof displacement record # 1 (Loma Prieta record #1)**



Time in seconds



Figure A.15

Normalized inelastic roof displacement record # 1 (Loma Prieta record #1)

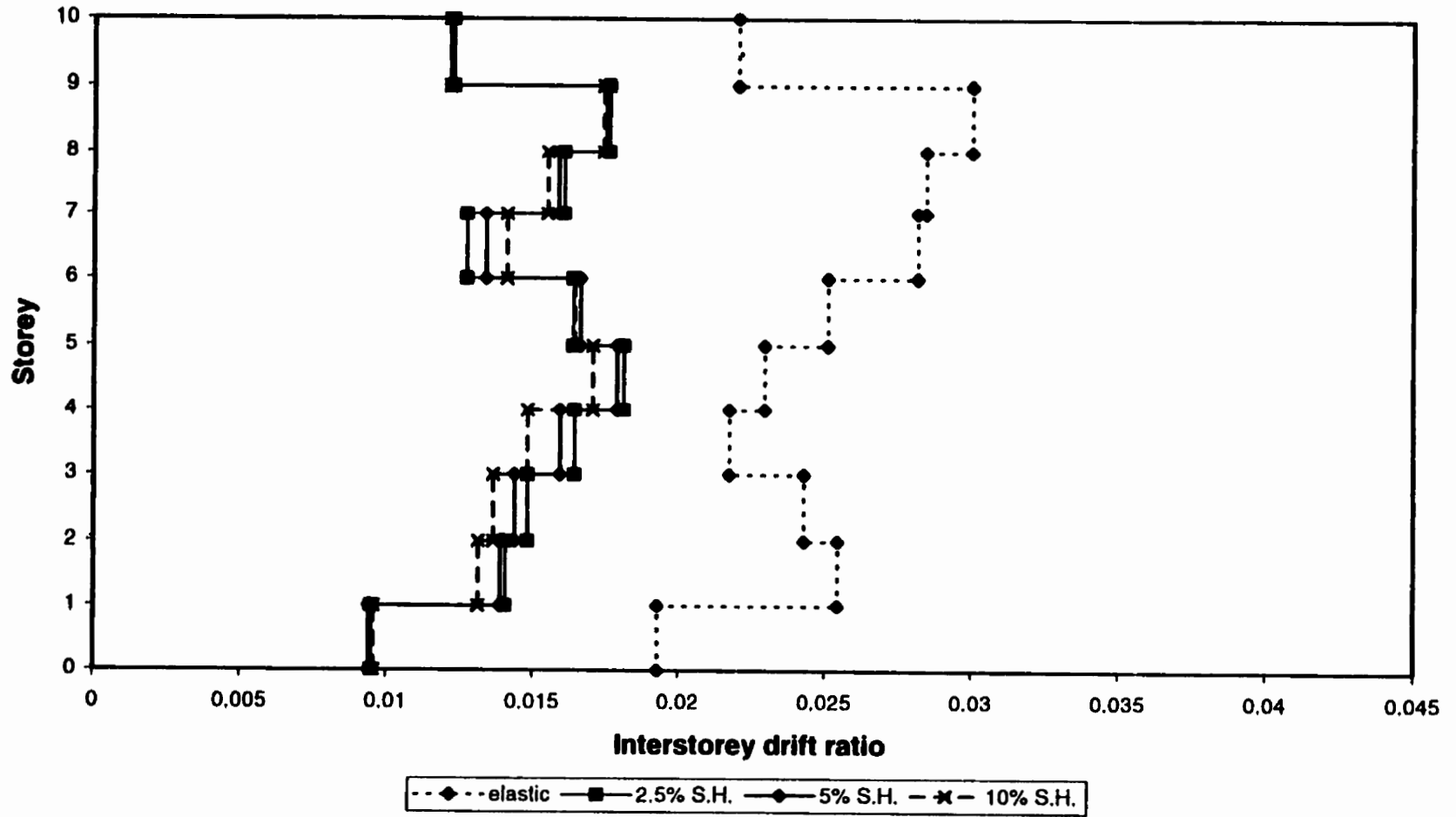


**Figure A.16**  
**Maximum interstorey drift ratio for record # 1 (Loma Prieta record # 1)**

2.27	1.55	1.84	1.44	2.07	1.69
5.97	4.15	5.53	4.21	5.94	4.16
2.42	2.39	2.16	2.16	2.38	2.44
1.55	1.61	1.84	1.84	1.60	1.55
3.19	2.93	3.82	3.82	2.93	3.19
4.21	3.43	4.18	3.70	3.90	3.72
2.21	1.82	2.04	1.93	1.94	2.09
2.35	1.83	2.17	1.96	2.05	2.11
2.01	1.70	1.79	1.78	1.70	2.00
1.30	1.04	1.08	1.08	1.01	1.33

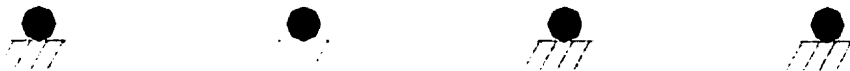
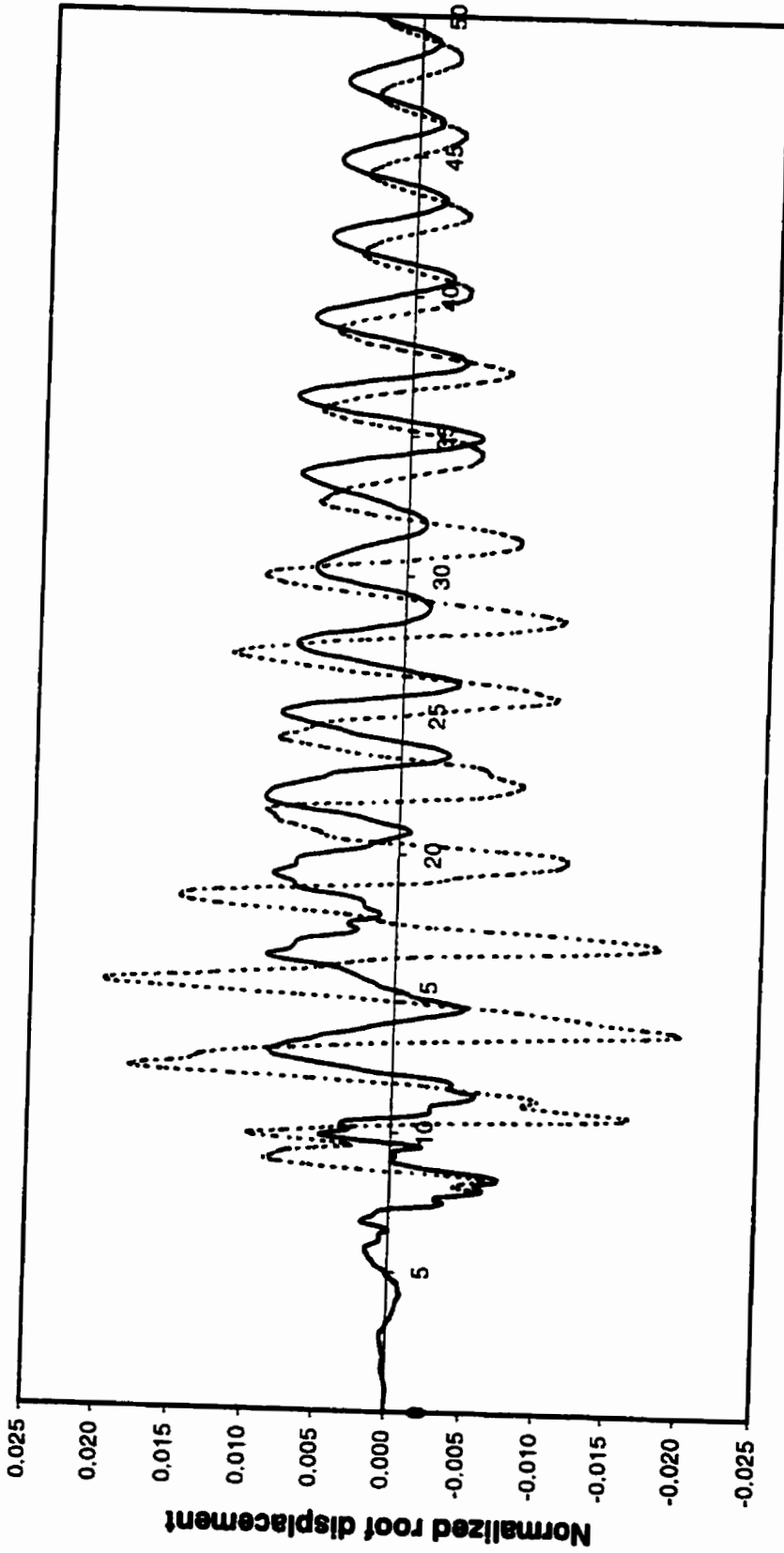


**Figure A.17**  
**Strength deterioration in percent for record # 2 (Loma Prieta record # 2)**  
**5% strain hardening ratio**



Time in seconds

.....elastic — inelastic 5% S.H.

**Figure A.18**  
**Normalized roof displacement record # 2 (Loma Prieta record #2)**

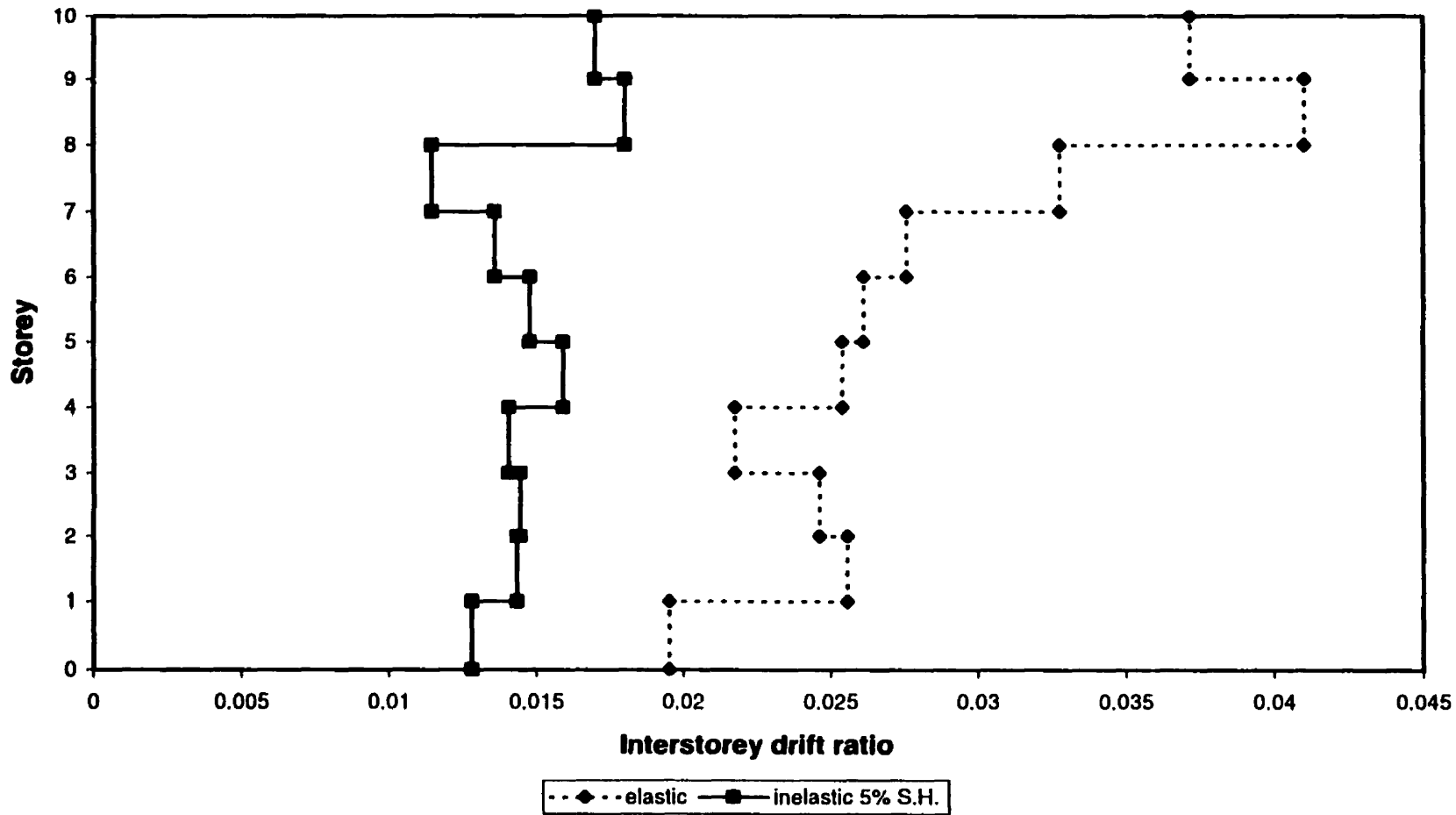


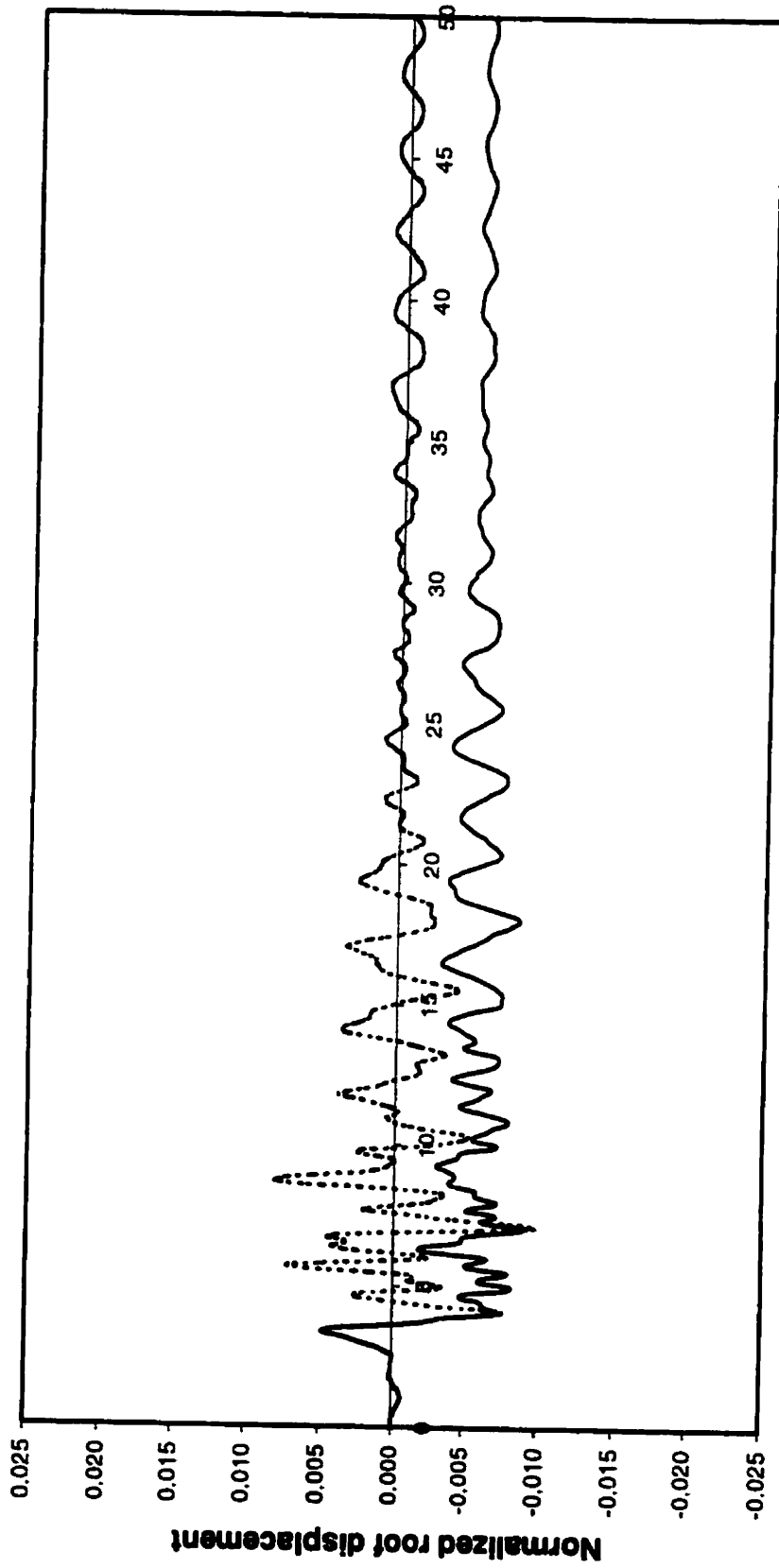
**Figure A.19**  
**Maximum interstorey drift ratio for record # 2 (Loma Prieta record # 2)**



1.75	1.49	1.32	1.30	1.46	1.72
3.10	2.68	2.92	2.92	2.84	3.05
0.60	0.58	0.61	0.61	0.58	0.63
0.46	0.44	0.44	0.44	0.45	0.46
0.13	0.10	0.13	0.13	0.10	0.13
0.14	0.14	0.13	0.13	0.14	0.14
0.16	0.16	0.15	0.16	0.16	0.16
0.27	0.25	0.25	0.25	0.25	0.27
0.66	0.55	0.55	0.55	0.55	0.65
0.77	0.61	0.61	0.61	0.61	0.78



**Figure A.20**  
**Strength deterioration in percent for record # 3 (Northridge record)**  
**5% strain hardening ratio**



Time in seconds

..... elastic — inelastic 5% S.H.

**Figure A.21**  
**Normalized roof displacement record # 3 (Northridge record)**

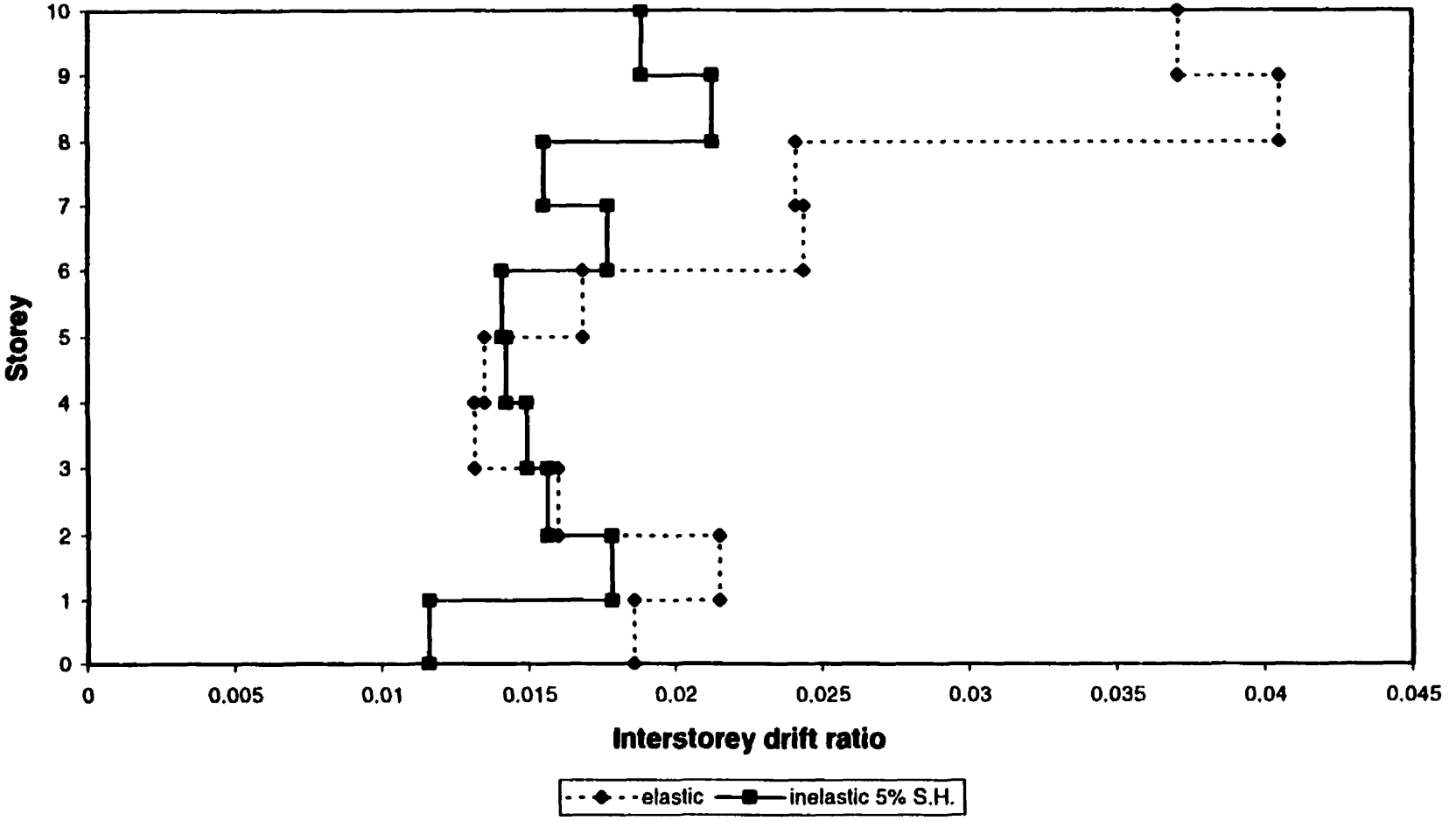
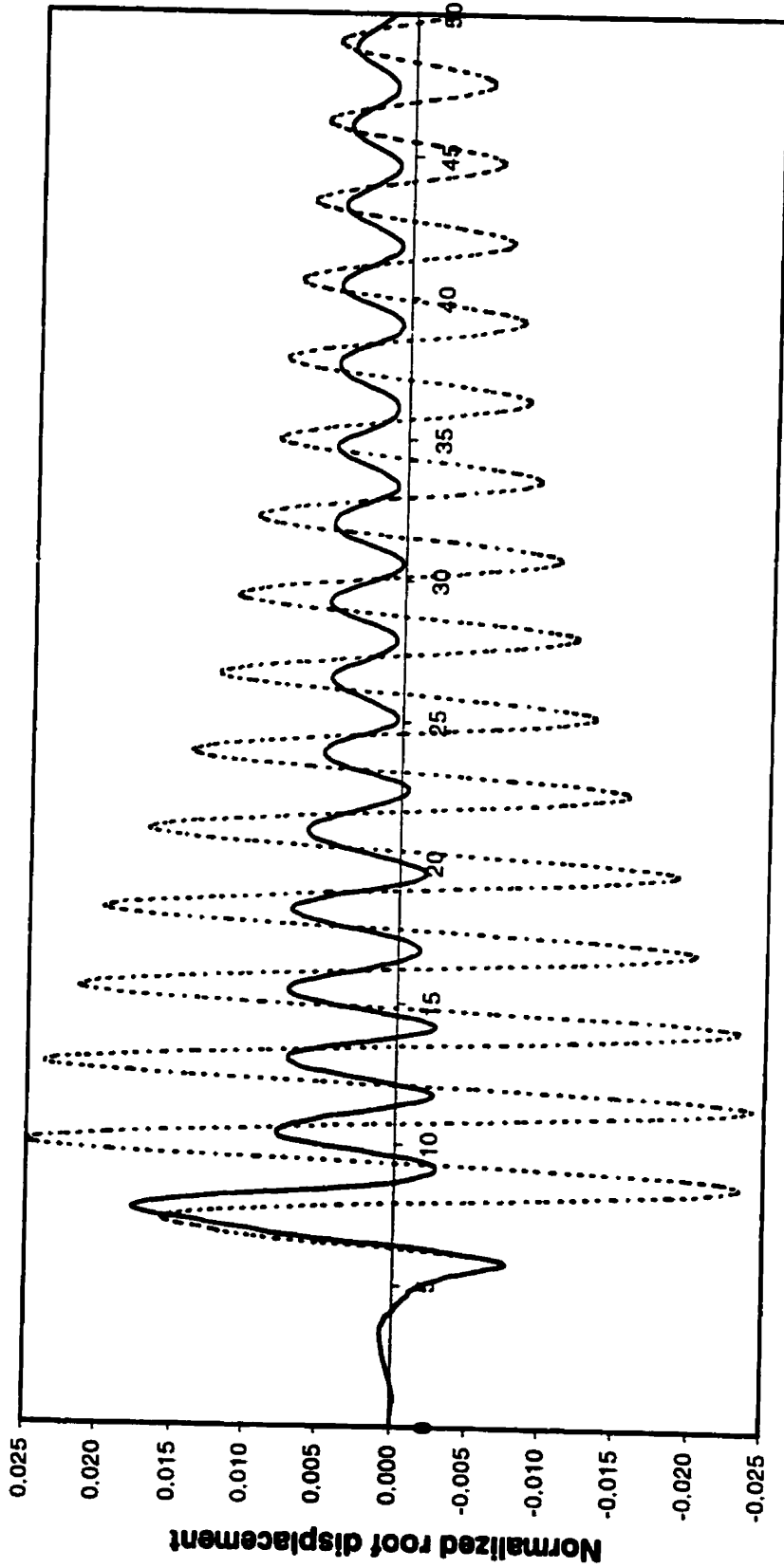


**Figure A.22**  
**Maximum interstorey drift ratio for record # 3 (Northridge record)**

0.00	0.00	0.00	0.00	0.00	0.00
0.00	0.30	0.00	0.38	0.00	0.29
0.00	0.35	0.14	0.00	0.10	0.00
0.49	1.14	0.62	1.27	0.52	1.08
1.31	1.26	1.38	1.38	1.26	1.30
2.29	2.17	2.33	2.33	2.17	2.28
1.44	1.33	1.42	1.41	1.33	1.44
2.74	1.69	1.77	1.77	1.69	1.81
2.05	1.94	2.00	1.99	1.94	2.05
2.18	1.95	1.98	1.98	1.94	2.14



**Figure A.23**  
**Strength deterioration in percent for record # 4 (Long Beach)**  
**5% strain hardening ratio**



Time in seconds

.....elastic — inelastic 5% S.H.

**Figure A.24**  
**Normalized roof displacement record # 4 (Long Beach record)**

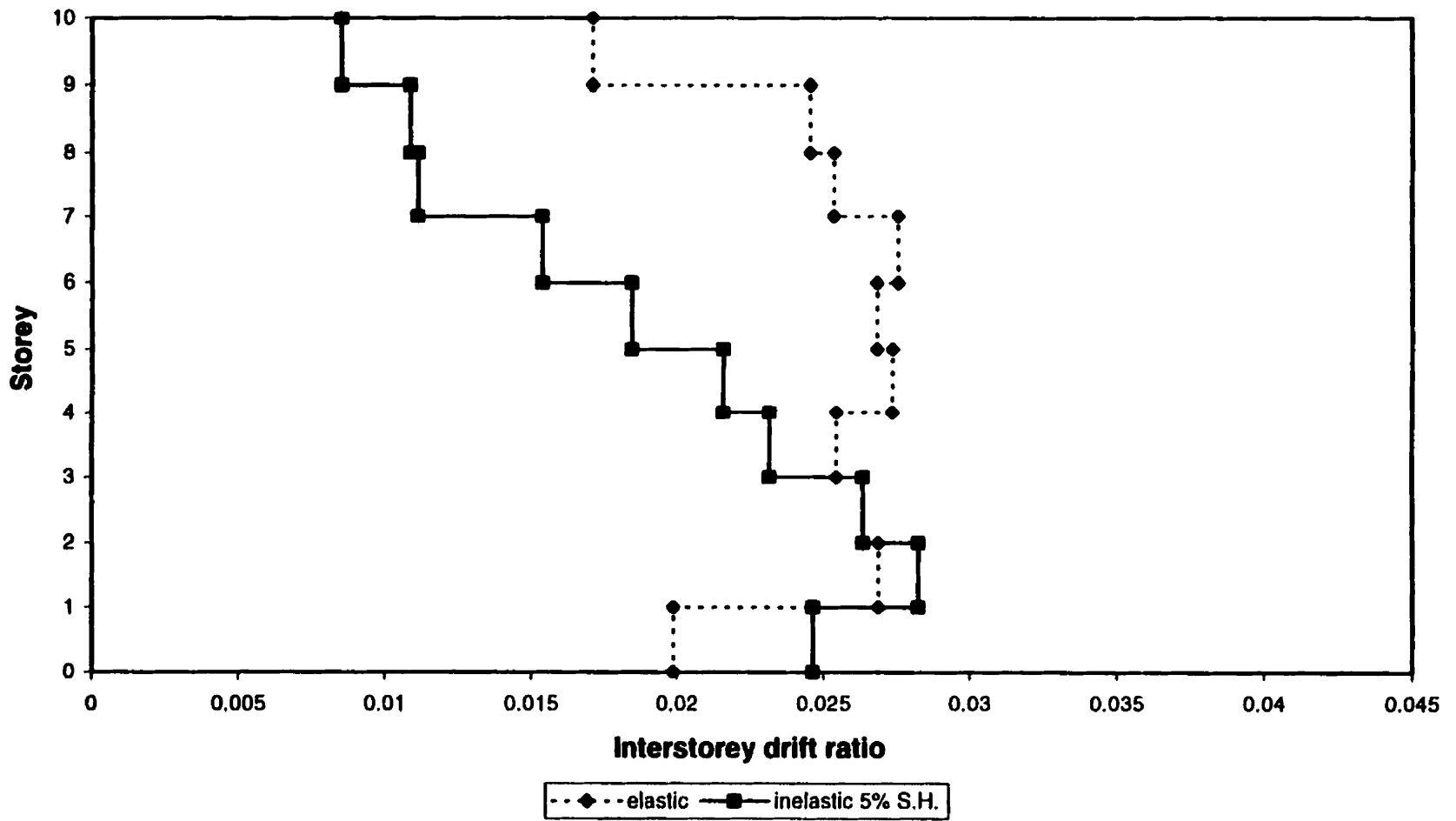


**Figure A.25**  
**Maximum interstorey drift ratio for record # 4 (Long Beach record)**

0.82	1.52	0.74	1.43	0.81	1.72
5.33	4.97	5.87	5.63	5.23	5.10
10.16	10.10	9.56	9.56	10.11	10.19
5.87	8.36	6.44	8.89	5.97	8.20
2.57	5.42	2.84	5.84	2.55	5.43
1.09	2.18	1.10	2.38	0.96	2.36
0.45	0.55	0.25	0.59	0.22	0.61
0.68	0.54	0.48	0.48	0.54	0.68
0.81	0.71	0.72	0.72	0.71	0.81
0.71	0.53	0.54	0.55	0.53	0.73



**Figure A.26**  
**Strength deterioration in percent for record # 5 (Morgan Hill)**  
**2.5% strain hardening ratio**

0.83	1.65	0.73	1.54	0.79	1.64
5.49	5.16	6.13	5.88	5.43	5.24
9.22	9.31	9.83	9.82	9.28	9.23
5.92	3.72	6.48	3.92	6.02	3.66
2.51	4.70	2.78	5.13	2.48	4.77
1.09	2.03	1.10	0.75	0.93	0.73
0.30	0.50	0.27	0.56	0.21	0.58
0.56	0.45	0.48	0.48	0.45	0.56
0.83	0.72	0.74	0.74	0.72	0.82
0.58	0.41	0.42	0.42	0.41	0.73



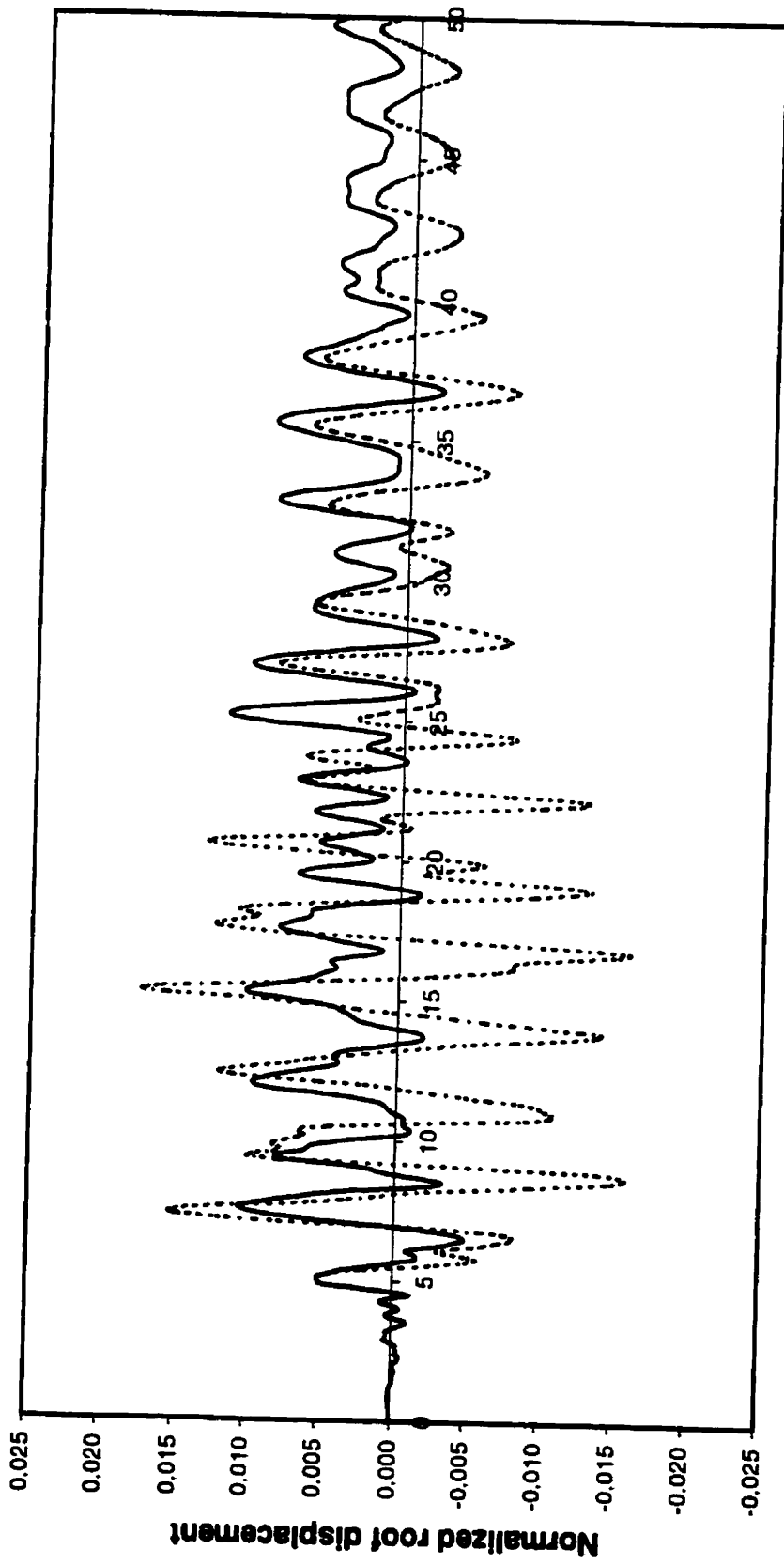
**Figure A.27**  
**Strength deterioration in percent for record # 5 (Morgan Hill)**  
**5% strain hardening ratio**



0.82	1.51	0.69	1.40	0.76	1.51
4.75	4.40	5.04	4.78	4.68	4.48
9.71	9.59	9.14	9.13	9.51	9.41
5.77	3.64	6.39	4.01	5.82	3.57
2.42	2.14	2.76	2.22	2.38	2.16
1.08	0.60	1.08	1.08	0.90	1.08
0.27	0.45	0.24	0.50	0.18	0.52
0.53	0.43	0.46	0.46	0.43	0.53
0.82	0.74	0.75	0.75	0.73	0.85
0.57	0.55	0.57	0.57	0.56	0.76



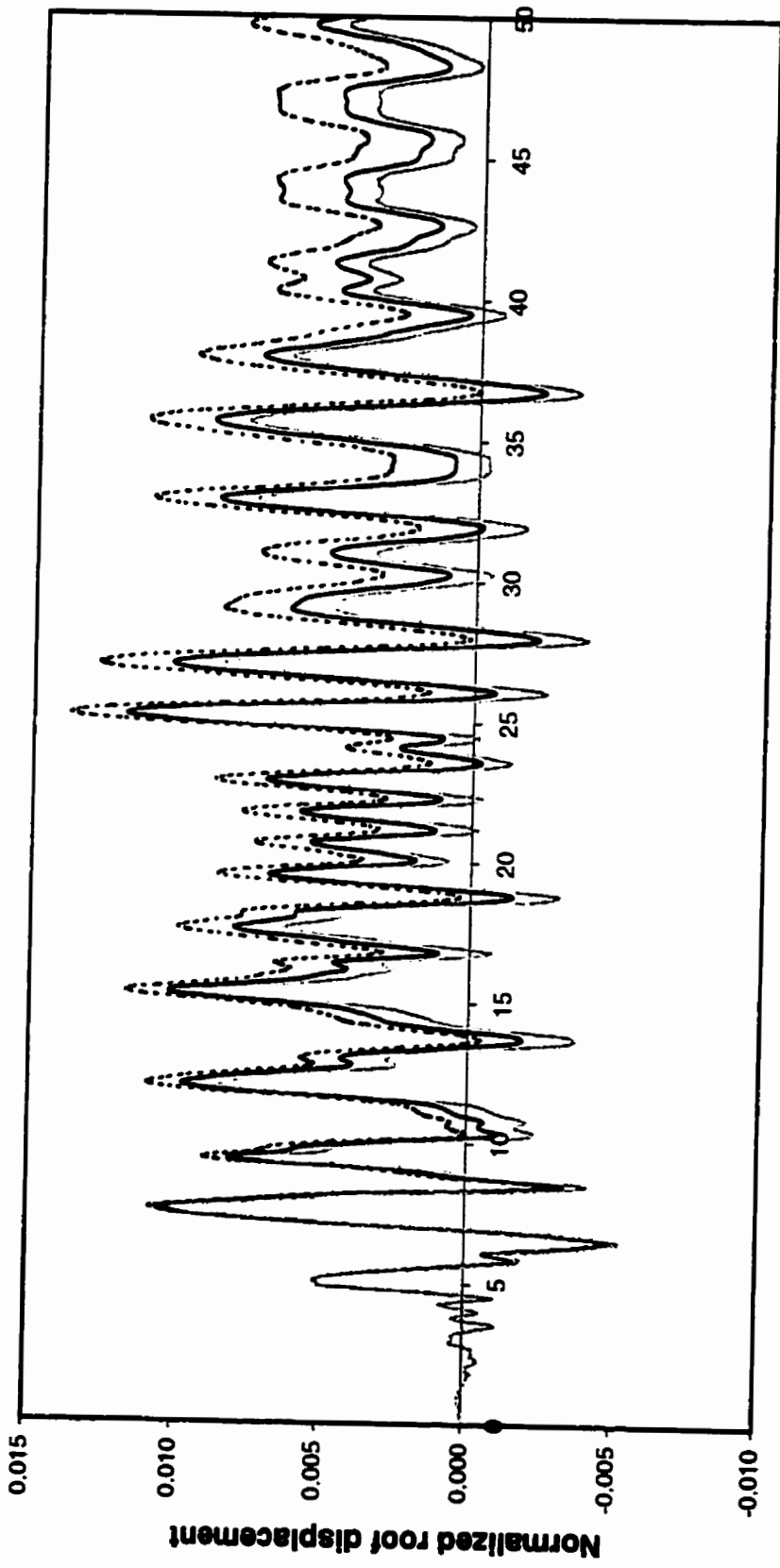
**Figure A.28**  
**Strength deterioration in percent for record # 5 (Morgan Hill)**  
**10% strain hardening ratio**



**Time in seconds**

..... elastic — inelastic 5% S.H.

**Figure A.29**  
**Normalized roof displacement record # 5 (Morgan Hill record)**



**Time in seconds**  
 ..... 2.5% S.H. — 5% S.H. .... 10% S.H.

**Figure A.30**  
**Normalized inelastic roof displacement record # 5 (Morgan Hill)**

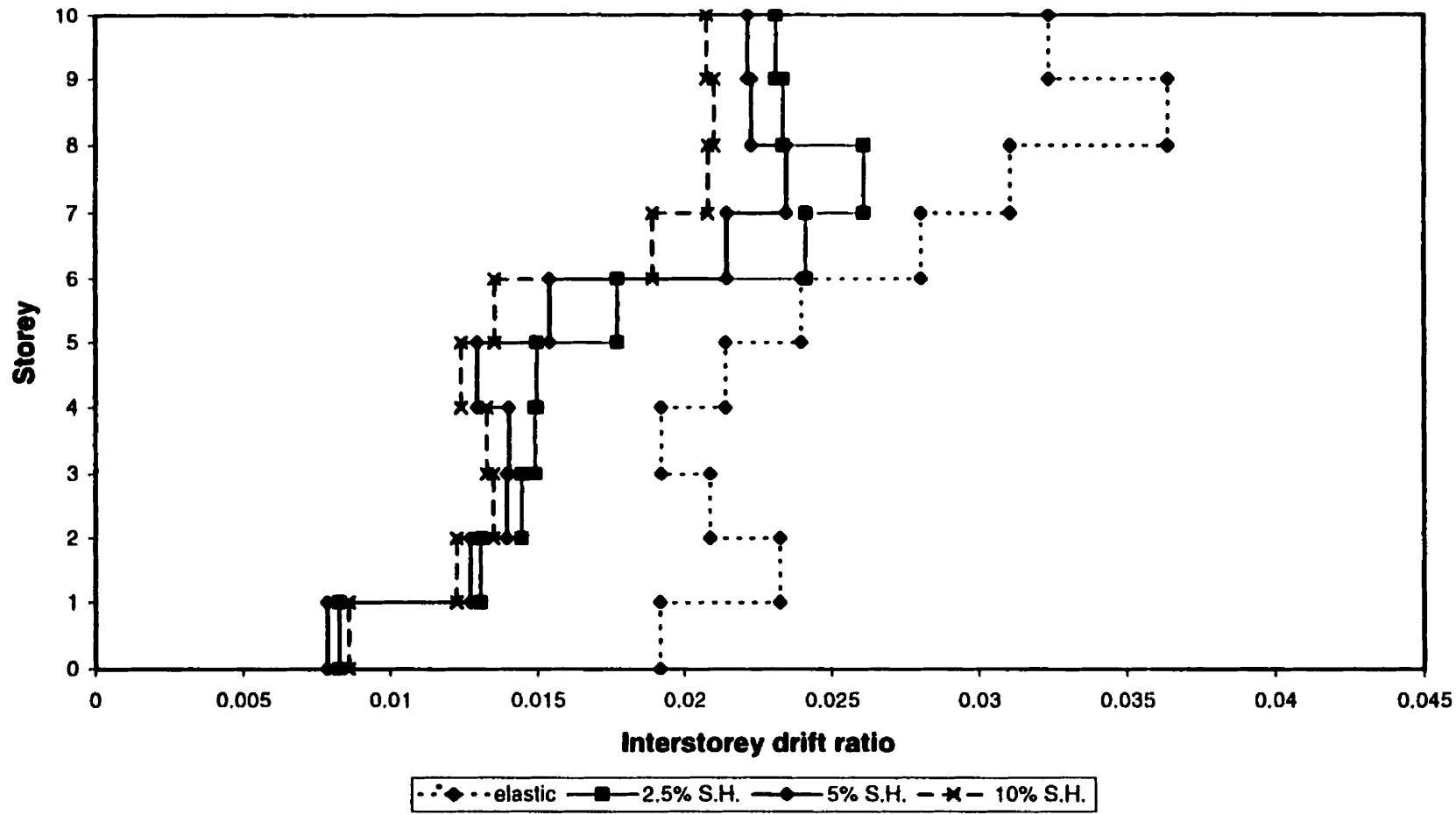


**Figure A.31**  
**Maximum interstorey drift ratio for record # 5 (Morgan Hill record)**

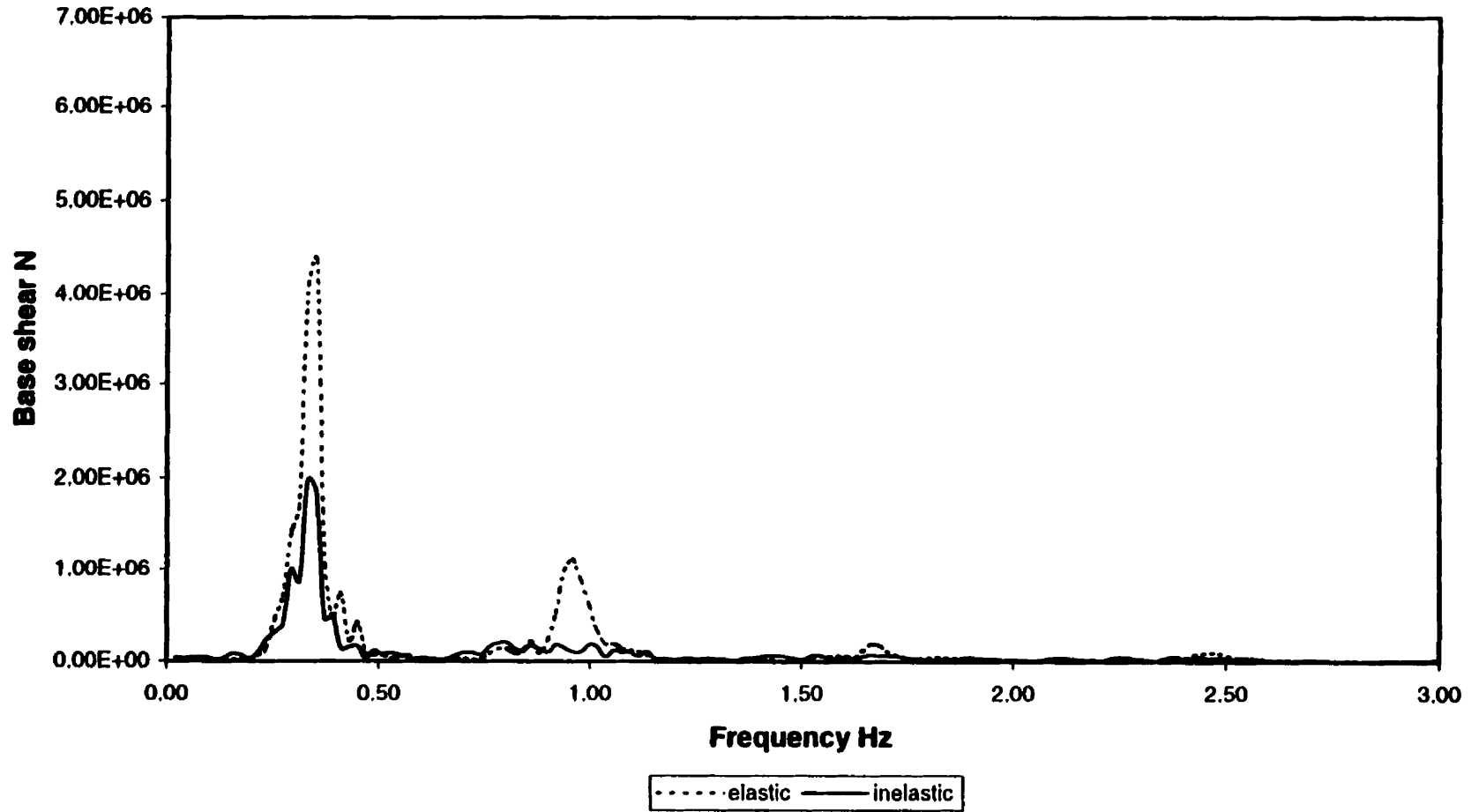


**Figure A.32**  
**Fourier spectrum for base shear history record #1**  
**(Loma Prieta record # 1)**

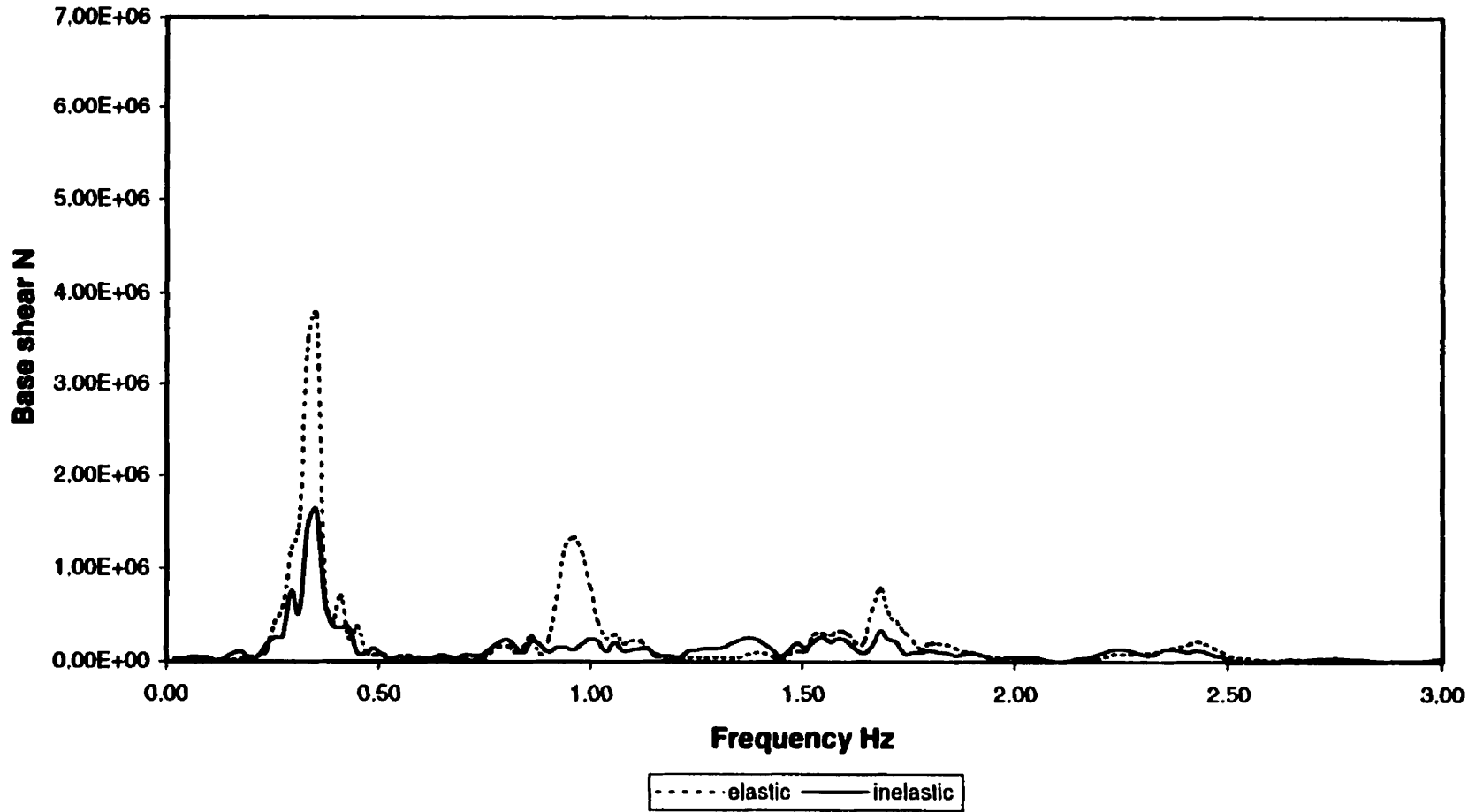


**Figure A.33**  
**Fourier spectrum for base shear history record #2**  
**(Loma Prieta record # 2)**

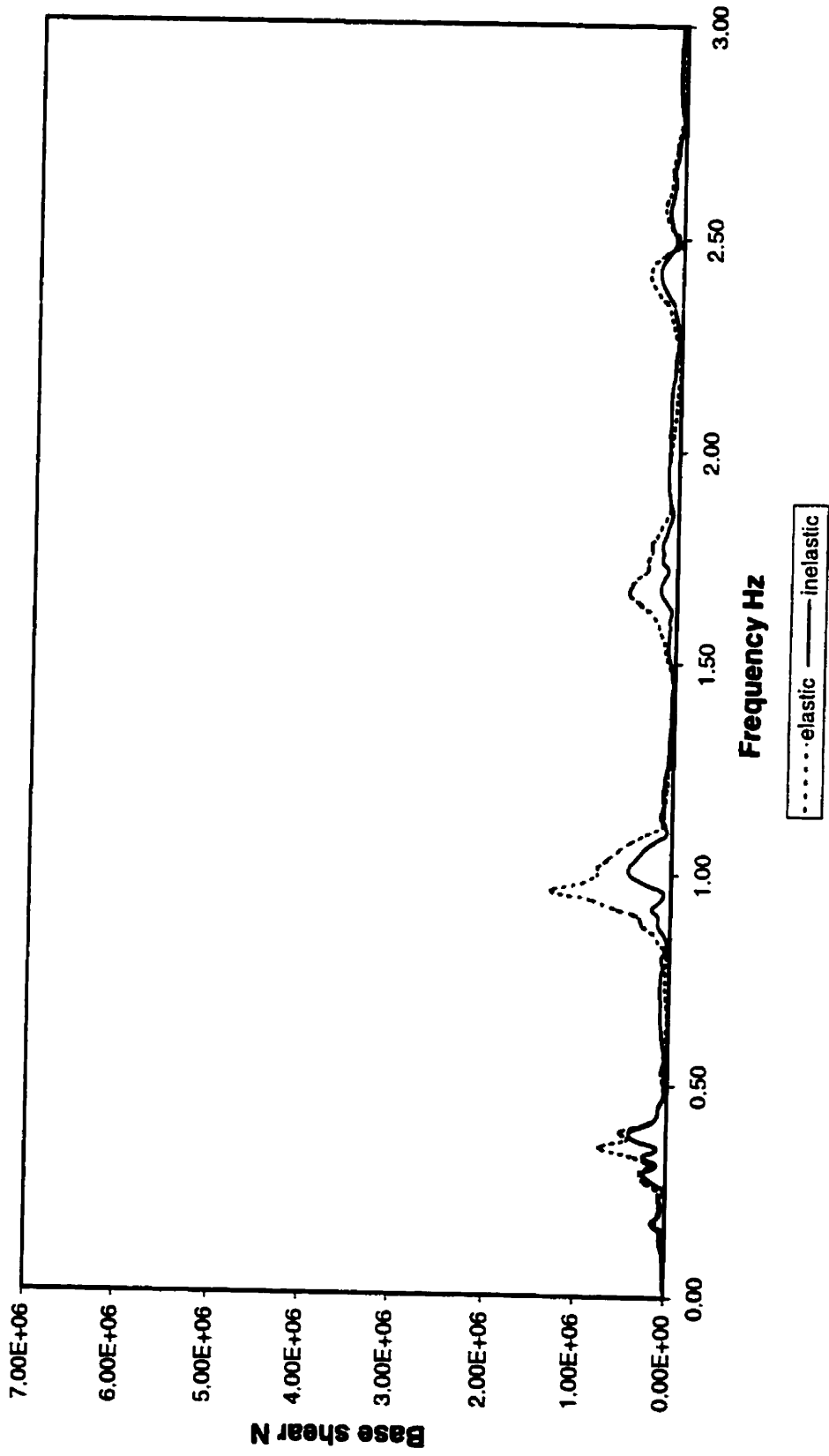


**Figure A.34**  
**Fourier spectrum for base shear history record #3**  
**(Northridge record)**

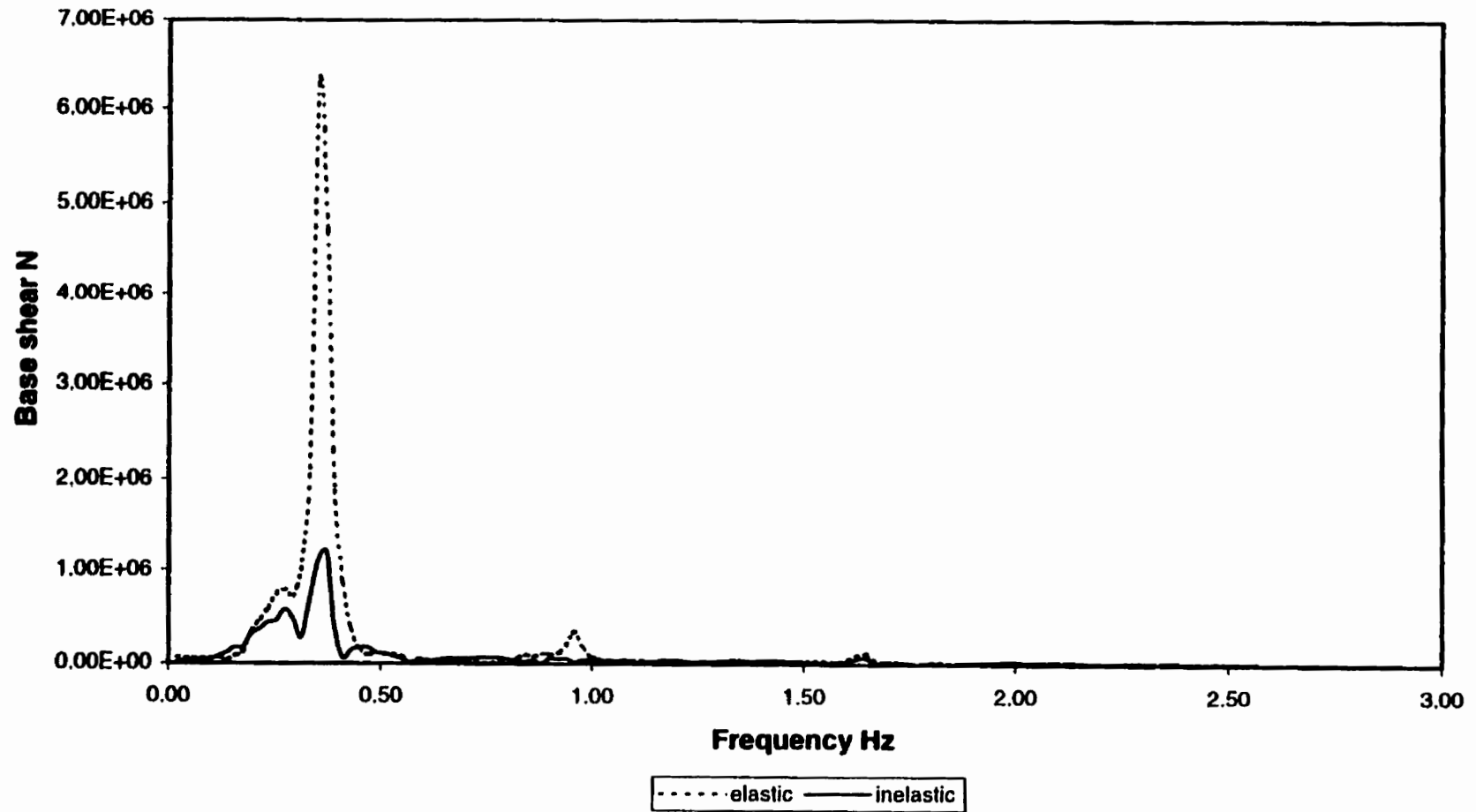


**Figure A.35**  
**Fourier spectrum for base shear history record #4**  
**(Long Beach record)**



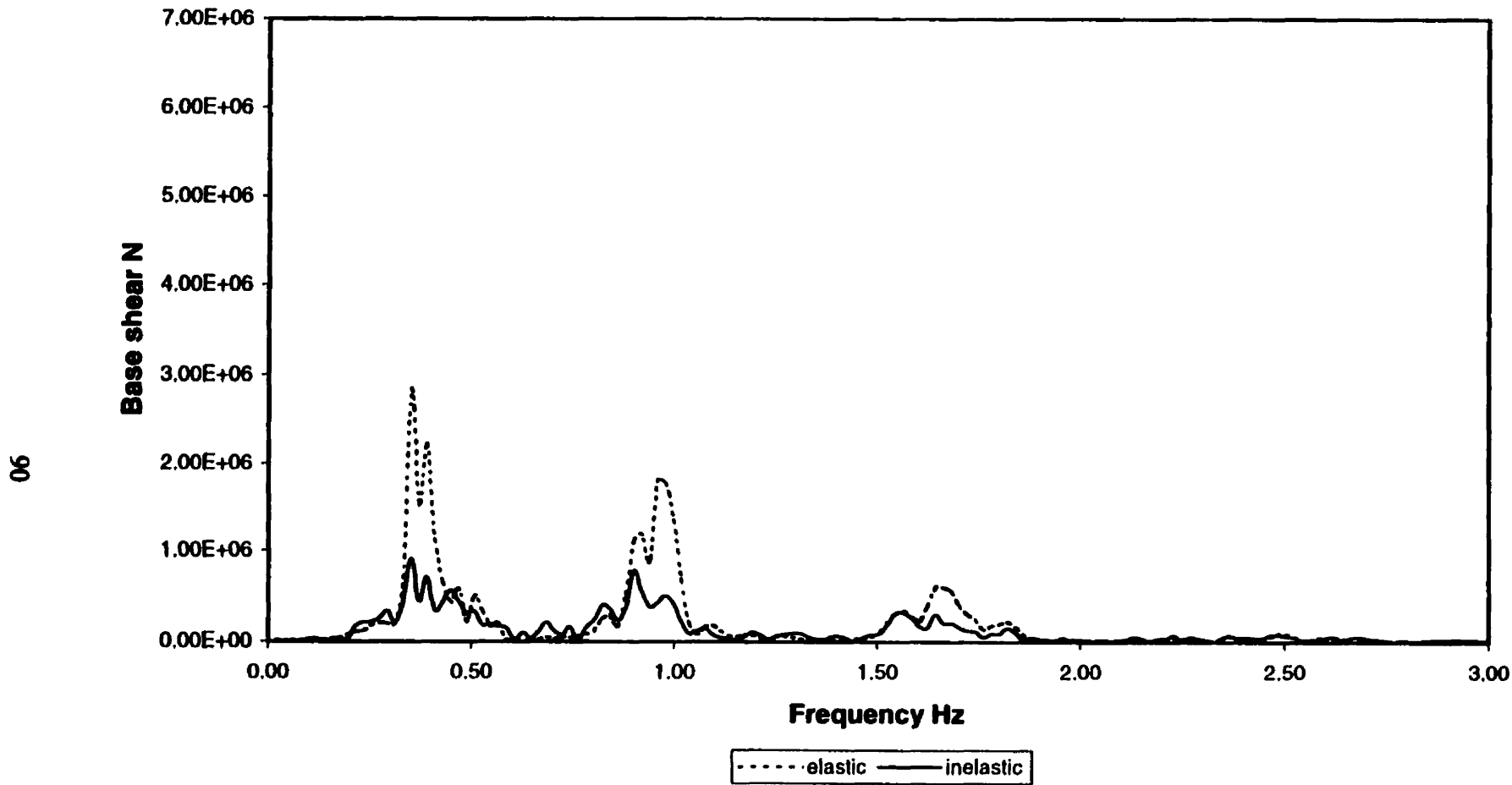


**Figure A.36**  
**Fourier spectrum for base shear history record #5**  
**(Morgan Hill record)**

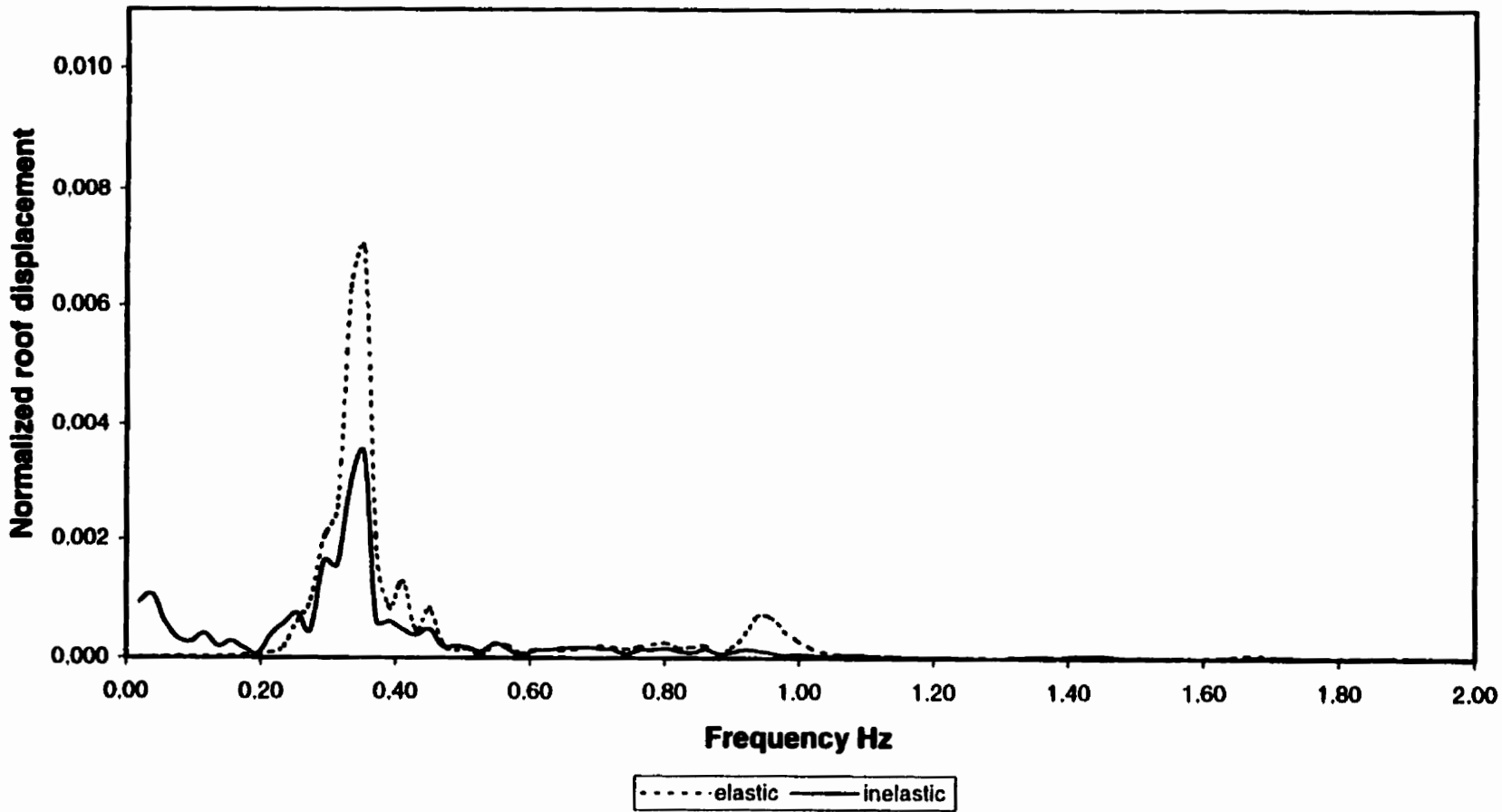


**Figure A.37**  
**Fourier spectrum for roof displacement history record #1**  
**(Loma Prieta record # 1)**

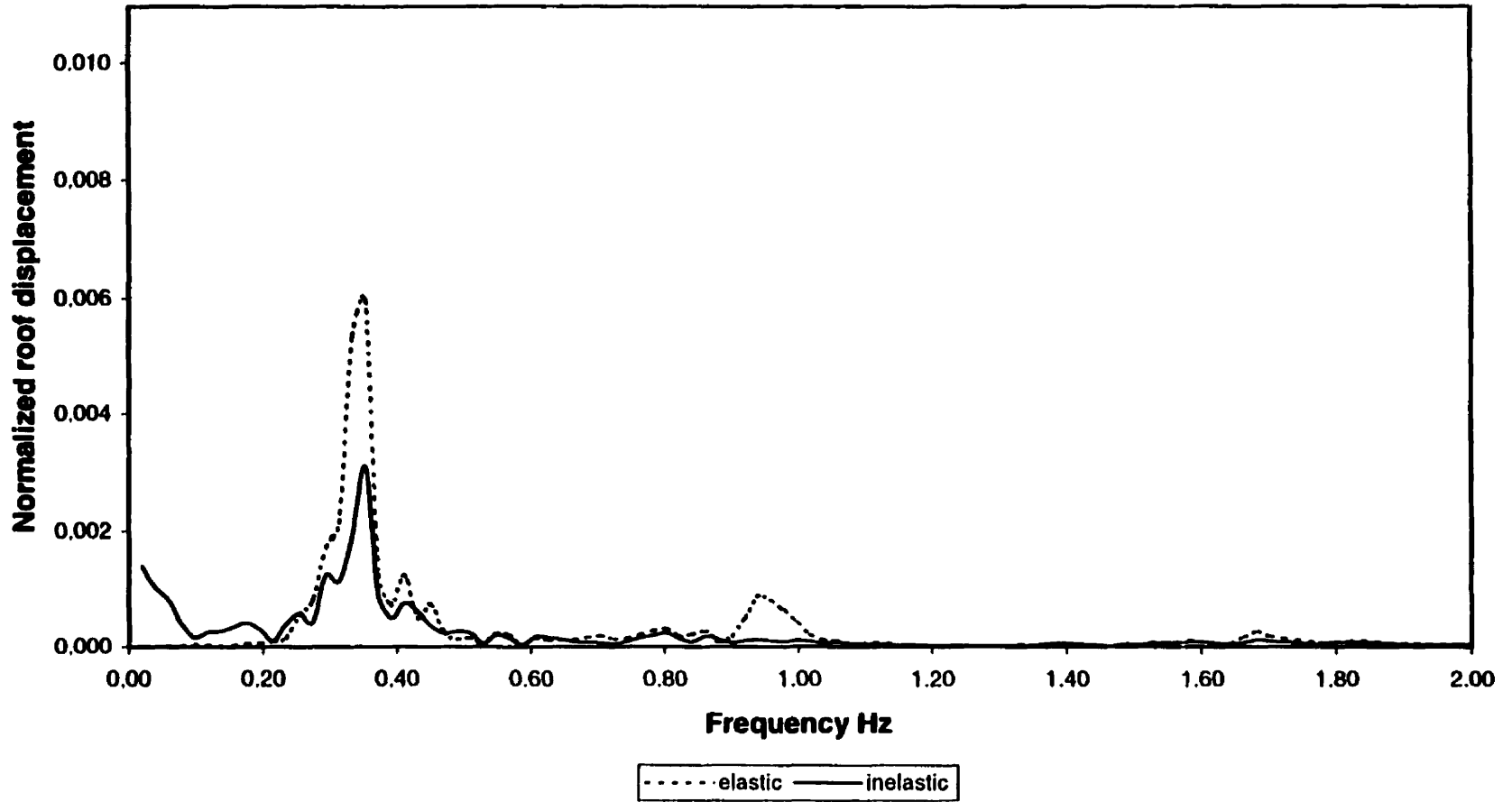


**Figure A.38**  
**Fourier spectrum for roof displacement history record #2**  
**(Loma Prieta record # 2)**

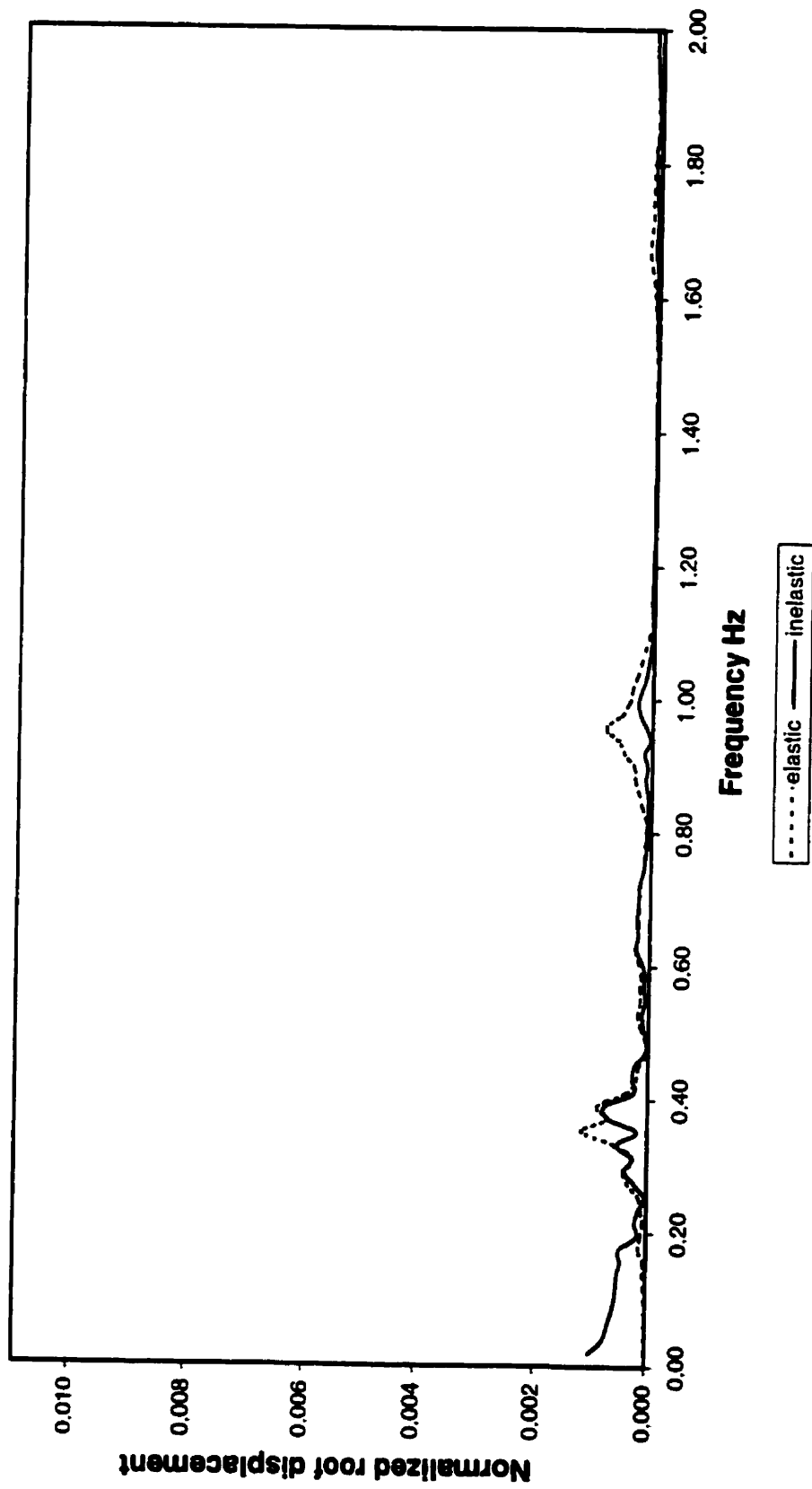


**Figure A.39**  
**Fourier spectrum for roof displacement history record #3**  
**(Northridge record)**

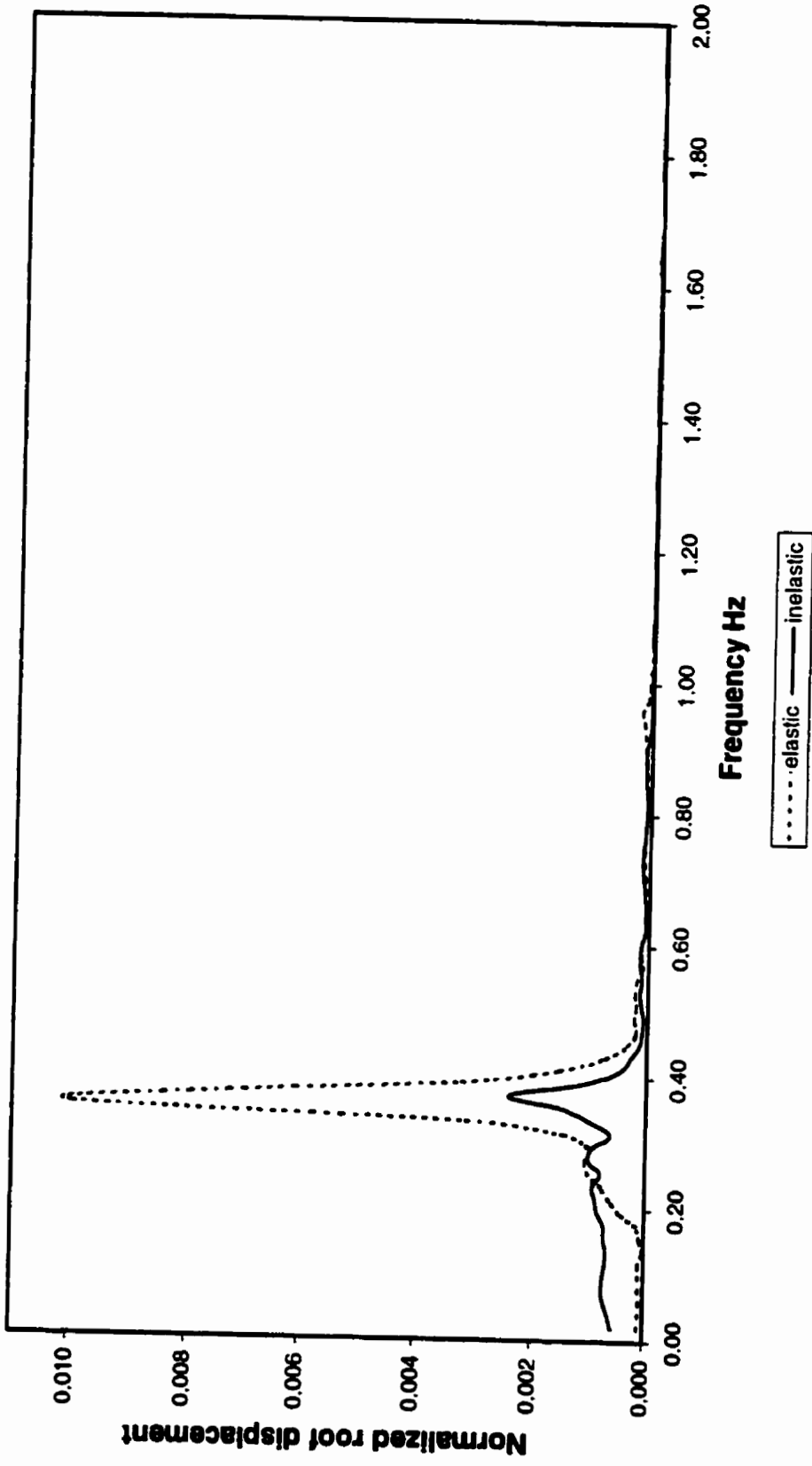


**Figure A.40**  
**Fourier spectrum for roof displacement history record #4**  
**(Long Beach record)**

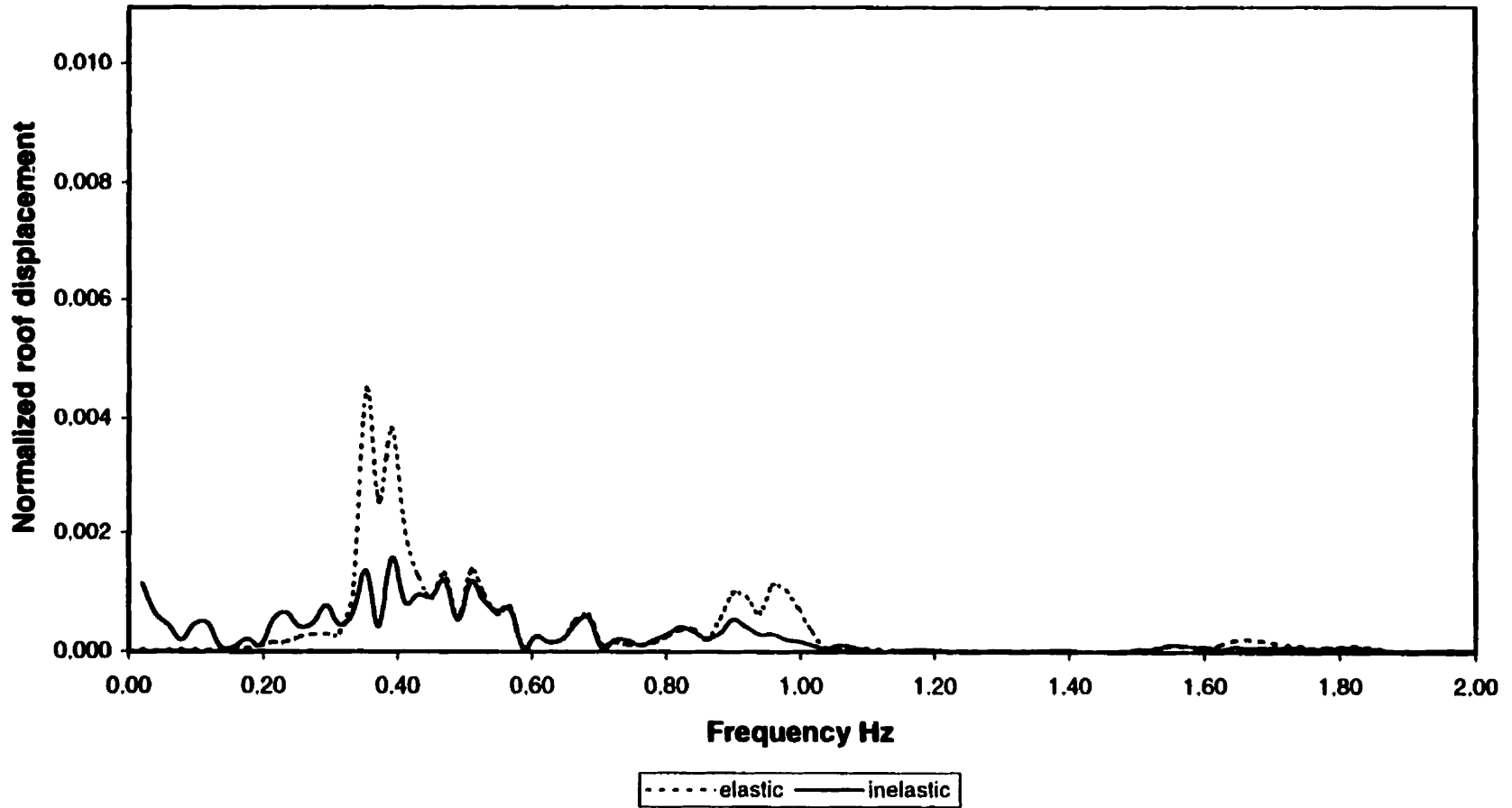


**Figure A.41**  
**Fourier spectrum for roof displacement history record #5**  
**(Morgan Hill record)**

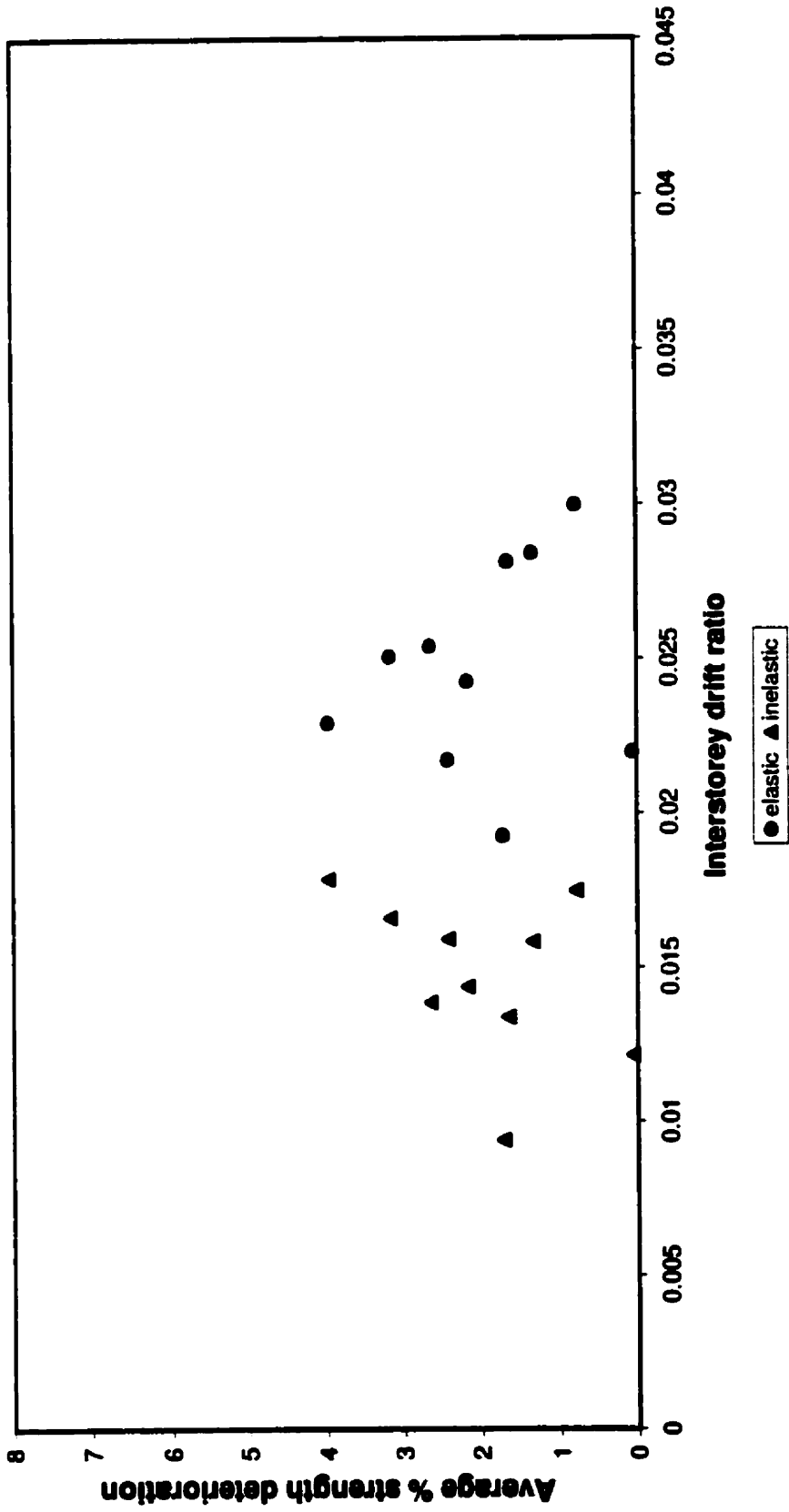


**Figure A.42**  
**% strength deterioration versus maximum interstorey drift ratio**  
**record #1 (Loma Prieta record # 1)**

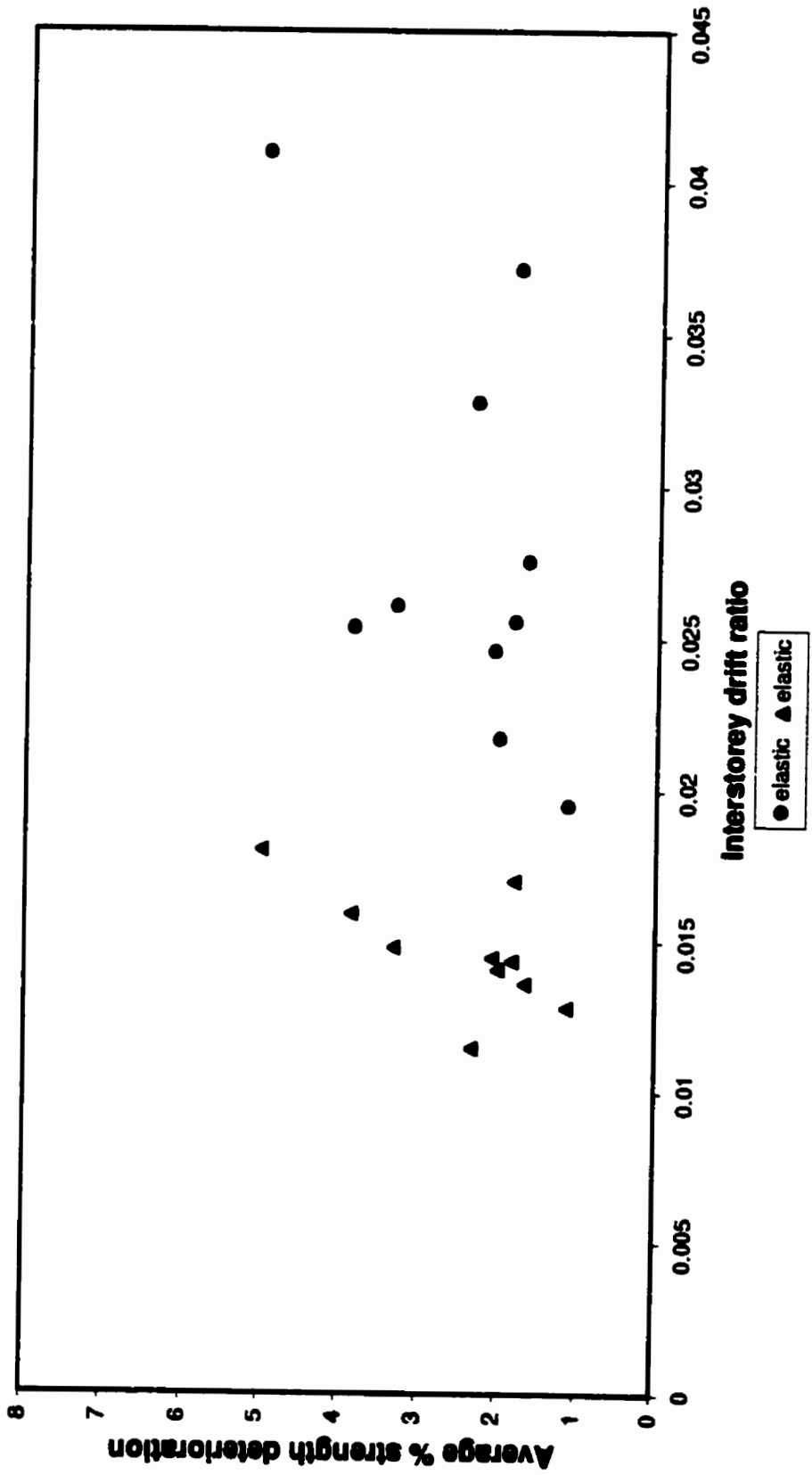


**Figure A.43**  
**% strength deterioration versus maximum interstorey drift ratio**  
**record #2 (Loma Prieta record # 2)**



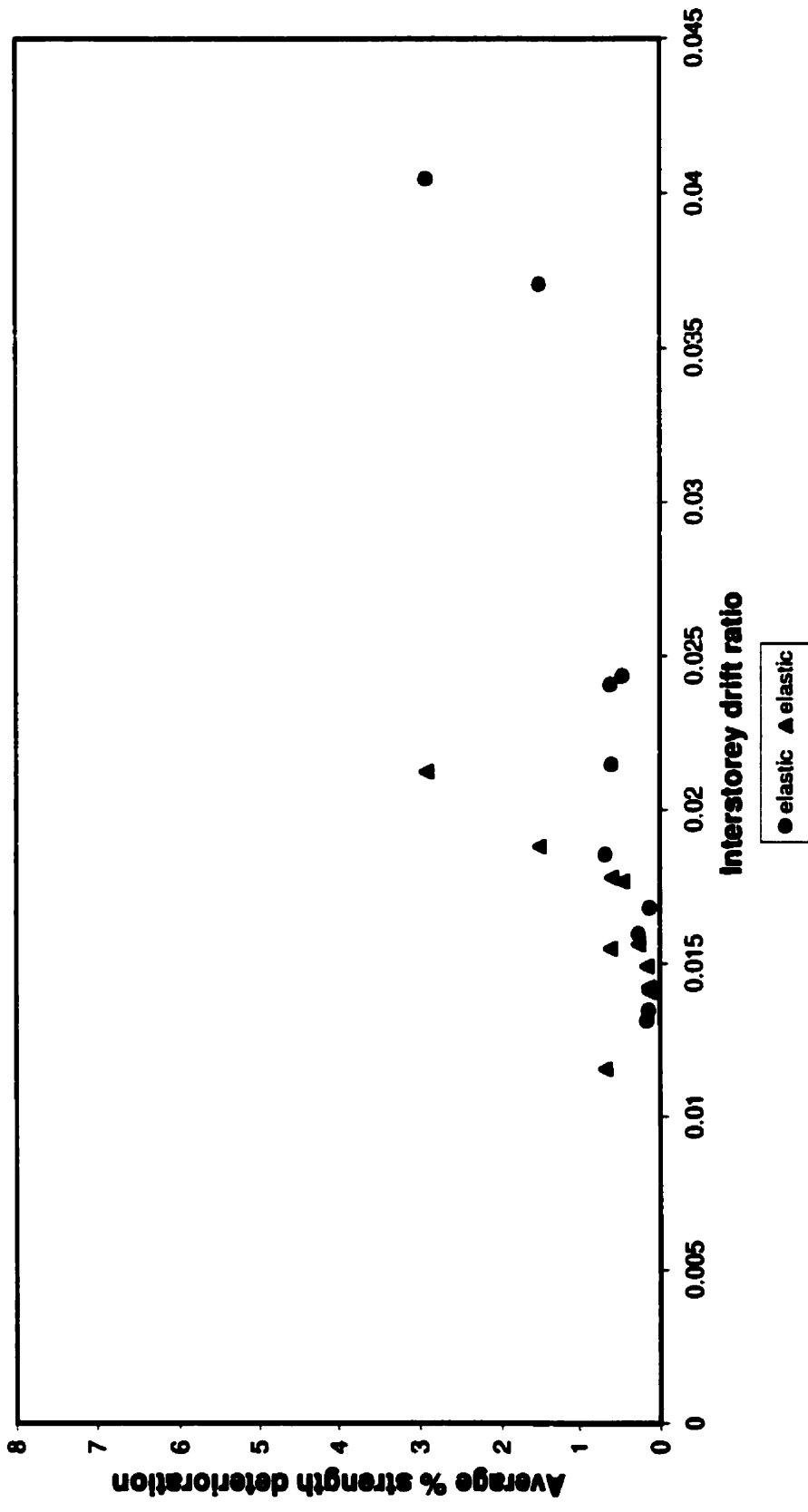


**Figure A.44**  
**% strength deterioration versus maximum interstorey drift ratio**  
**record #3 (Northridge record)**

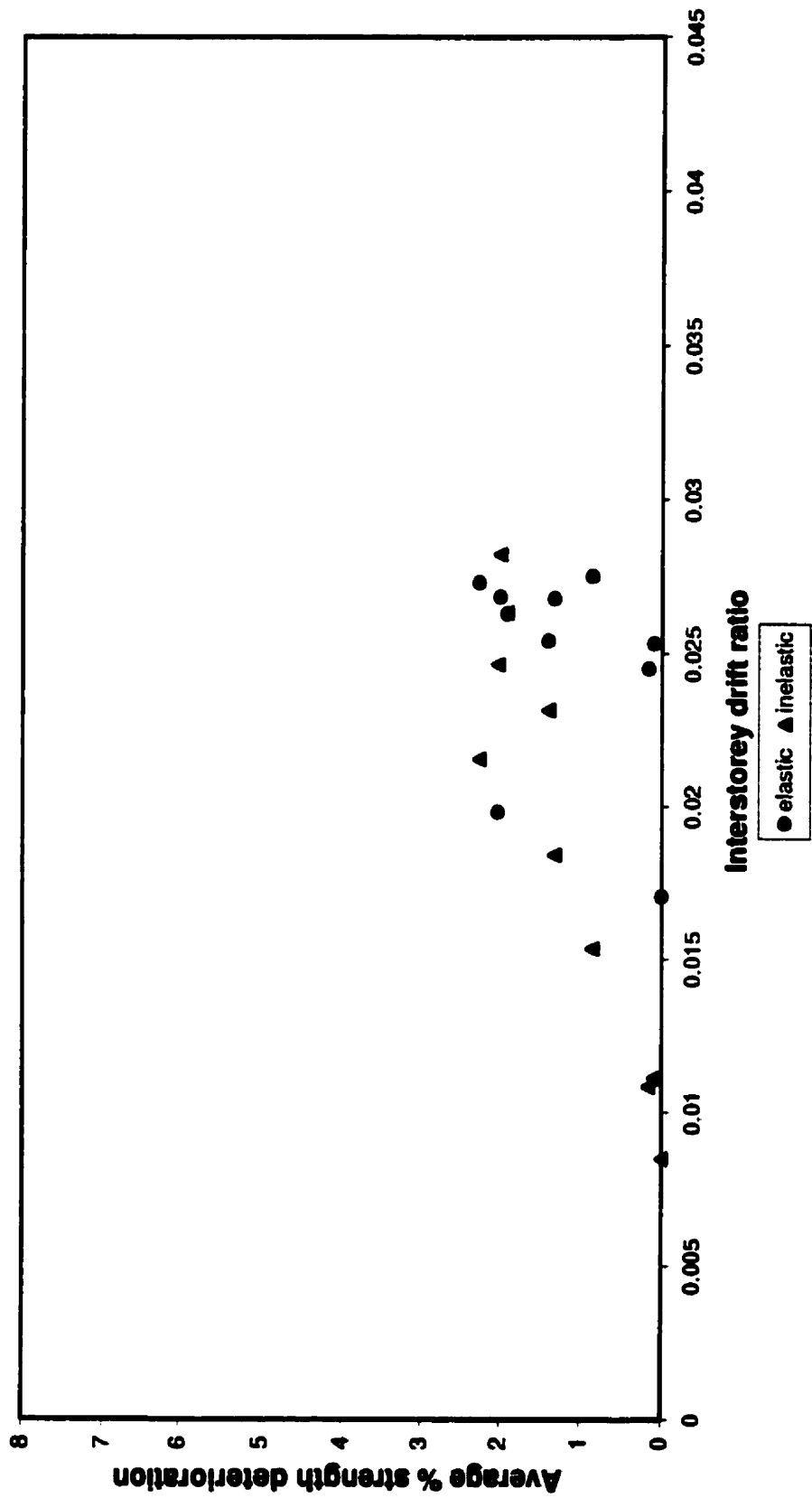


**Figure A.45**  
**% strength deterioration versus maximum interstorey drift ratio**  
**record #4 (Long Beach record)**

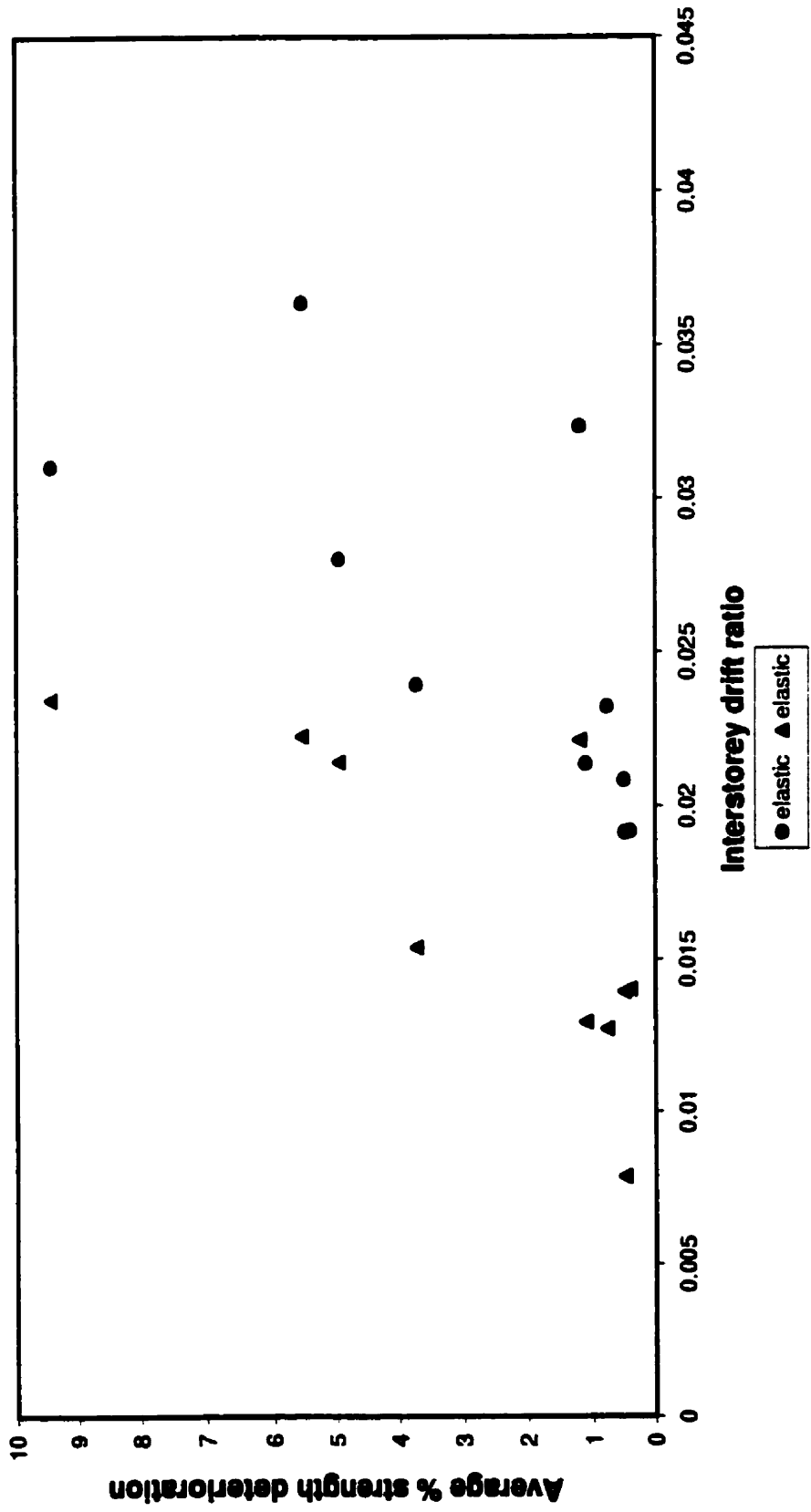


**Figure A.46**  
**% strength deterioration versus maximum interstorey drift ratio**  
**record #5 (Morgan Hill record)**

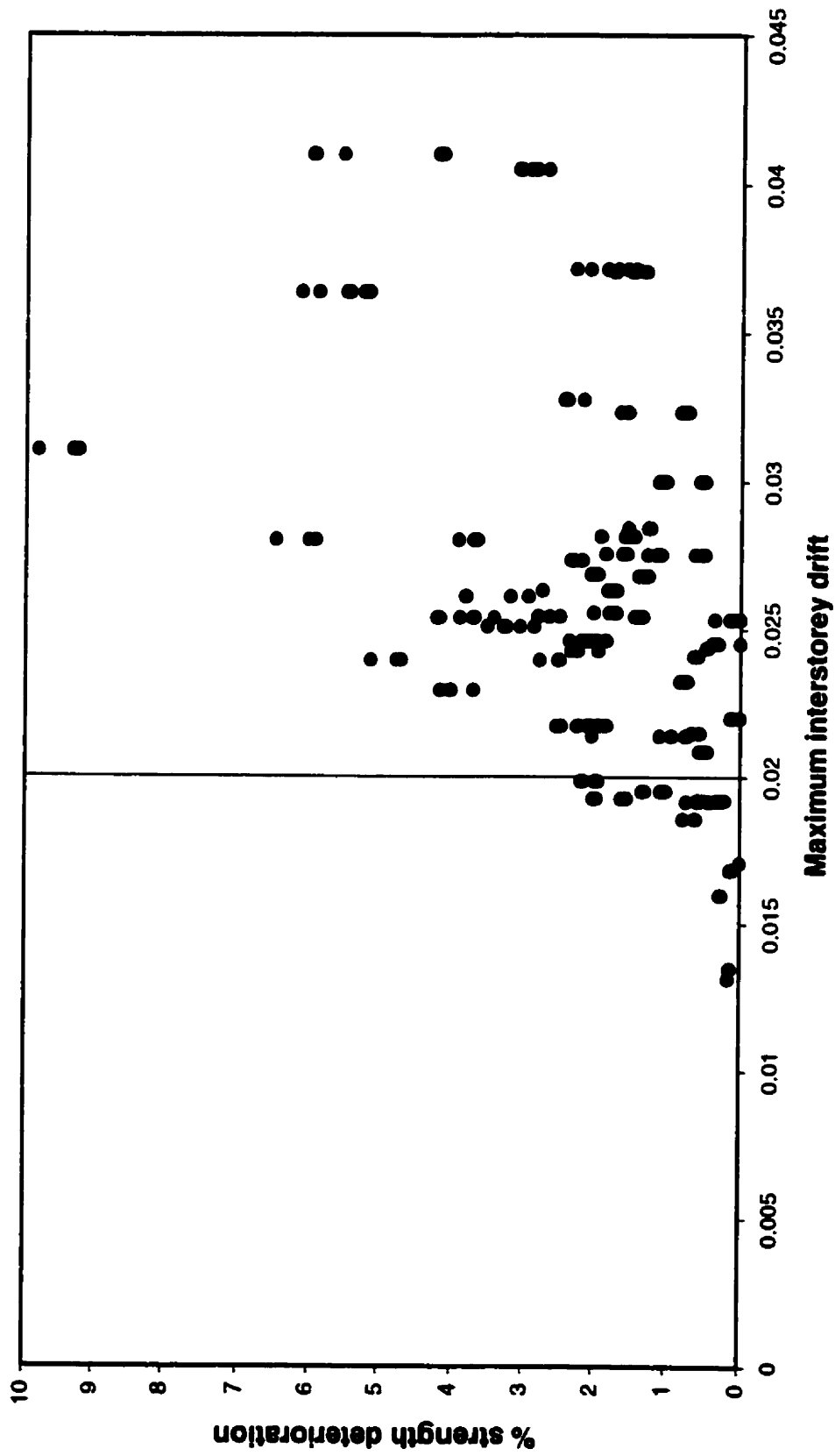


**Figure A.47**  
**Elastic maximum interstorey drift ratio versus damage**

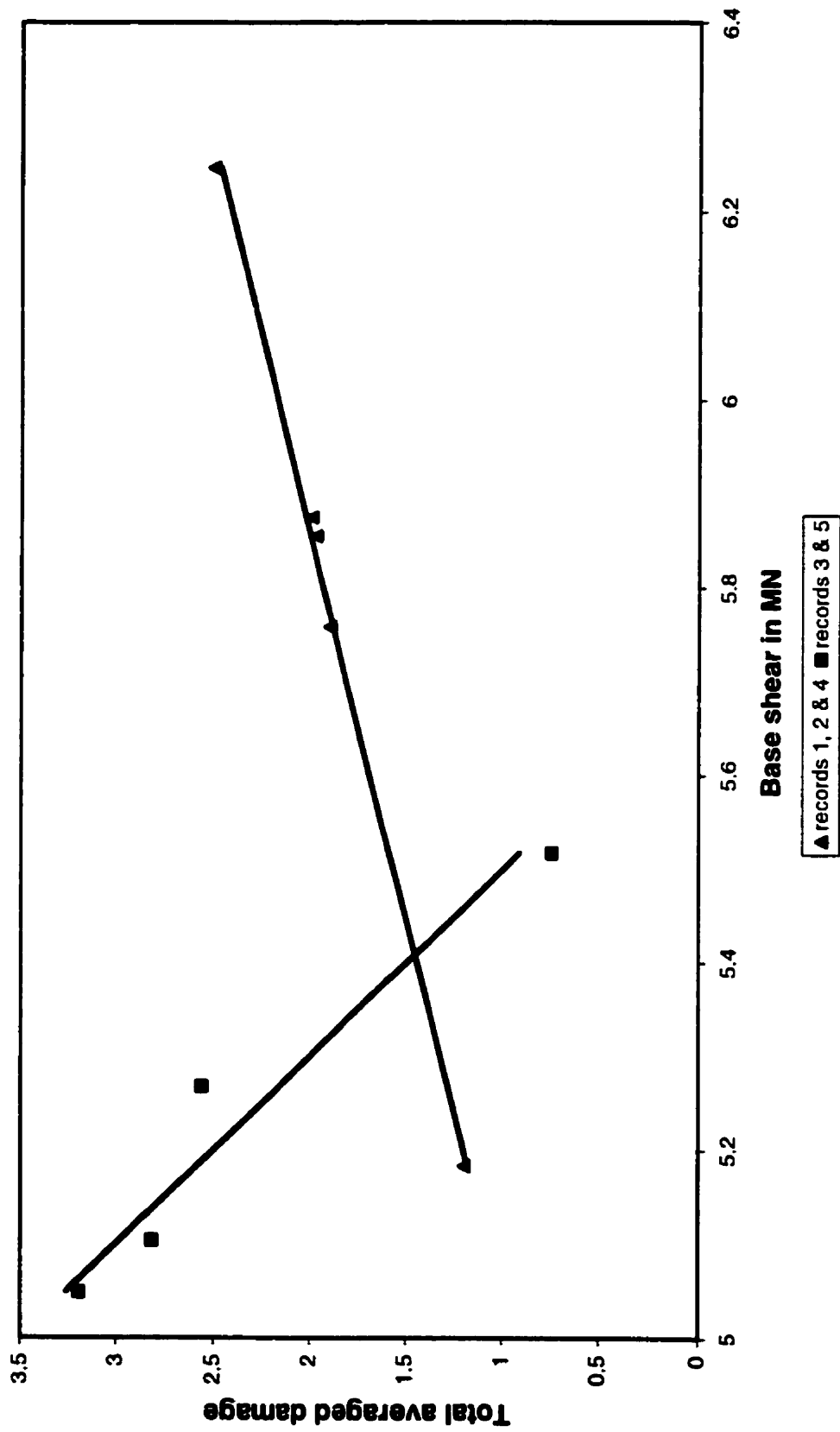


**Figure A.48**  
**Base shear versus total averaged damage**

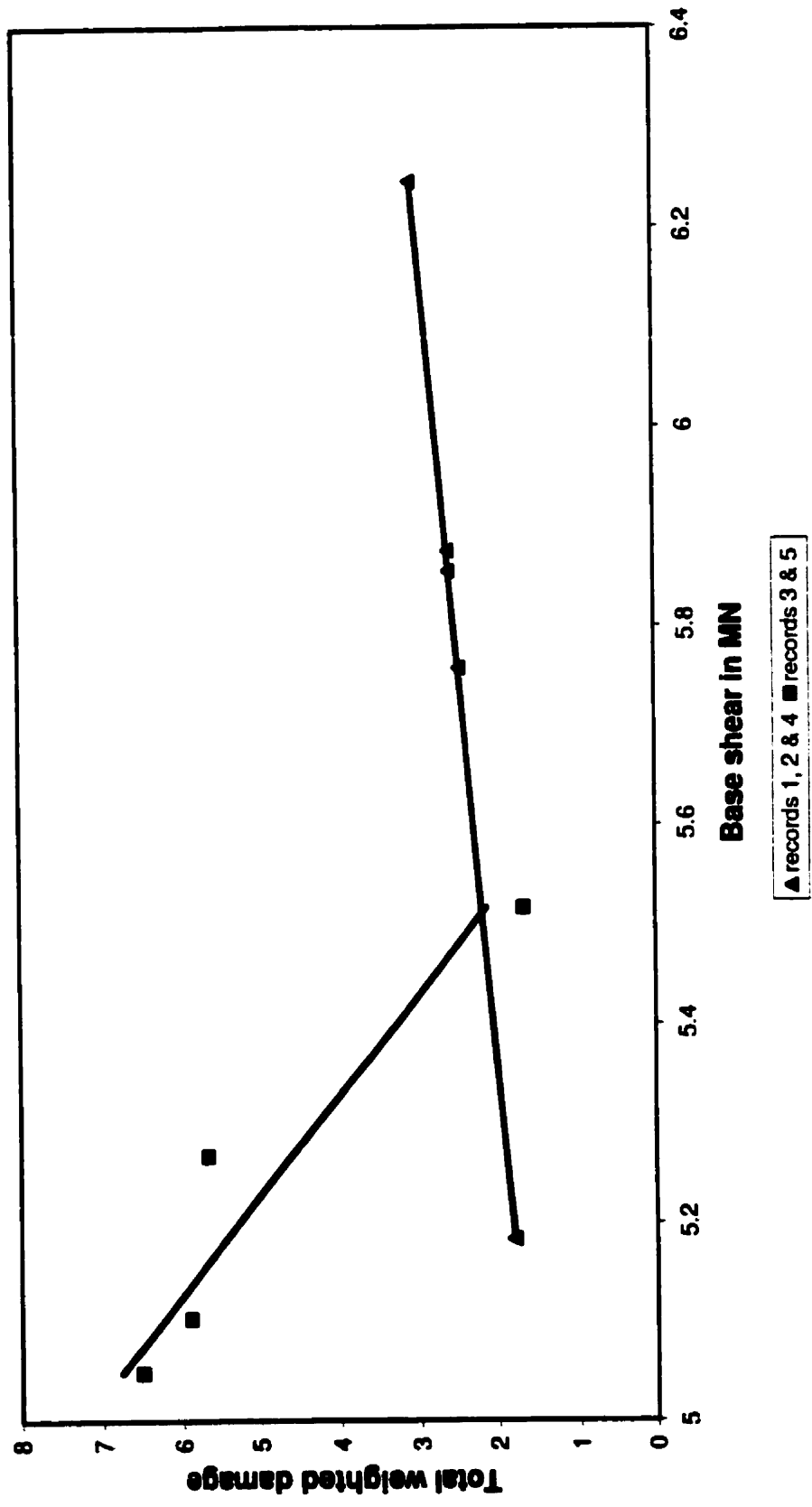


**Figure A.49**  
**Base shear versus total weighted damage**

## APPENDIX B

### FORTRAN PROGRAM FOR CALCULATING THE RESPONSE SPECTRUM OF GROUND ACCELERATION RECORDS

CC—PROGRAM TO CALCULATE THE RESPONSE SPECTRUM OF GROUND ACCELERATION  
CC THE PROGRAM IS MODIFIED FROM A PROGRAM ACCOMPANYING THE EXAMPLE  
CC MANUALS OF THE PROGRAM ABAQUS  
CC

```
PROGRAM RESPON
  IMPLICIT REAL*8 (A-H,O-Z)
  DIMENSION A(2,2),B(2,2),Q(4000),QP(4000),QPP(4000),
1ACC(4000),TAB(8),FR(1000),QM(1000),QPM(1000),
1QPPM(1000)
  parameter(one=1.d0,two=2.d0,zero=0.d0,dt=5.d-3,fact=-1.316d-2)
  DATA NACC/4000/
C   DATA NACC/2500/
  DATA FREQMIN/0.01d0/
  DATA FREQMAX/10.d0/
  DATA INT/1000/
C   STORAGE ALLOCATED FOR A MAXIMUM OF 2500 TIMEPOINTS
C   IN THE EARTHQUAKE HISTORY
CC READ ACCELERATION HISTORY FROM FILE.
CC DISPLACEMENT SPECTRUM
CC WILL BE WRITTEN TO FILE *.DIS, VELOCITY SPECTRUM TO FILE *.VEL.
C
C**** TIME INTEGRATION FOR LINEAR ACCELERATION (EXACT SOLUTION)
C   DATA DAMP DENOTES DAMPING AS PERCENTAGE OF CRITICAL DAMPING
C   DATA FREQMIN AND FREQMAX DEFINE FREQUENCY RANGE
C   DATA INT DEFINES NUMBER OF POINTS IN FREQUENCY RANGE
C** THIS INPUT ASSUMES THAT 301020I.INP HAS BEEN COPIED TO QUAKE.AMP
  OPEN(UNIT=1,STATUS='OLD',FILE='LO3.ABQ')
  OPEN(UNIT=15,STATUS='UNKNOWN',FILE='LO3sc.DIS')
  OPEN(UNIT=16,STATUS='UNKNOWN',FILE='LO3sc.VEL')
  FRAC=ONE/DBLE(INT-1)
  DAMP=2.d-2
C*** INITIATE AMAT,BMAT BEFORE TIME INTEGRATION
  DO 10 I=1,2
  DO 10 J=1,2
  A(I,J)=ZERO
  B(I,J)=ZERO
  10 CONTINUE
C** READ AMPLITUDE DATA AND STORE ON ACC(2500)
  ACC(1)=0.
  READ(1,31) (ACC(I2), I2=2,(NACC-1))
  31 FORMAT(8(E10.4E1))
  ACC=ACC*FACT
  DFREQ=FREQMAX-FREQMIN
C** CHOOSE DAMPING.
C** DAMPING MUST BE LESS THAN CRITICAL (BETWEEN 0.0 AND 1.0).
C   DO 300 IKSI=1,3
  IF(DAMP.GT.ONE) WRITE(6,11)
  11 FORMAT(/,3X,50HTHIS PROGRAM IS WRITTEN FOR UNDERDAMPED CASES
ONLY)
```

```

C** CHOOSE FREQUENCY FROM THE RANGE (FREQMIN, FREQMAX)
  DO 200 IFREQ=1, INT
    FREQIN=FREQMIN+FRAC*DFREQ*DBLE(IFREQ-1)
C** FREQMIN MUST BE GREATER THAN ZERO
    PI=TWO*ASIN(ONE)
    VXSI=DAMP
    FREQ=FREQIN*TWO*PI
    DEN=SQRT(ONE-VXSI*VXSI)
    VRATIO=ONE/DEN
    FREQE=DEN*FREQ
    XSIWT=VXSI*FREQ*DT
    ETAU=EXP(-XSIWT)
    SINWT=SIN(FREQE*DT)
    COSWT=COS(FREQE*DT)
    A(1,1)=ETAU*(VXSI*VRATIO*SINWT+COSWT)
    A(1,2)=ETAU*SINWT/FREQE
    A(2,1)=-ETAU*FREQ*VRATIO*SINWT
    A(2,2)=ETAU*(COSWT-VXSI*VRATIO*SINWT)
C
    TXSI=(TWO*VXSI*VXSI-ONE)/FREQ/FREQ/FREQE/DT
    XSIF=VXSI/FREQ/FREQE
    FREQI=ONE/FREQ/FREQ
C
    B(1,1)=ETAU*(-(XSIF+TXSI)*SINWT-
1          (FREQI+TWO*VXSI*FREQI/FREQ/DT)*COSWT)+
2          TWO*VXSI*FREQI/FREQ/DT
    B(1,2)=ETAU*(TXSI*SINWT+TWO*VXSI*FREQI/FREQ/DT*COSWT)+
1          FREQI-TWO*VXSI*FREQI/FREQ/DT
    B(2,1)=ETAU*(-(FREQE*COSWT-VXSI*FREQ*SINWT)*(TXSI+XSIF)+
1          (FREQE*SINWT+VXSI*FREQ*COSWT)*(FREQI+TWO*VXSI*FREQI/
1          FREQ/DT))-FREQI/DT
    B(2,2)=ETAU*((FREQE*COSWT-VXSI*FREQ*SINWT)*TXSI-
1          (FREQE*SINWT+VXSI*FREQ*COSWT)*TWO*VXSI*FREQI/
2          FREQ/DT)+FREQI/DT
    DO 100 IT=1, NACC
      IF(IT.EQ.1) THEN
C* INITIAL CONDITIONS
        T=0.d0
        Q(1)=0.d0
        QP(1)=0.d0
        QPP(1)=ACC(1)
      ELSE
        T=T+DT
        Q(IT)=A(1,1)*Q(IT-1)+A(1,2)*QP(IT-1)+B(1,1)*ACC(IT-
1)+B(1,2)
1          *ACC(IT)
        QP(IT)=A(2,1)*Q(IT-1)+A(2,2)*QP(IT-1)+B(2,1)*ACC(IT-1)+
1          B(2,2)*ACC(IT)
        QPP(IT)=ACC(IT)-QP(IT)*TWO*VXSI*FREQ-Q(IT)*FREQ*FREQ
      ENDIF
100 CONTINUE
    QMAX=0.d0
    QPMAX=0.d0
    QPPMAX=0.d0
    DO 110 II=1, NACC
      QABS=ABS(Q(II))
      QPABS=ABS(QP(II))

```



```
QPPABS=ABS(QPP(II))
QMAX=MAX(QMAX,QABS)
QPMAX=MAX(QPMAX,QPABS)
QPPMAX=MAX(QPPMAX,QPPABS)
110 CONTINUE
QM(IFREQ)=QMAX
QPM(IFREQ)=QPMAX
QPPM(IFREQ)=QPPMAX
FR(IFREQ)=FREQIN
200 CONTINUE
DO 210 LI=1,INT
WRITE(15,211) FR(LI),QM(LI)
WRITE(16,211) FR(LI),QPM(LI)
210 CONTINUE
211 FORMAT(1X,E12.5,1H,,E12.5)
DAMP=DAMP+0.02d0
300 CONTINUE
990 CONTINUE
STOP
END
```

## APPENDIX C

### SAMPLE DRAIN-2DX INPUT FILES

#### B.1 Sample elastic analysis input file

```

•STARTXX
  nr021          0 1 1 1          elastic dynamic analysis
*NODECOORDS
!BASE NODES
C      1          0.          0.
C      2          8.          0.
C      3          16.         0.
C      4          24.         0.
!GRID EDGES
C     11          0.          5.
C     14          24.         5.
C    101          0.         41.
C    104          24.         41.
! GRID GENERATION
G     11          14          104          101          1          10
*RESTRAINTS
S 111          1          4          1
*MASSES
! TRANSLATIONAL MASSES
! ROOF EDGES
S 110 135341.          101          104          3
0.06543
! ROOF CENTER
S 110  91023.          102          103
0.06543
! TYPICAL FLOOR EDGES
G 110 160766.          11          14          3          91          10
0.06543
! TYPICAL FLOOR CENTER
G 110 109950.          12          13          92          10
0.06543
! ROTATIONAL MASSES
! ROOF EDGES
S 001 53614.7          101          104          3
0.06543
! ROOF CENTER
S 001 107229.4          102          103
0.06543
! TYPICAL FLOOR EDGES
G 001 33119.3          11          14          3          91          10
0.06543
! TYPICAL FLOOR CENTER
G 001 126238.6          12          13          92          10
0.06543
*ELEMENTGROUP
  02  0  2          4.85E-3          BEAMS & COLUMNS OF THE
STRUCTURE
  11  0  1
!STIFNESS DATA
! W 840 X 210

```

1	2.E11	0.	0.0268	3.11E-3	4.	4.	2.
! W 840 X 176							
2	2.E11	0.	0.0224	2.46E-3	4.	4.	2.
! W 760 X 147							
3	2.E11	0.	0.0187	1.66E-3	4.	4.	2.
! W 610 X 113							
4	2.E11	0.	0.0144	8.75E-4	4.	4.	2.
! W 360 X 990							
5	2.E11	0.	0.1260	5.19E-3	4.	4.	2.
! W 360 X 818							
6	2.E11	0.	0.1040	3.92E-3	4.	4.	2.
! W 360 X 744							
7	2.E11	0.	0.0948	3.42E-3	4.	4.	2.
! W 360 X 509							
8	2.E11	0.	0.0649	2.05E-3	4.	4.	2.
! W 360 X 551							
9	2.E11	0.	0.0701	2.26E-3	4.	4.	2.
! W 360 X 421							
10	2.E11	0.	0.0537	1.60E-3	4.	4.	2.
! W 360 X 287							
11	2.E11	0.	0.0366	9.97E-4	4.	4.	2.
! YIELD SURFACE MY VERY LARGE FOR ELASTIC ANALYSIS							
1	1	1.0E10	1.0E10				
! ELEMENT GENERATION							
! BEAMS FLOORS 1-4							
1	11	12		1	1	1	
3	13	14		1	1	1	
4	21	22		1	1	1	
6	23	24		1	1	1	
7	31	32		1	1	1	
9	33	34		1	1	1	
10	41	42		1	1	1	
12	43	44		1	1	1	
! BEAMS FLOORS 5 & 6							
13	51	52		2	1	1	
15	53	54		2	1	1	
16	61	62		2	1	1	
18	63	64		2	1	1	
! BEAMS FLOORS 7 & 8							
19	71	72		3	1	1	
21	73	74		3	1	1	
22	81	82		3	1	1	
24	83	84		3	1	1	
! BEAMS FLOORS 9 & 10							
25	91	92		4	1	1	
27	93	94		4	1	1	
28	101	102		4	1	1	
30	103	104		4	1	1	
! COLUMNS AXES # 1							
31	1	11	10	7	1	1	
34	31	41		7	1	1	
35	41	51		9	1	1	
36	51	61		9	1	1	
37	61	71		10	1	1	
38	71	81		10	1	1	
39	81	91		11	1	1	
40	91	101		11	1	1	

! COLUMNS AXES # 2							
41	2	12		10	5	1	1
44	32	42			5	1	1
45	42	52			6	1	1
46	52	62			6	1	1
47	62	72			7	1	1
48	72	82			7	1	1
49	82	92			8	1	1
50	92	102			8	1	1
! COLUMNS AXES # 3							
51	3	13		10	5	1	1
54	33	43			5	1	1
55	43	53			6	1	1
56	53	63			6	1	1
57	63	73			7	1	1
58	73	83			7	1	1
59	83	93			8	1	1
60	93	103			8	1	1
! COLUMNS AXES # 4							
61	4	14		10	7	1	1
64	34	44			7	1	1
65	44	54			9	1	1
66	54	64			9	1	1
67	64	74			10	1	1
68	74	84			10	1	1
69	84	94			11	1	1
70	94	104			11	1	1

\*SECTION

SECTION FOR CALCULATING BASE

0.			
SHEAR			
1	31	-12.0	0
	1.0	0.0	0.
	0.0	1.0	0.
	0.	0.	1.0
	0.	0.	0.
	0.	0.	0.
	0.	0.	0.
1	41	-4.0	1
1	51	4.0	1
1	61	12.0	1

\*GENDISP

INTERSTOREY DRIFT 1ST FLOOR

4	1	-1.0
14	1	1.0
11	2	-0.20833
14	2	0.20833

\*GENDISP

INTERSTOREY DRIFT 2ND FLOOR

14	1	-1.0
24	1	1.0
21	2	-0.16667
24	2	0.16667

\*GENDISP

INTERSTOREY DRIFT 3RD FLOOR

24	1	-1.0
34	1	1.0
31	2	-0.16667
34	2	0.16667

\*GENDISP

INTERSTOREY DRIFT 4TH FLOOR

34	1	-1.0
----	---	------

44	1	1.0	
41	2	-0.16667	
44	2	0.16667	
*GENDISP			
44	1	-1.0	INTERSTOREY DRIFT 5TH FLOOR
54	1	1.0	
51	2	-0.16667	
54	2	0.16667	
*GENDISP			
54	1	-1.0	INTERSTOREY DRIFT 6TH FLOOR
64	1	1.0	
61	2	-0.16667	
64	2	0.16667	
*GENDISP			
64	1	-1.0	INTERSTOREY DRIFT 7TH FLOOR
74	1	1.0	
71	2	-0.16667	
74	2	0.16667	
*GENDISP			
74	1	-1.0	INTERSTOREY DRIFT 8TH FLOOR
84	1	1.0	
81	2	-0.16667	
84	2	0.16667	
*GENDISP			
84	1	-1.0	INTERSTOREY DRIFT 9TH FLOOR
94	1	1.0	
91	2	-0.16667	
94	2	0.16667	
*GENDISP			
94	1	-1.0	INTERSTOREY DRIFT 10TH FLOOR
104	1	1.0	
101	2	-0.16667	
104	2	0.16667	

```

*RESULTS
!NODAL DISPLACEMENT
NSD 001 102
!NODAL VELOCITY
NSV 001 102
! ELEMENT OUTPUT
E 000
! SECTION OUTPUT
S 001
! GENERALIZED DISPLACEMENT
GD 001

```

```

*ELEMLOAD
BMGL
DEAD & LIVE LOADS ON BEAMS
G 1 2
   1 1 0.0 103200. 137600. 0. 103200.
-137600.
   2 1 0.0 87840. 117120. 0. 87840.
-117120.
   1 27 1 1.
   28 30 1 1.

```

```

*NODALOAD
GRLD
NODAL LOADS FROM SIDE FRAMES

```

```

G      0. -103200.      0.      11      14      91
10
S      0. -87840.      0.      101     104      3
*ACCNREC
  EQ      nr2.txt(8(f10.3))      NORTH RIDGE REC # 2
  1928    8    0    2      0.01873    0.02    0.
*PARAMETERS
OD      0      0      20    0.1    0      0
DT    0.005    0.005
*GRAV
E      BMGL
N      GRLD
*ACCN
      51.2050000    1
1      EQ
*STOP

```

### B.1 Sample elastic analysis input file

```

*STARTXX
  nr02n      0 1 1 1      DYNAMIC NON LINER TIME HISTORY
ANALYSIS
*NODECOORDS
!BASE NODES
C      1      0.      0.
C      2      8.      0.
C      3     16.      0.
C      4     24.      0.
!GRID EDGES
C      11     0.      5.
C      14     24.      5.
C     101     0.     41.
C     104     24.     41.
! GRID GENERATION
G      11     14     104     101     1     10
*RESTRAINTS
S 111      1      4      1
*MASSES
! TRANSLATIONAL MASSES
! ROOF EDGES
S 110  135341.      101     104     3
0.06543
! ROOF CENTER
S 110   91023.      102     103
0.06543
! TYPICAL FLOOR EDGES
G 110  160766.      11      14      3      91      10
0.06543
! TYPICAL FLOOR CENTER
G 110  109950.      12      13      92      10
0.06543
! ROTATIONAL MASSES
! ROOF EDGES

```

```

S 001 53614.7      101      104      3
0.06543
! ROOF CENTER
S 001 107229.4    102      103
0.06543
! TYPICAL FLOOR EDGES
G 001 33119.3     11       14       3       91      10
0.06543
! TYPICAL FLOOR CENTER
G 001 126238.6   12       13       92      10
0.06543
*ELEMENTGROUP
  02  0  2      4.85E-3      BEAMS & COLUMNS OF THE
STRUCTURE
  11  0  11
!STIFNESS DATA
! W 840 X 210
  1  2.E11      .050      0.0268    3.11E-3   4.   4.   2.
! W 840 X 176
  2  2.E11      .050      0.0224    2.46E-3   4.   4.   2.
! W 760 X 147
  3  2.E11      .050      0.0187    1.66E-3   4.   4.   2.
! W 610 X 113
  4  2.E11      .050      0.0144    8.75E-4   4.   4.   2.
! W 360 X 990
  5  2.E11      .050      0.1260    5.19E-3   4.   4.   2.
! W 360 X 818
  6  2.E11      .050      0.1040    3.92E-3   4.   4.   2.
! W 360 X 744
  7  2.E11      .050      0.0948    3.42E-3   4.   4.   2.
! W 360 X 509
  8  2.E11      .050      0.0649    2.05E-3   4.   4.   2.
! W 360 X 551
  9  2.E11      .050      0.0701    2.26E-3   4.   4.   2.
! W 360 X 421
  10 2.E11      .050      0.0537    1.60E-3   4.   4.   2.
! W 360 X 287
  11 2.E11      .050      0.0366    9.97E-4   4.   4.   2.
! YIELD SURFACES
! W 840 X 210
  1  2  2.202E6    2.202E6    8.04E6    8.04E6    1.   0.   1.   0.
! W 840 X 176
  2  2  1.770E6    1.770E6    6.72E6    6.72E6    1.   0.   1.   0.
! W 760 X 147
  3  2  1.323E6    1.323E6    5.61E6    5.61E6    1.   0.   1.   0.
! W 610 X 113
  4  2  8.640E5     8.642E5    4.32E6    4.32E6    1.   0.   1.   0.
! W 360 X 990
  5  2  5.670E6    5.670E6    37.8E6    37.8E6    1.   0.   1.   0.
! W 360 X 818
  6  2  4.590E6    4.590E6    31.2E6    31.2E6    1.   0.   1.   0.
! W 360 X 744
  7  2  4.110E6    4.110E6    28.44E6    28.44E6    1.   0.   1.   0.
! W 360 X 509
  8  2  2.751E6    2.571E6    19.47E6    19.47E6    1.   0.   1.   0.
! W 360 X 551
  9  2  2.982E6    2.982E6    21.03E6    21.03E6    1.   0.   1.   0.

```

! W 360 X 421									
10	2	2.253E6	2.253E6	16.11E6	16.11E6	1.	0.	1.	0.
! W 360 X 990									
11	2	1.521E6	1.521E6	10.98E6	10.98E6	1.	0.	1.	0.
! ELEMENT GENERATION									
! BEAMS FLOORS 1-4									
1	11	12		1	1	1			
3	13	14		1	1	1			
4	21	22		1	1	1			
6	23	24		1	1	1			
7	31	32		1	1	1			
9	33	34		1	1	1			
10	41	42		1	1	1			
12	43	44		1	1	1			
! BEAMS FLOORS 5 & 6									
13	51	52		2	2	2			
15	53	54		2	2	2			
16	61	62		2	2	2			
18	63	64		2	2	2			
! BEAMS FLOORS 7 & 8									
19	71	72		3	3	3			
21	73	74		3	3	3			
22	81	82		3	3	3			
24	83	84		3	3	3			
! BEAMS FLOORS 9 & 10									
25	91	92		4	4	4			
27	93	94		4	4	4			
28	101	102		4	4	4			
30	103	104		4	4	4			
! COLUMNS AXES # 1									
31	1	11	10	7	7	7			
34	31	41		7	7	7			
35	41	51		9	9	9			
36	51	61		9	9	9			
37	61	71	10	10	10	10			
38	71	81	10	10	10	10			
39	81	91	11	11	11	11			
40	91	101	11	11	11	11			
! COLUMNS AXES # 2									
41	2	12	10	5	5	5			
44	32	42		5	5	5			
45	42	52		6	6	6			
46	52	62		6	6	6			
47	62	72		7	7	7			
48	72	82		7	7	7			
49	82	92		8	8	8			
50	92	102		8	8	8			
! COLUMNS AXES # 3									
51	3	13	10	5	5	5			
54	33	43		5	5	5			
55	43	53		6	6	6			
56	53	63		6	6	6			
57	63	73		7	7	7			
58	73	83		7	7	7			
59	83	93		8	8	8			
60	93	103		8	8	8			
! COLUMNS AXES # 4									



61	4	14	10	7	7	7
64	34	44		7	7	7
65	44	54		9	9	9
66	54	64		9	9	9
67	64	74		10	10	10
68	74	84		10	10	10
69	84	94		11	11	11
70	94	104		11	11	11
*SECTION			SECTION FOR CALCULATING BASE			
0.						
SHEAR						
1	31	-12.0	0			
	1.0	0.0	0.			
	0.0	1.0	0.			
	0.	0.	1.0			
	0.	0.	0.			
	0.	0.	0.			
	0.	0.	0.			
1	41	-4.0	1			
1	51	4.0	1			
1	61	12.0	1			
*GENDISP						
	4	1	-1.0	INTERSTOREY DRIFT 1ST FLOOR		
	14	1	1.0			
	11	2	-0.20833			
	14	2	0.20833			
*GENDISP						
	14	1	-1.0	INTERSTOREY DRIFT 2ND FLOOR		
	24	1	1.0			
	21	2	-0.16667			
	24	2	0.16667			
*GENDISP						
	24	1	-1.0	INTERSTOREY DRIFT 3RD FLOOR		
	34	1	1.0			
	31	2	-0.16667			
	34	2	0.16667			
*GENDISP						
	34	1	-1.0	INTERSTOREY DRIFT 4TH FLOOR		
	44	1	1.0			
	41	2	-0.16667			
	44	2	0.16667			
*GENDISP						
	44	1	-1.0	INTERSTOREY DRIFT 5TH FLOOR		
	54	1	1.0			
	51	2	-0.16667			
	54	2	0.16667			
*GENDISP						
	54	1	-1.0	INTERSTOREY DRIFT 6TH FLOOR		
	64	1	1.0			
	61	2	-0.16667			
	64	2	0.16667			
*GENDISP						
	64	1	-1.0	INTERSTOREY DRIFT 7TH FLOOR		
	74	1	1.0			
	71	2	-0.16667			
	74	2	0.16667			
*GENDISP						

```

      74   1   -1.0
      84   1    1.0
      81   2  -0.16667
      84   2   0.16667
*GENDISP
      84   1   -1.0
      94   1    1.0
      91   2  -0.16667
      94   2   0.16667
*GENDISP
      94   1   -1.0
     104   1    1.0
     101   2  -0.16667
     104   2   0.16667
*RESULTS
!NODAL DISPLACMENT
NSD  001    102
!NODAL VELOCITY
NSV  001    102
! ELEMENT OUTPUT
E    001
! SECTION OUTPUT
S    001
! GENERALIZED DISPLACMENT
GD   001
*ELEMLOAD
  BMGL
  G   1   2
      1   1    0.0    103200.    137600.    0.    103200.
-137600.
      2   1    0.0    87840.    117120.    0.    87840.
-117120.
      1  27    1    1.
      28  30    1    1.
*•NODALOAD
  GRLD
  G   0.  -103200.    0.    11    14    91
  10
  S   0.  -87840.    0.    101   104    3
*ACCNREC
  EQ      nr2.txt(8(f10.3))    northridge  REC # 2
  1928   8    0    2    .018730    0.02    0.
*PARAMETERS
OD   0    0
DT  .0025    .0025
*GRAV
E    BMGL
N    GRLD
*ACCN
      51.2050000    1
1    EQ
*STOP

```

## APPENDIX D

### FORTRAN SUBROUTINE TO SEPARATE COMPLETE CYCLES AND CALCULATE DAMAGE

```
c
c  program to calculate the damage based on the Daali-korol formula
c  subroutine for range-pair counting of random data distribution
c  developed by Dr. Sudip Bhattacharjee
c
c  returns damage at beam ends
c
c
c  subroutine rpr (th,nline,a,d1,d2)
c  dimension ntr(1000),dat(20000),idat(20000),sig(10000),dsec(2)
c  dimension th(1.5000)
c
c  nlimit=20000
c
c  nstep=1000
c  do 5000 j=1,nline
c  itme=2
c
c  dat1=th(jel,1)
c  dat2=th(jel,2)
c  if (dat2 .gt. dat1) then
c    k2=1
c  else
c    k2=-1
c  endif
c  nf=2
c  ni=1
c  dat(ni)=dat1
c  idat(ni)=-k2
c  k0=-k2
c  imax=0
200 continue
c  itme=itme+1
c  nf=nf+1
c  datf=th(jel,itme)
c  kr=0
c  if (k2 .eq. 1 .and. datf .gt. dat2) then
c    kr=1
c  endif
c  if (k2 .eq. -1 .and. datf .lt. dat2) then
c    kr=1
c  endif
c  endif
c  if (kr .eq. 0) then
c    ni=ni+1
c    dat(ni)=dat2
c    idat(ni)=k2
c    k3=-k2
c  else
c    k3=k2
c    if (nf .lt. nline) then
```

```

        dat2=datf
        go to 200
    endif
endif
if (nf .lt. nline) then
    kr=1
    dat0=dat(1)
    if (k0 .eq. -1 .and. dat2 .lt. dat0) kr=0
    if (k0 .eq. 1 .and. dat2 .gt. dat0) kr=0
    if (ni .eq. nlimit) kr=0
    if (kr .eq. 1) then
        dat2=datf
        k2=k3
        go to 200
    endif
endif
300 continue
c count the stress cycles
    idiff=0
    do 399 i=1,ni
        ki=idat(i)
        if (ki .eq. 0) go to 399
        il=i+1
        do 310 j=il,ni
            kj=idat(j)
            if (kj .eq. 0) go to 320
310 continue
320 continue
            dat0=dat(i)
            itmp=0
            j1=j-1
            temp=dat0
            do 330 m=i1,j-1
                if (ki .eq. -1) then
                    if (dat(m) .gt. temp) then
                        itmp=m
                        temp=dat(m)
                    endif
                else
                    if (dat(m) .lt. temp) then
                        itmp=m
                        temp=dat(m)
                    endif
                endif
            do 330 m=i1,j-1
330 continue
c
            if (itmp.ne.0)then
                idat(itmp)=0
                idiff=idiff+1
                diff=abs(dat0-temp)
                sig(idiff)=diff
                nfr(idiff)=1
            end if
c
399 continue
    if (nf .lt. nline-1) then
        dat(1)=dat(ni)

```

```
        idat(1)=idat(ni)
        dat2=datf
        k2=k3
        ni=1
        k0=idat(1)
        go to 200
    endif
c
    imax=idiff
    dsec(jel)=0
    do 400 k=1,imax
        dummm=200*a*sig(k)**1.65
        dsec(jel)=dsec(jel)+dummm
    400 continue
    5000 continue
    d1=dsec(1)
    d2=dsec(2)
    end
```

## **VITA AUCTORIS**

**NAME:** Karim Helmi

**PLACE OF BIRTH:** Cairo, Egypt

**DATE OF BIRTH:** 1971

**EDUCATION:** 1993, B. Sc. in Civil Engineering, University of Alexandria  
Alexandria, Egypt

1998 Joined the M.A.Sc. program at the University of  
Windsor, Windsor, Ontario